# ASSESSMENT OF THE POTENTIAL IMPACT OF DIFFUSION FLAMES ON THE AP600 CONTAINMENT WALL AND PENETRATIONS

**Revision 1**

**April 1997**

---

Westinghouse Electric Corporation
Energy Systems Business Unit
P.O. Box 355
Pittsburgh, PA 15230-0355

# AP600 DOCUMENT COVER SHEET

TDC: _____ IDS: I _____ S _____

Form 58202G(5/94) [t:\xxxx.wpf:1x] AP600 CENTRAL FILE USE ONLY:

0058.FRM RFS#: RFS ITEM #:

| AP600 DOCUMENT NO. | REVISION NO. | | ASSIGNED TO |
|---|---|---|---|
| PRA-GSR-004 | 1 | Page 1 of 1 | |

ALTERNATE DOCUMENT NUMBER: WORK BREAKDOWN #: 3.2.4.17

DESIGN AGENT ORGANIZATION: Westinghouse (FAI)

TITLE: Assessment of the Potential Impact of Diffusion Flames on the AP600 Containment Wall and Penetrations

| ATTACHMENTS: | DCP #/REV. INCORPORATED IN THIS DOCUMENT REVISION: |
|---|---|
| CALCULATION/ANALYSIS REFERENCE: | |

| ELECTRONIC FILENAME | ELECTRONIC FILE FORMAT | ELECTRONIC FILE DESCRIPTION |
|---|---|---|
| | | |



**COMPLETE 1 IF WORK PERFORMED UNDER DESIGN CERTIFICATION OR COMPLETE 2 IF WORK PERFORMED UNDER FOAKE.**

1 ☒ **DOE DESIGN CERTIFICATION PROGRAM** - GOVERNMENT LIMITED RIGHTS STATEMENT [See page 2]

Copyright statement: A license is reserved to the U.S. Government under contract DE-AC03-90SF18495.

☐ DOE CONTRACT DELIVERABLES (DELIVERED DATA)
Subject to specified exceptions, disclosure of this data is restricted until September 30, 1995 or Design Certification under DOE contract DE-AC03-90SF18495, whichever is later.

EPRI CONFIDENTIAL: NOTICE: 1 ☒ 2 ☐ 3 ☐ 4 ☐ 5 ☐ CATEGORY: A ☒ B ☐ C ☐ D ☐ E ☐ F ☐

2 ☐ **ARC FOAKE PROGRAM** - ARC LIMITED RIGHTS STATEMENT [See page 2]

Copyright statement: A license is reserved to the U.S. Government under contract DE-FC02-NE34267 and subcontract ARC-93-3-SC-001.

☐ ARC CONTRACT DELIVERABLES (CONTRACT DATA)
Subject to specified exceptions, disclosure of this data is restricted under ARC Subcontract ARC-93-3-SC-001.

| ORIGINATOR | SIGNATURE/DATE | |
|---|---|---|
| C. L. Haag | C L Haag | 5/1/97 |
| AP600 RESPONSIBLE MANAGER | SIGNATURE* | APPROVAL DATE |
| B. A. McIntyre | B A McIntyre | 5/1/97 |

*Approval of the responsible manager signifies that document is complete, all required reviews are complete, electronic file is attached and document is released for use.

Form 58202G(5/94)

## LIMITED RIGHTS STATEMENTS

**DOE GOVERNMENT LIMITED RIGHTS STATEMENT**

(A) These data are submitted with limited rights under government contract No. DE-AC03-90SF18495. These data may be reproduced and used by the government with the express limitation that they will not, without written permission of the contractor, be used for purposes of manufacturer nor disclosed outside the government; except that the government may disclose these data outside the government for the following purposes, if any, provided that the government makes such disclosure subject to prohibition against further use and disclosure:

(I) This "Proprietary Data" may be disclosed for evaluation purposes under the restrictions above.

(II) The "Proprietary Data" may be disclosed to the Electric Power Research Institute (EPRI), electric utility representatives and their direct consultants, excluding direct commercial competitors, and the DOE National Laboratories under the prohibitions and restrictions above.

(B) This notice shall be marked on any reproduction of these data, in whole or in part.

**ARC LIMITED RIGHTS STATEMENT:**

This proprietary data, furnished under Subcontract Number ARC-93-3-SC-001 with ARC may be duplicated and used by the government and ARC, subject to the limitations of Article H-17.F. of that subcontract, with the express limitations that the proprietary data may not be disclosed outside the government or ARC, or ARC's Class 1 & 3 members or EPRI or be used for purposes of manufacture without prior permission of the Subcontractor, except that further disclosure or use may be made solely for the following purposes:

This proprietary data may be disclosed to other than commercial competitors of Subcontractor for evaluation purposes of this subcontract under the restriction that the proprietary data be retained in confidence and not be further disclosed, and subject to the terms of a non-disclosure agreement between the Subcontractor and that organization, excluding DOE and its contractors.

## DEFINITIONS

**CONTRACT/DELIVERED DATA** — Consists of documents (e.g. specifications, drawings, reports) which are generated under the DOE or ARC contracts which contain no background proprietary data.

## EPRI CONFIDENTIALITY / OBLIGATION NOTICES

**NOTICE 1:** The data in this document is subject to no confidentiality obligations.

**NOTICE 2:** The data in this document is proprietary and confidential to Westinghouse Electric Corporation and/or its Contractors. It is forwarded to recipient under an obligation of Confidence and Trust for limited purposes only. Any use, disclosure to unauthorized persons, or copying of this document or parts thereof is prohibited except as agreed to in advance by the Electric Power Research Institute (EPRI) and Westinghouse Electric Corporation. Recipient of this data has a duty to inquire of EPRI and/or Westinghouse as to the uses of the information contained herein that are permitted.

**NOTICE 3:** The data in this document is proprietary and confidential to Westinghouse Electric Corporation and/or its Contractors. It is forwarded to recipient under an obligation of Confidence and Trust for use only in evaluation tasks specifically authorized by the Electric Power Research Institute (EPRI). Any use, disclosure to unauthorized persons, or copying this document or parts thereof is prohibited except as agreed to in advance by EPRI and Westinghouse Electric Corporation. Recipient of this data has a duty to inquire of EPRI and/or Westinghouse as to the uses of the information contained herein that are permitted. This document and any copies or excerpts thereof that may have been generated are to be returned to Westinghouse, directly or through EPRI, when requested to do so.

**NOTICE 4:** The data in this document is proprietary and confidential to Westinghouse Electric Corporation and/or its Contractors. It is being revealed in confidence and trust only to Employees of EPRI and to certain contractors of EPRI for limited evaluation tasks authorized by EPRI. Any use, disclosure to unauthorized persons, or copying of this document or parts thereof is prohibited. This Document and any copies or excerpts thereof that may have been generated are to be returned to Westinghouse, directly or through EPRI, when requested to do so.

**NOTICE 5:** The data in this document is proprietary and confidential to Westinghouse Electric Corporation and/or its Contractors. Access to this data is given in Confidence and Trust only at Westinghouse facilities for limited evaluation tasks assigned by EPRI. Any use, disclosure to unauthorized persons, or copying of this document or parts thereof is prohibited. Neither this document nor any excerpts therefrom are to be removed from Westinghouse facilities.

## EPRI CONFIDENTIALITY / OBLIGATION CATEGORIES

**CATEGORY "A"** — (See Delivered Data) Consists of CONTRACTOR Foreground Data that is contained in an issued reported.

**CATEGORY "B"** — (See Delivered Data) Consists of CONTRACTOR Foreground Data that is not contained in an issued report, except for computer programs.

**CATEGORY "C"** — Consists of CONTRACTOR Background Data except for computer programs.

**CATEGORY "D"** — Consists of computer programs developed in the course of performing the Work.

**CATEGORY "E"** — Consists of computer programs developed prior to the Effective Date or after the Effective Date but outside the scope of the Work.

**CATEGORY "F"** — Consists of administrative plans and administrative reports.

## TABLE OF CONTENTS

## LIST OF FIGURES

## LIST OF TABLES

## 1.0 BACKGROUND AND APPROACH

The potential impact on the AP600 containment shell and penetrations of standing diffusion flames is a severe accident issue and not a design basis issue. The plant configuration including the IRWST vent exit configuration and locations have been derived as part of the AP600 design basis. The assessment presented in this report is directed toward determining the response of this given plant configuration to the proposed severe accident events. A generally deterministic assessment is described in the report and subsequently interpreted in the probabilistic context of the AP600 PRA to place its significance in the severe accident context.

The general approach used to address the potential impact of diffusion flames on the AP600 containment wall and its penetrations included a review of the Mark III HCOG data, the use of the hydrogen generation scenarios defined in the AP600 PRA, the use of the AP600 containment and IRWST specific geometry, the assessment of the IRWST gas space and vent design for the PRA hydrogen generation scenarios, the assessment of the valve vault rooms for the PRA accident scenarios, quantification of the diffusion flames (flame height and flame temperature), determination of the local containment walls and penetrations thermal responses, and an assessment of the structural significance of the local heating of the containment wall.

## 2.0 REVIEW OF MARK III HCOG DATA

The Mark III Hydrogen Control Owners Group (HCOG) sponsored and conducted a series of hydrogen combustion experiments in 1/4 scale models of Mark III nuclear reactor containments. Several attributes of the HCOG data were considered to facilitate the data's application to the AP600 IRWST assessment. These attributes included the hydrogen release flow rates, the diffusion flame behavior in terms of its location, maximum flame height, radiant heat fluxes and pressurization due to diffusion flame light-off.

The 1/4 scale model facility included a simulation of the distributed igniter system installed in Mark III containments, a suppression pool and the release of hydrogen through submerged spargers in the suppression pool. The test facility and results (Tamanini, 1988) were reviewed. The two-volume test program and results document plus selected video tapes were examined. Tests with both high (approximately 1 kg/sec) and low (approximately 0.4 kg/sec) hydrogen release rates were reviewed and observed. These tests demonstrated the formation and maintenance of diffusion flames anchored to the suppression pool surface which were initiated by the igniters in the test facility. The diffusion flame burning mode was maintained as long as the hydrogen source was maintained above an extinction level and sufficient oxygen was available to support combustion on the suppression pool surface. The general similarities in the

test configuration as compared to the AP600 IRWST with hydrogen release through submerged spargers was judged to support the applicability of the HCOG's test results to the AP600 IRWST and sparger configuration. The release flow rates of hydrogen incorporated in the HCOG test program correspond to the range of flow rates expected during severe accident hydrogen discharge through the ADS valves into the IRWST water pool for the AP600. During the peak hydrogen flow rate intervals complete combustion by diffusion flames located on the pool surface are observed in the HCOG tests.

Several observations were made during the HCOG test data review:

- During the peak hydrogen flow rate intervals complete combustion of diffusion flames located on the pool surface are observed. At low hydrogen flow rates less stable diffusion flames are observed and less than 100% combustion resulted.

- As oxygen in the region above the suppression pool was depleted, secondary or lifted flames were observed in the HCOG experiments which moved from the pool surface to a higher elevation in the plant. The flames moved to a region in the containment which had sufficient oxygen to support the continued burning.

- Pressure rise in the suppression pool region was gradual due to continued global heating during the burn with an initial light-off pressure of between 1.5 and 3.5 psid.

- The co-injection of steam and hydrogen through the submerged spargers had no affect on the observed diffusion flame behavior.

- Intermittent diffusion flame extinction was observed for diffusion flames on the pool surface for hydrogen flow rates in the range of 0.01 to 0.11 kg/s. Total diffusion flame extinction for hydrogen injection rates of 0.03 to 0.07 kg/s were observed, given that the background hydrogen concentration was less than 4%. The hydrogen injection rate which caused total diffusion flame extinction was seen to decrease as the background hydrogen concentration increased. Thus, for a background hydrogen concentration of approximately 4.5%, the observed hydrogen injection rate leading to extinction was in the range of 0.01 kg/s.

These observations from the HCOG experiments suggest that for the AP600 IRWST during burns reducing the oxygen concentration in the IRWST gas space, that the diffusion flame could move from the pool surface to the vent exits given the flappers are open to the rest of the

containment. The diffusion flame burning rates and locations are seen to be a function of the oxygen concentration in the IRWST gas space. Likewise, the extinction of a diffusion flame on the pool surface is dependent on the hydrogen injection flow rate. The conditions causing diffusion flame extinction for a flame attached to an IRWST vent were not examined in the HCOG experiments.

## 3.0 AP600 PRA HYDROGEN SCENARIOS

A three stage ADS scenario plus several of the accident scenarios defined in Chapter 41 of the AP600 PRA were used in this assessment. As discussed in the AP600 PRA the equivalent of 100% fuel-clad metal-water reaction for the cladding surrounding the active fuel was considered to be oxidized for the hydrogen burn analyses. This would yield approximately 640 kg of hydrogen for the AP600 design. A three stage ADS scenario was defined to assess the potential for diffusion flames at the IRWST vent exits. This scenario was a transient initiated by a loss of feedwater and, representing the 1D accident class discussed in Chapter 41 of the AP600 PRA. Its key feature is that it only considers the operation of the first three stages of the ADS system and not the state 4 ADS valves. This results in a bounding hydrogen release rate to the IRWST and a maximum IRWST water level which minimizes the gas volume in the IRWST. All hydrogen produced in-vessel is discharged through the ADS spargers and into the IRWST gas space for this three stage ADS. This results in high hydrogen concentrations in the limited IRWST gas space. It is important to note that the failure frequency of the 4th stage ADS is very low ($10^{-3}$ per year). Under most circumstances the 4th stage ADS will be actuated. When the 4th stage ADS is actuated, most hydrogen would bypass the IRWST and be directly released to the containment. The level of hydrogen buildup in the IRWST would be much lower and unlikely to support any standing flames. A series of scenario analysis from the AP600 PRA show that the operation of the 4th stage ADS prevents formation of diffusion flames at the IRWST vents.

The MAAP4 computer code was used to model the hydrogen generation and release sequences. A combination of parameters that control the amount of calculated clad oxidation and hydrogen production were selected to approximate the 100% oxidation of the active fuel cladding zirconium inventory. The MAAP4 simulation for the three stage ADS scenario yielded approximately 110% oxidation of the active cladding. This provides some conservatism in the amount of hydrogen burned in containment for this assessment. The calculated duration of hydrogen evolution rates was sufficiently large to support a diffusion flame burning of approximately 5000 sec. The peak calculated hydrogen release rate was 1.2 kg/s. The hydrogen release history for the three stage ADS MAAP4 simulation is provided in Figure 1.

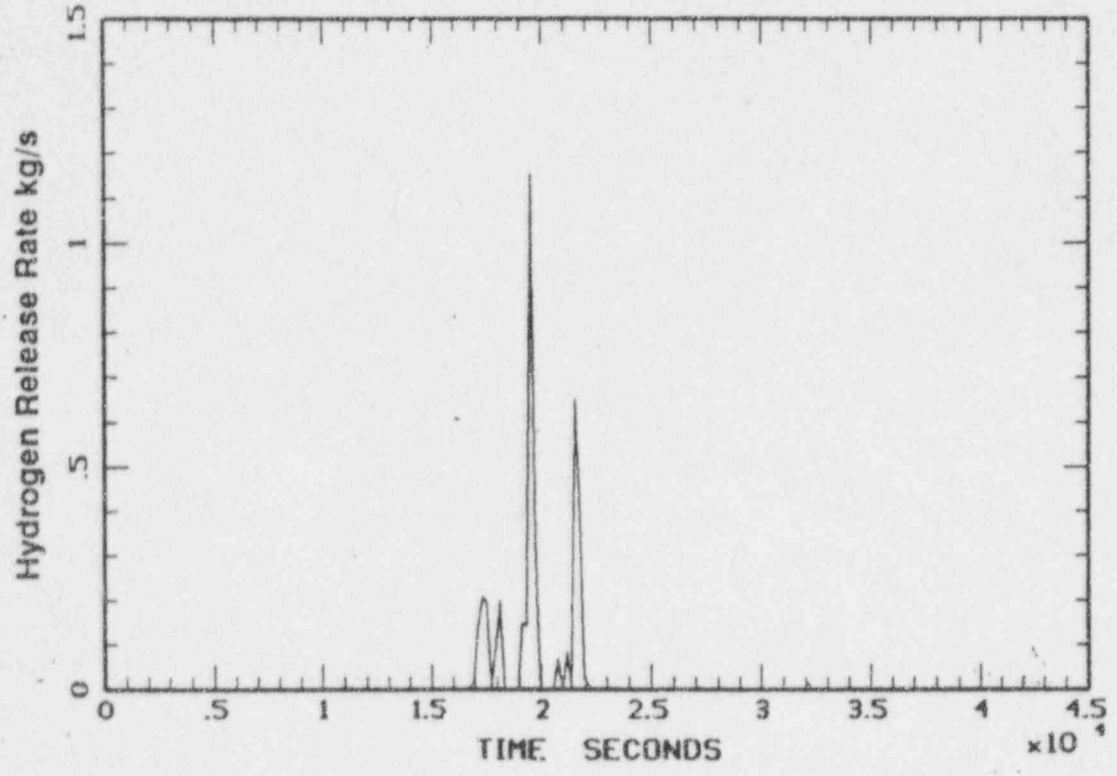


Note: All in-vessel hydrogen is released to IRWST through first three stages of ADS system for this bounding sequence.

Figure 1 Hydrogen Release History for Three Stage ADS Sequence

Five additional accident scenarios (see Table 1) were assessed with MAAP4 to investigate a range of hydrogen release histories and locations. These hydrogen release histories involved extended intervals of hydrogen generation during the boil-off of the vessel water inventory and relatively brief intervals of peak generation rates during core reflood. Each of these five sequences included the operation of all fourth stage ADS valves so they were fully depressurized sequences. The fourth stage ADS valves discharge directly to the steam generator compartments. Thus, a large flow path for hydrogen release from the primary system that does not involve the IRWST is provided by the operation of each fourth stage ADS valve.

These five sequences include cases (3BE-FRF1 and 3BE-FN1) initiated by a direct vessel injection (DVI) line break which release hydrogen in the valve vault rooms. This alternate hydrogen release location is used to assess the potential for diffusion flames being produced on the core makeup tank (CMT) room floor at elevation 107′ 2″ in the AP600 containment. Two DVI line break sequences were assessed to investigate the impact of flooding the break elevation on the potential of producing a standing diffusion flame at the valve vault room exits. Lastly, a sensitivity case (3BR-FR1*) was evaluated to investigate the impact of uncovering the ADS spargers in the IRWST water pool given the operation of all four stages of ADS valves. The hydrogen release histories for each of the five sequences with fourth stage ADS operation are presented in Figures 2 through 6. The containment node receiving the principal hydrogen release was found to be steam inerted for each of these five sequences except for the 3BE-FRF1 sequence. In this sequence the release point for the hydrogen and steam mixture escaping the primary system was submerged in the water that flooded that compartment. Thus, as the three stage ADS was used to assess the IRWST vents, the 3BE-FRF1 sequence was used to assess the effect of a standing diffusion flame at the exit in the ceiling of each valve vault room.

## 4.0 IRWST AND CMT FLOOR CONFIGURATIONS

Figure 7 depicts the IRWST cross section and sparger and igniter locations. The spargers are the locations where hydrogen produced by clad oxidation in the RPV is discharged following actuation of the first three stages of the ADS. The irregular geometric shape of the IRWST cross section suggests that it be represented in the IRWST vent assessment by two nodes. The node boundary used to divide the IRWST into a sparger region and a "PRHR" region is also shown in Figure 7. The IRWST vent design is summarized in Table 2. The IRWST vents are one directional flow devices. Each of the containment outer wall vents is located in the roof of the IRWST just inside the containment wall. The vents run straight up through the IRWST roof and then make a 90° turn away from the containment wall. Hinged flaps are provided at each exit to prevent significant exchange of air between the containment

Table 1

Accident Sequences with Fourth Stage ADS Operation

| Accident Sequence Designator | Sequence Description | Principal Release Location | Total Mass $H_2$ Released (kg) |
|---|---|---|---|
| 3BE-FRF1 | Full depressurized with failure of gravity injection (DVI line break with valve vault room flooded) | Valve Vault Room | 710 |
| 3BL-FN | Full depressurized with failure of gravity recirculation (15 cm hot leg break) | Steam Generator Compartment | 710 |
| 3BE-FN1 | Fully depressurized with failure of gravity injection (DVI line break with valve vault not flooded) | Valve Vault Room | 710 |
| 3BR-FR1 | Large LOCA with failure of accumulators | Steam Generator Compartment | 540 |
| 3BR-FR1* | Sensitivity case for 3BR-FR1 sequence with ADS sparger uncovered | Steam Generator Compartment | 540 |

**Note:** Chapter 41 of the AP600 PRA provides a description and discussion of these sequences.

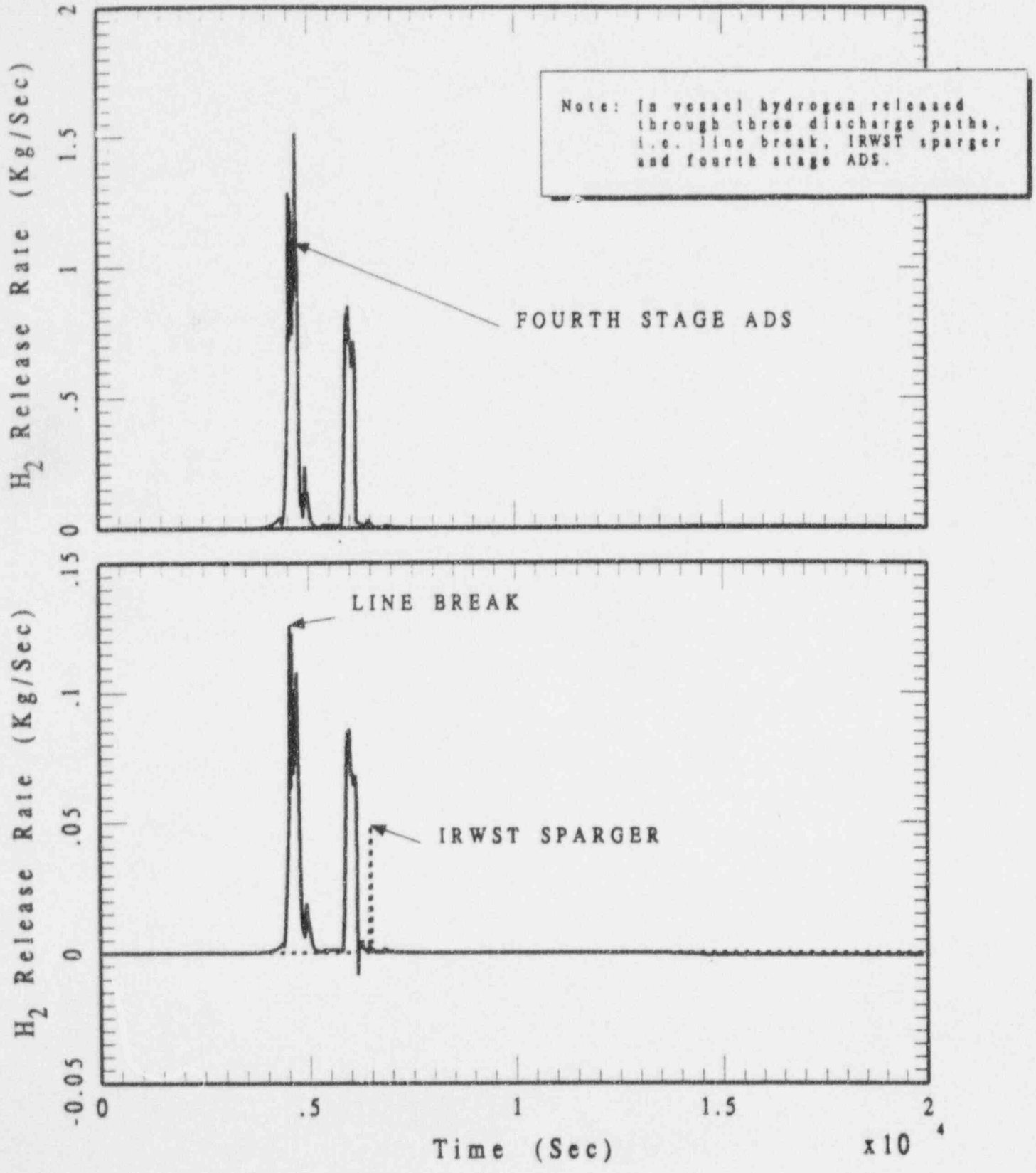


Figure 2 Hydrogen Release History for 3BE-FRF1 Sequence

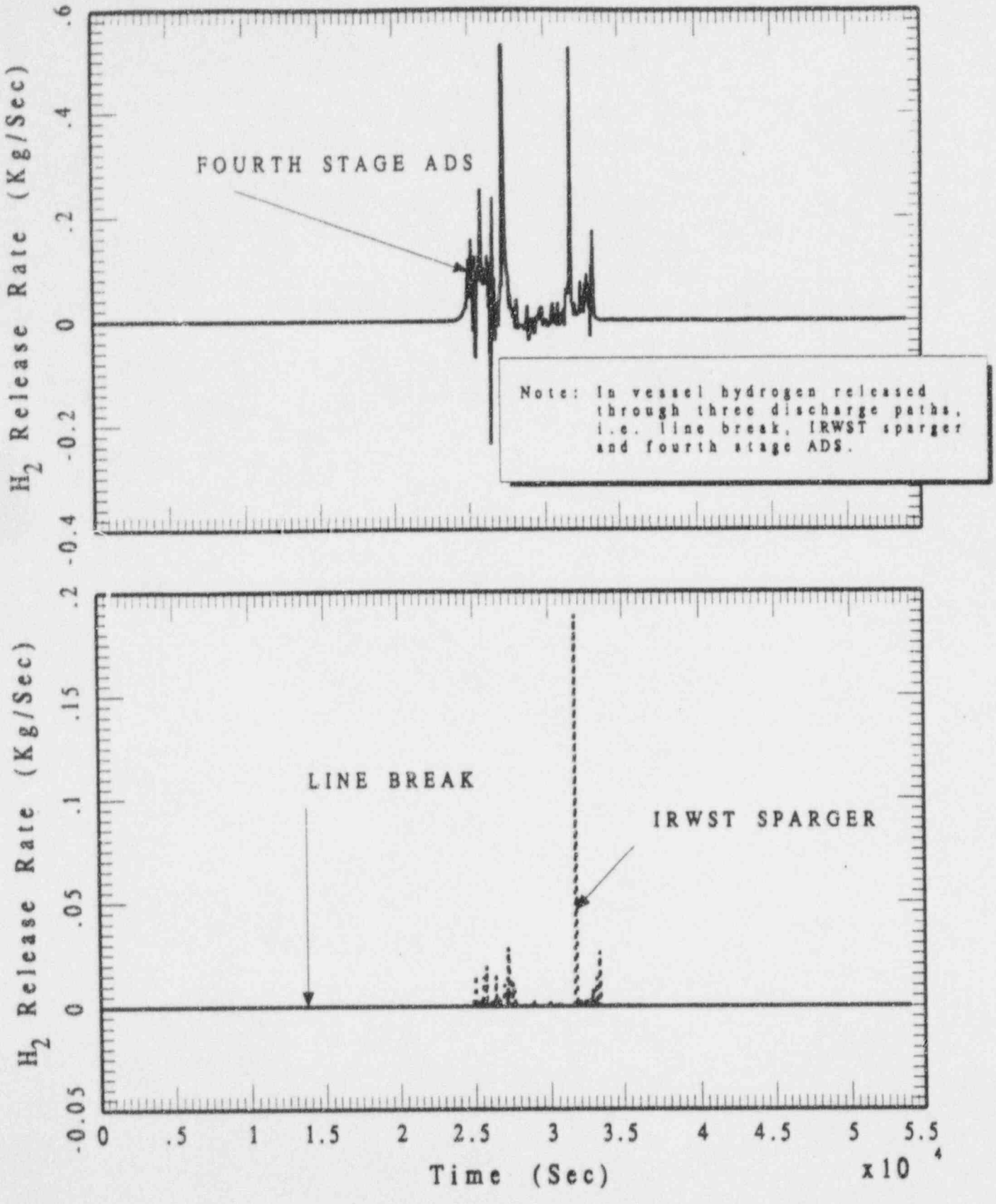


Figure 3 Hydrogen Release History for 3BL-FN Sequence.

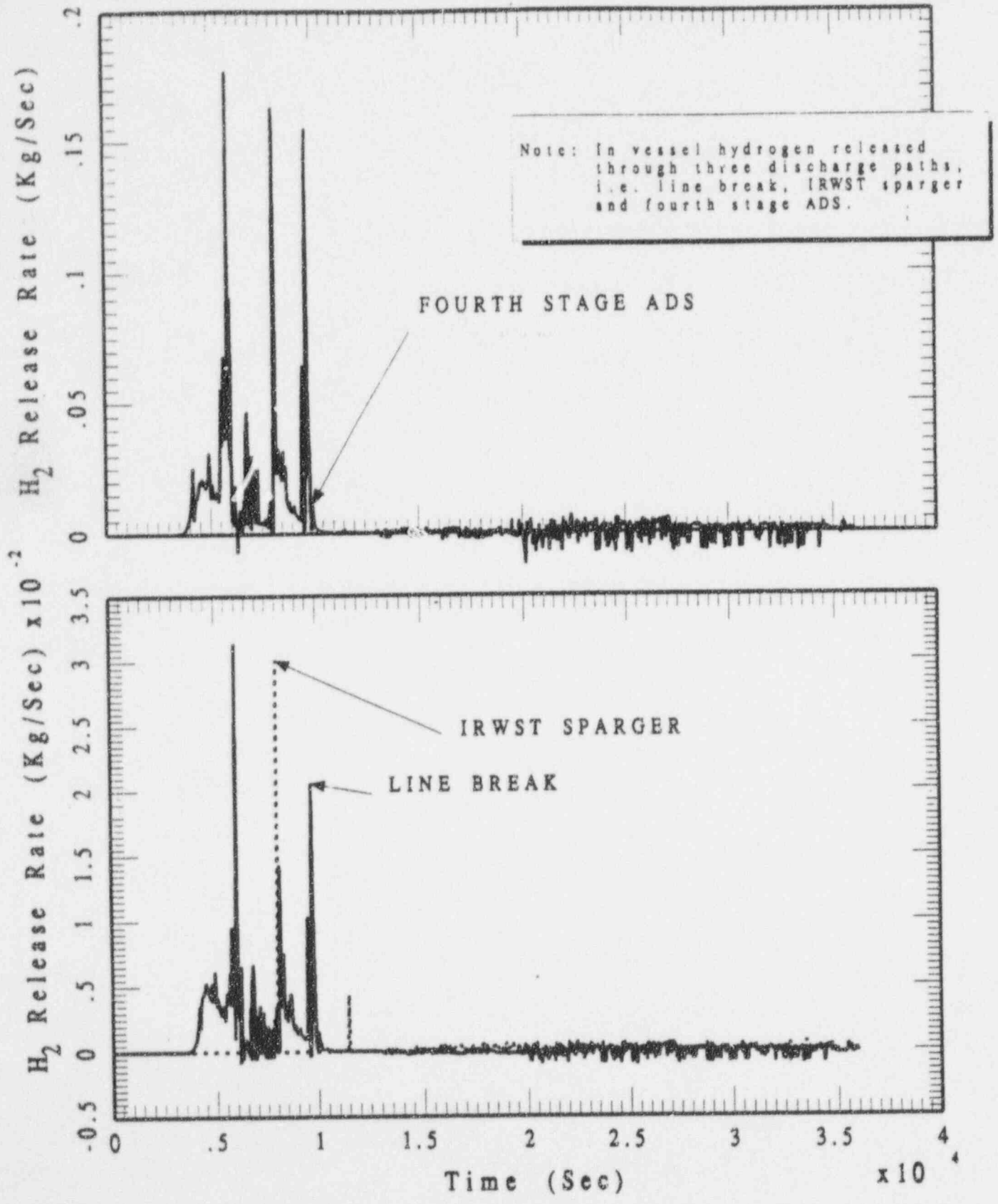


Figure 4 Hydrogen Release History for 3BE-FN1 Sequence.

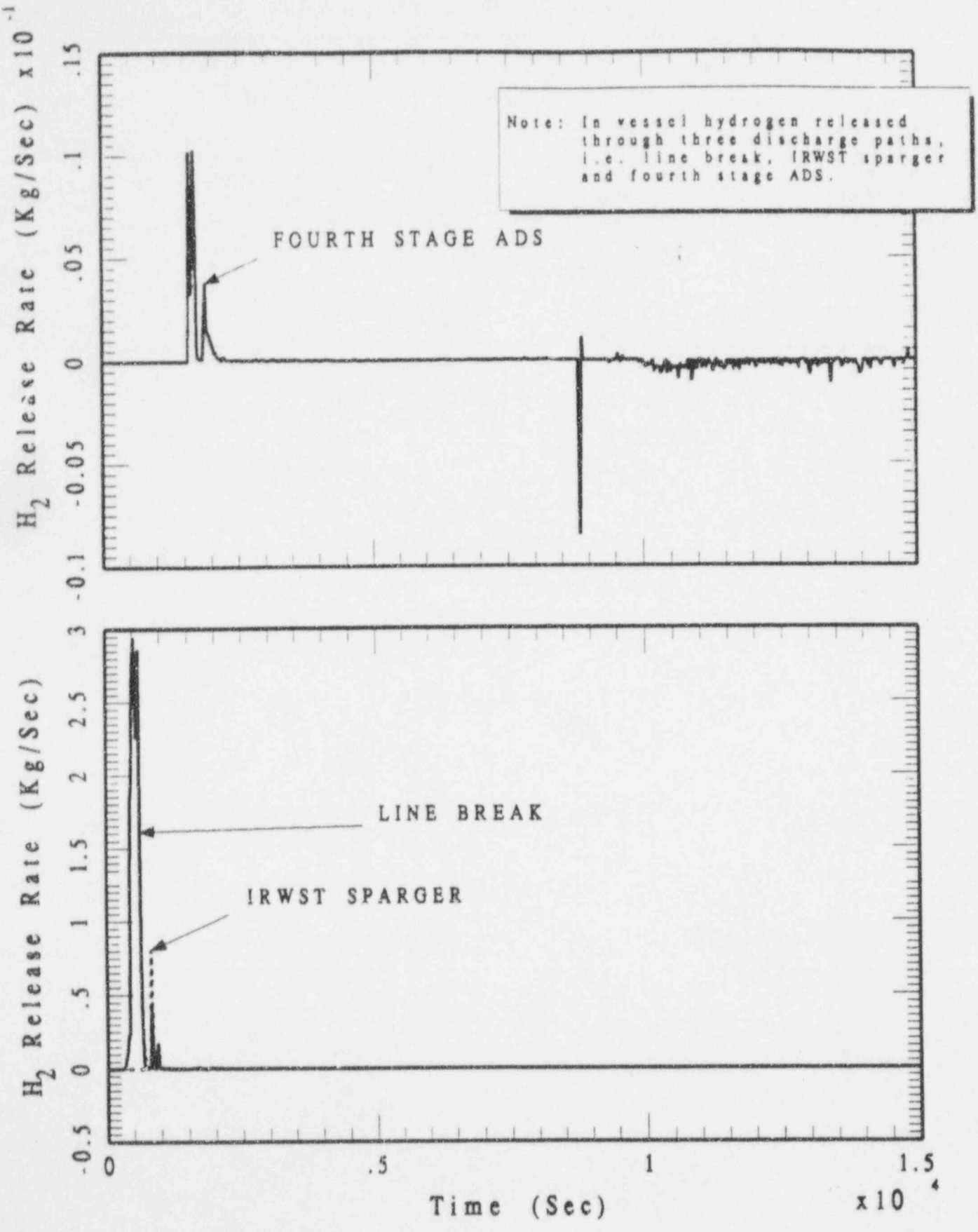


Figure 5 Hydrogen Release History for 3BR-FR1 Sequence.

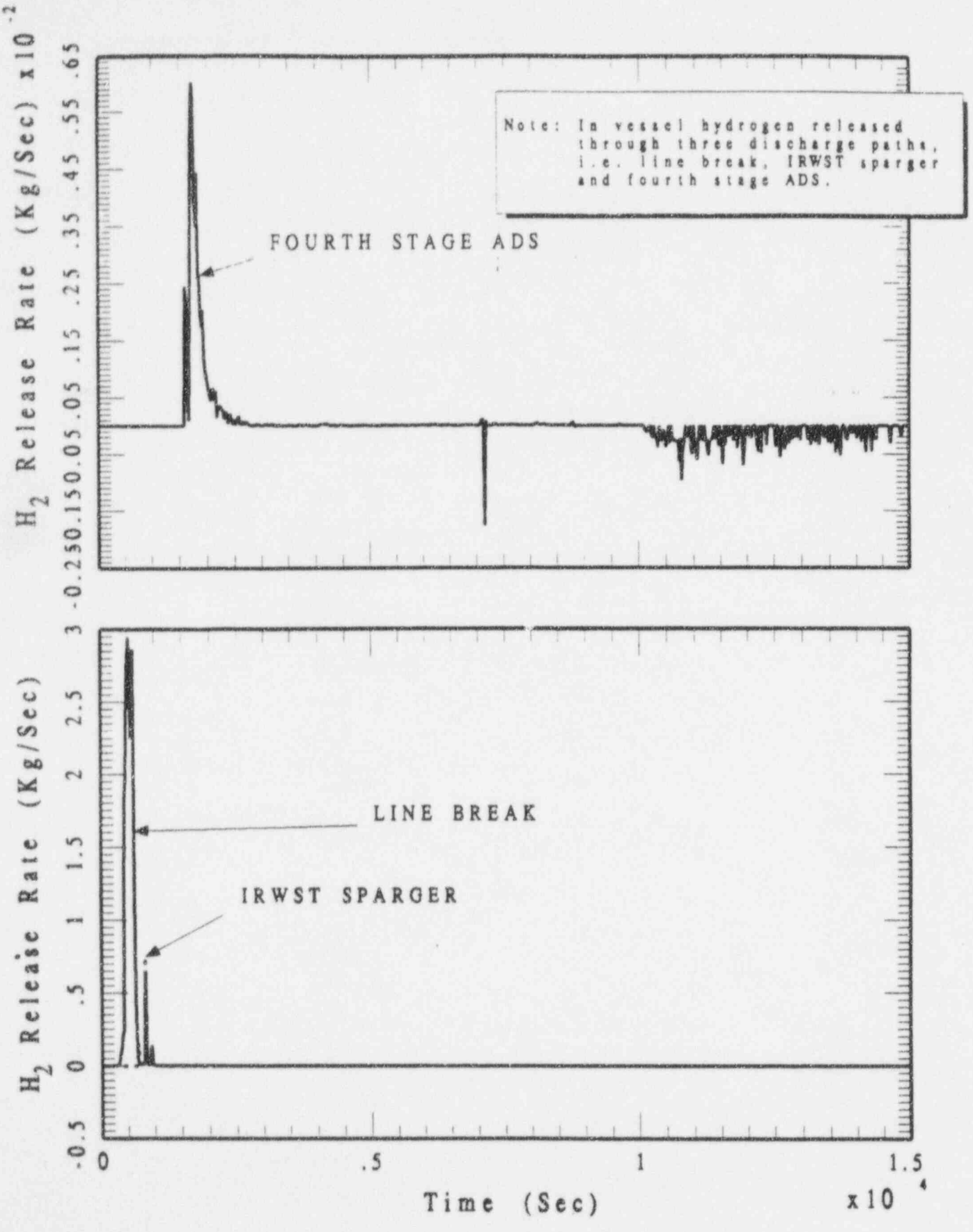


Figure 6 Hydrogen Release History for 3BR-FR1* Sequence.

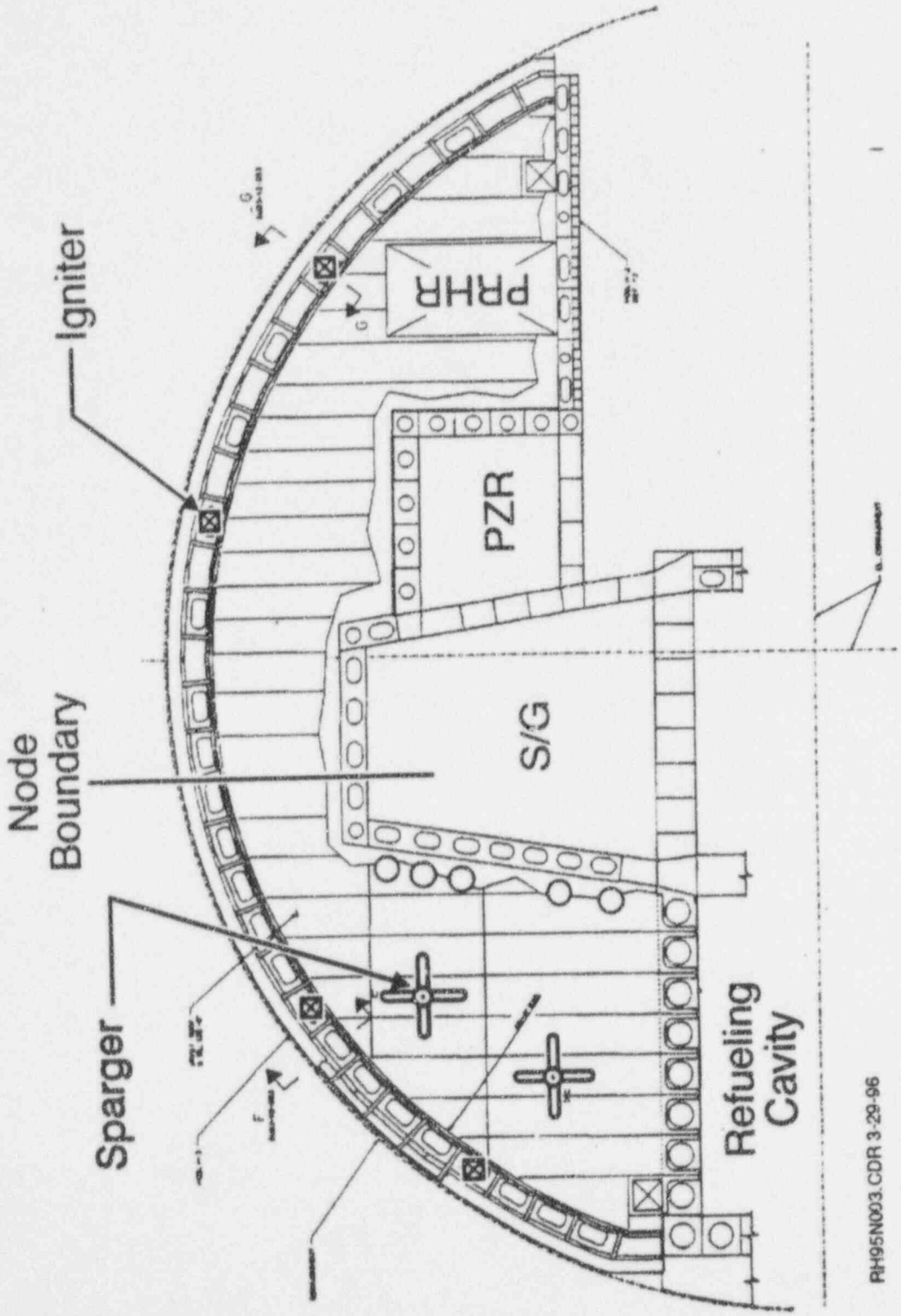


Figure 7 IRWST Cross-Section with Sparger and Igniter Locations.

Table 2

IRWST Vent Configuration

| Vent | Type | Location | Number | Size | Total Area |
|---|---|---|---|---|---|
| Outer wall | IRWST roof | sparger side | 12 | .9 m (3′) x .45 m (1.5′)(1) | 4.5 $m^2$ (48.9 $ft^2$) |
| | | behind SG | 4 | .9 m (3′) x .45 m (1.5′)(1) | 1.5 $m^2$ (16.3 $ft^2$) |
| | | PRHR side | 5(3) | .9 m (3′) x .45 m (1.5′)(1) | 1.9 $m^2$ (20.4 $ft^2$)(3) |
| SG wall | IRWST roof | SG wall | 5 | 0.6 m (2′) pipe(2) | 1.3 $m^2$ (14.4 $ft^2$) |
| | | | | | 9.3 $m^2$ (100.0 $ft^2$) |

Notes:

(1) Actual opening is 35″ x 17″ with 6″ radius corners.

(2) 0.6 m (24″) pipe schedule XXS has .58 m (23″) ID.

(3) Note that there are 7 vents on the PRHR side of the IRWST, however 2 of them are being reserved for venting from the containment back into the IRWST to prevent implosion of the IRWST during a LOCA or SLB and as a result will not be available for venting out of the IRWST.

and the IRWST gas space during normal plant operation. The lowest point of the containment wall vent's discharge is 15 cm(6 inches) above the operating deck, which is intended to prevent water on the operating deck from draining back into the IRWST through the vents.

The vents along the steam generator wall are also located in the roof of the IRWST next to that wall. The vents run straight up through the roof of the IRWST. Flow through the steam generator wall vents discharges vertically through hinged flaps. These vents also discharge 15 cm (6 in) above the operating deck elevation.

The IRWST gas space is connected to the refueling cavity by large overflow openings. A total of six rectangular weir openings each 0.38 m (1.25 ft) high and 0.91 m (3 ft) wide (2.1 $m^2$ or 22.5 $ft^2$ total area) are provided in the IRWST design. Each overflow runs straight through the wall between the IRWST and the refueling cavity. Single or multiple flaps will be provided on each overflow opening to prevent significant exchange of air between the IRWST and the containment during normal operation.

The existence of the flappers on each of the IRWST vent paths to prevent mixing with the air in the rest of the containment regions also impacts the diffusion flame assessment. The availability of the various gas flow paths between the IRWST gas space and the balance of the containment regions depends upon the relative differential pressures which influence whether the flow path (flapper) is open or closed.

Considerations of the IRWST geometry and the referenced vent design which prevents mixing during normal operation were used to produce a revised model for use in MAAP4 to perform the diffusion flame assessment for the IRWST vents. The MAAP4 representation of the AP600 includes two nodes for the IRWST and additional junctions such that the assessment included the effects of the flappers. Figure 8 describes the IRWST nodalization and flow junctions. The circled numbers in Figure 8 identify the containment regions as labeled in the figure. The arrows connecting the different containment nodes have arrow heads to represent if two-directional flow is possible or only one-directional flow due to the behavior of the flapper valves. Junction 25 represents the two vents on the PRHR side of the IRWST used to vent from the containment back into the IRWST.

Figure 9 depicts the floor plan for the core makeup tank (CMT) room floor which is at elevation 107' 2" in the AP600 containment. The CMT floor is one level below the operating deck. The two geometrically independent dead-end valve vault rooms are beneath the CMT floor. Each valve vault room has a grating covered opening in its ceiling which is the only gas flow path to or from the valve vaults. Each valve vault room contains a direct vessel injection (DVI) line

| No. | Description | Total Area ($m^2$) | No. of Vents | Vent Dimensions | Hydraulic Diameter (m) | $\Delta P_{open}$ $\Delta P_{close}$ (Pa) |
|---|---|---|---|---|---|---|
| Junction #8 | IRWST overflow | 2.09 | 6 | 3' x 1.25' | 0.54 | 500<br>499 |
| Junction #16 | IRWST vents on sparger side | 4.52 | 12 | 3' x 1.5'<br>(3' x 2.75')* | 0.61** | 271.6<br>100 |
| Junction #22 | Connecting middle passage to PRHR side | 27.45 | --- | --- | --- | --- |
| Junction #23 | IRWST vents on PRHR side | 1.895 | 5 | 3' x 1.5'<br>(3' x 2.75')* | 0.611** | 271.6<br>100 |
| Junction #24 | Connecting sparger side to middle passage | 34.45 | --- | --- | --- | --- |
| Junction #25 | IRWST back-vents | 0.757 | 2 | 3' x 1.5' | --- | --- |
| Junction #26 | 24" pipe vents | 1.337 | 5 | 23" ID | 0.584 | 135.8<br>50 |
| Junction #27 | IRWST vents middle narrow passage | 1.5 | 4 | 3' x 1.5'<br>(3' x 2.75')* | 0.61** | 271.6<br>100 |

*Total flapper area per vent
**Based on fully opened area of flaps at each vent

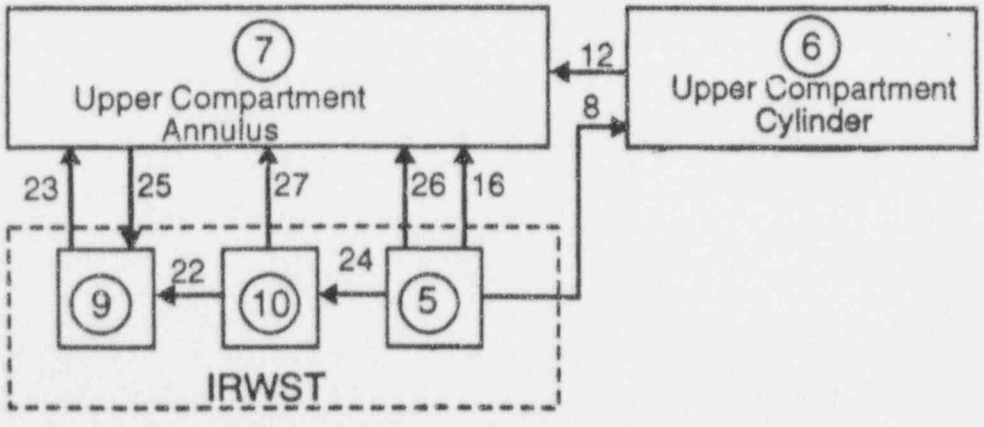


Figure 8 Three region nodalization of the IRWST and flow junctions.

and its isolation valves which separate the IRWST from the RPV downcomer. For a DVI line break between the RPV and these isolation valves, in-vessel hydrogen and steam could be released to the valve vault room. If the DVI line isolation valves are closed the valve vault room would not be flooded, yet if they are opened, the valve vault room would be flooded and the DVI line break elevation submerged.

Figure 9 identifies the location and dimensions of valve vault room exits. The north valve vault room exit location has a direct line of sight to the containment wall and several electrical penetrations. It does not have a direct line of sight to either the equipment or personnel hatches. The south valve vault room exit orientation and location has only a limited view of the local containment wall. The close proximity of the CMT, which is approximately 6.4 m (21 ft) tall, and the refueling cavity wall greatly inhibit this exit's view of the containment wall. However, although the south exit is significantly displaced from the equipment and personnel hatches, it does have a direct line of sight to them. The electrical penetrations are not in the south exit's direct line of sight. This geometry is considered in the evaluation of the thermal response of the containment wall and penetrations to a standing diffusion flame at either valve vault room exit.

The containment nodalization used in MAAP4 to assess the potential for producing a standing diffusion flame on the CMT floor at either valve vault room exit used a separate node for the valve vault room. It also used a single node model for the IRWST as the more detailed two node model described above was not necessary. This containment model was used to calculate its temperature and pressure responses, the flow rates between containment regions and subcompartments, and the gas concentrations in the containment regions.

## 5.0 DIFFUSION FLAME ASSESSMENT

The three stage ADS analysis represents the worst case scenario for potential existence of diffusion flames at the IRWST vents as it involves a release of all in-core hydrogen into the IRWST through the first three stages of ADS valves. In the expanded analysis, besides being released into the IRWST, hydrogen was also released directly into the containment through the fourth stage ADS. With an actuation of the fourth stage ADS, while the sparger is still submerged (3BE-FRF1 and 3BE-FN1) there was no likelihood of substantial build-up of hydrogen in the IRWST that may lead to potential existence of diffusion flames at the IRWST vents. If the sparger is uncovered due to IRWST draining (3BL-FN), moderately high concentrations of hydrogen and very high concentrations of steam may exist in the IRWST, whose conditions are unlikely to lead to potential existence of diffusion flames at the IRWST vents. The expanded analysis also shows that when the fourth stage ADS was not yet actuated

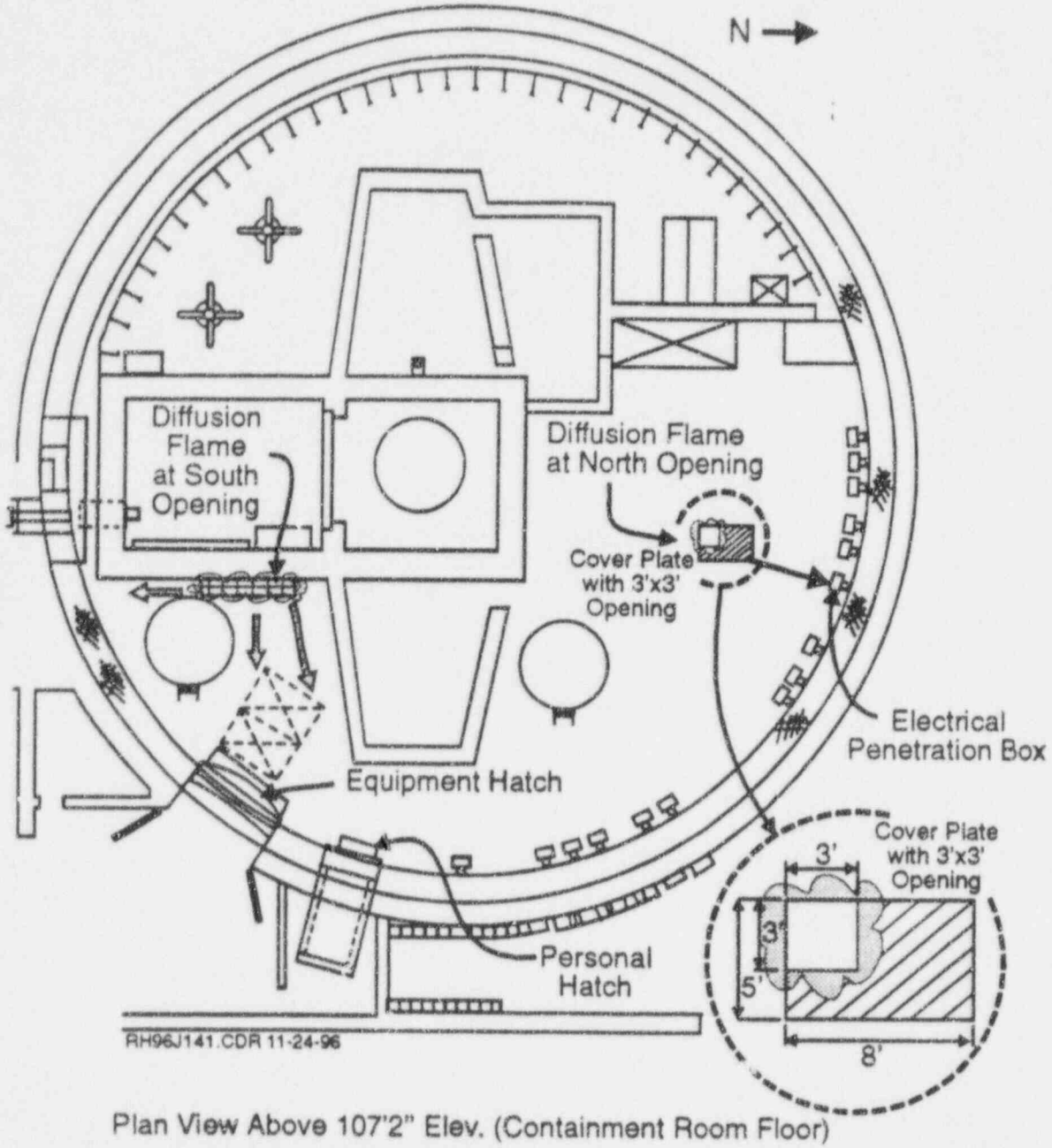


Plan View Above 107'2" Elev. (Containment Room Floor)

**Note:** Dimensions of south valve vault exit are 3 x 15 ft.

Figure 9 Plan View of CMT Room Floor.

during a hydrogen release (3BR-FR1 and 3BR-FR1*) the large break itself was enough to prevent hydrogen buildup in the IRWST.

## 5.1 IRWST Vents and Overflow Openings

The MAAP4 code with the two node IRWST model was used to quantify the hydrogen generation for the three stage ADS scenario and assess the potential and characteristics of diffusion flames which could be formed at the IRWST vents and overflow openings. Only scenarios involving the operation of first three ADS stages (no ADS stage four) could release a significant amount of hydrogen into the IRWST and have the potential of producing standing diffusion flames at the IRWST exits. The three stage ADS scenario was analyzed to determine the duration and height of standing diffusion flames at the IRWST exits.

The MAAP4 three stage ADS analysis showed that the diffusion flame criteria were satisfied inside the IRWST such that diffusion flames on the pool surface were briefly maintained while the oxygen in the IRWST was depleted. During the interval of the standing diffusion flame within the IRWST the hydrogen concentrations remained relatively high as they were in the range of 36 to 55%. The diffusion flame burning rate is limited by the availability of oxygen in the IRWST. The rate of oxygen being admitted to the IRWST through the existing venting configuration was found to be far less than the hydrogen release rate. The unburned and highly concentrated hydrogen then flowed out through the IRWST vents and overflow openings. The oxygen supply in the balance of containment (outside of the IRWST gas space) was sufficient to support the burning of the high concentration hydrogen streams such that diffusion flames burning at the operating deck level at the IRWST vent exits and overflow exits are considered possible. Thus, the thermal impact of standing diffusion flames was quantified.

The MAAP4 analyses were used to determine the diffusion flame heights at the vent exits and overflow openings and the duration of the respective standing diffusion flames. The height of the diffusion flame anchored at these openings was used to assess the radiation view factors and estimate the size of the affected region of the containment shell above the operating deck.

The correlation for the diffusion flame height was selected from the literature and incorporated in the MAAP4 code for these assessments.

$$\frac{H}{D} = a\, Q^{*} \qquad (5\text{-}1)$$

In this equation, H is the flame height (m), D is the hydraulic diameter (m) of the source gas

(in this case, the size of the vent), and $Q^*$ is a dimensionless heat release rate which is defined as

$$Q^* = \frac{Q}{\rho_\infty C_p T_\infty \sqrt{gD}\, D^2} \qquad (5\text{-}2)$$

where

$\rho_\infty$ is the density ($kg/m^3$) of gas in containment,

$C_p$ is the heat capacity (J/kg·K) of gas in containment,

$T_\infty$ is the temperature (K) of gas in containment,

g is the gravitational acceleration ($m/sec^2$),

and

Q is the heat release rate (w).

Among several applicable flame height correlations, we select the one which gives the highest flame height as a conservative approach, i. e., a = 4.16 and b = 0.4 (Steward, 1970). The correlation is applicable for a range of $1 < Q^* < 10^4$. A typical $Q^*$ value for the AP600 condition is about 2 for a vent flowrate of 2 kg/s, with 5% $H_2$ mass fraction from a 0.6 m diameter vent. The MAAP4 model used the time dependent vent flow rates and hydrogen mass fractions to calculate $Q^*$ variations and the concomitant flame height variations.

The flame height is proportional to the junction flow rate and the hydrogen concentration inside the IRWST. Both of these parameters are dependent upon the model selected to describe the junction (flapper) behavior. A variety of models were considered to assess this sensitivity and attempt to bound the standing diffusion flame heights. The bounding standing diffusion flame heights and durations from these sensitivity assessments were selected for further analysis and are included in the summary table presented in Section 6.

One additional result obtained from the MAAP4 analyses was the differential pressure produced in the IRWST during the hydrogen burn. The peak differential pressure calculated during a burn inside the IRWST for the IRWST roof was 0.73 psid and the peak differential pressure on the wall between the IRWST gas space and refueling cavity was also calculated as 0.73 psid. These differential pressures act outward from the IRWST gas space to the adjacent containment regions.

### 5.2 Valve Vault Room Exits

The MAAP4 code was used to quantify the hydrogen generation for the DVI line break cases (3BE-FRF1 and 3BE-FN1) and assess the potential and characteristics of standing diffusion flames which could be formed at the valve vault room ceiling exits.

The results for the DVI line break which is submerged by IRWST draining (3BE-FRF1) indicates that high hydrogen concentrations are produced in the valve vault room gas space. The steam that escapes the primary system with the hydrogen is condensed in the flooded cavity. The oxygen concentration in the valve vault room is too low to support combustion in that room. Thus, the composition of the gas mixture which exits the valve vault room could support a standing diffusion flame given an ignition source on the CMT floor.

The MAAP4 analyses were used to determine the diffusion flame heights at the ceiling exit and the duration of the various diffusion flame heights. The flame heights and exit locations were used to assess radiation view factors for the closest section of the containment wall, the closest electrical penetration and the equipment and personnel hatches. These results were used in a separate thermal assessment for each of these four items.

## 6.0 CONTAINMENT BOUNDARY RESPONSE

### 6.1 Containment Wall Thermal Response

Localized heating of the containment shell above the operating deck elevation by standing diffusion flames at the IRWST vents or overflow opening as illustrated in Figures 10 and 11 are assessed. The objective is to assess the physical extent of the affected zone of the containment shell and the maximum wall temperature produced by a standing diffusion flame. It should be noted that standing diffusion flames formed on the CMT floor at the valve vault room exits are further from the containment wall than those at the IRWST vents. Thus, they result in lower wall temperatures as discussed below. The IRWST vent assessment is accomplished by performing the following steps:

- Assess the diffusion flame temperature and height.
- Assess the induced (entrained) air velocity in the vicinity of the diffusion flame and containment wall.
- Quantify the convective heat transfer from the diffusion flame to the containment wall.

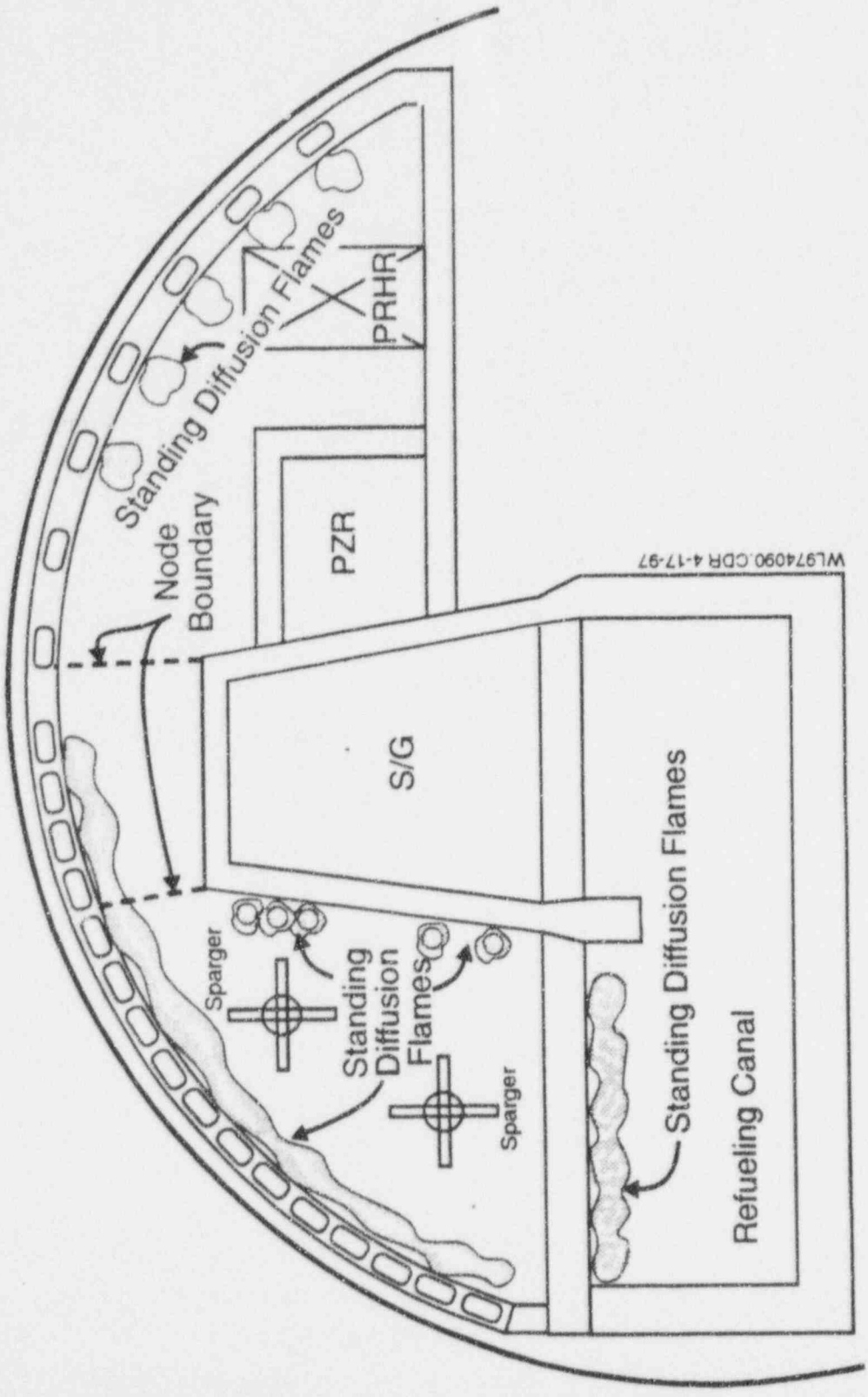


Figure 10 Locations of standing diffusion flames on IRWST vents and overflows.

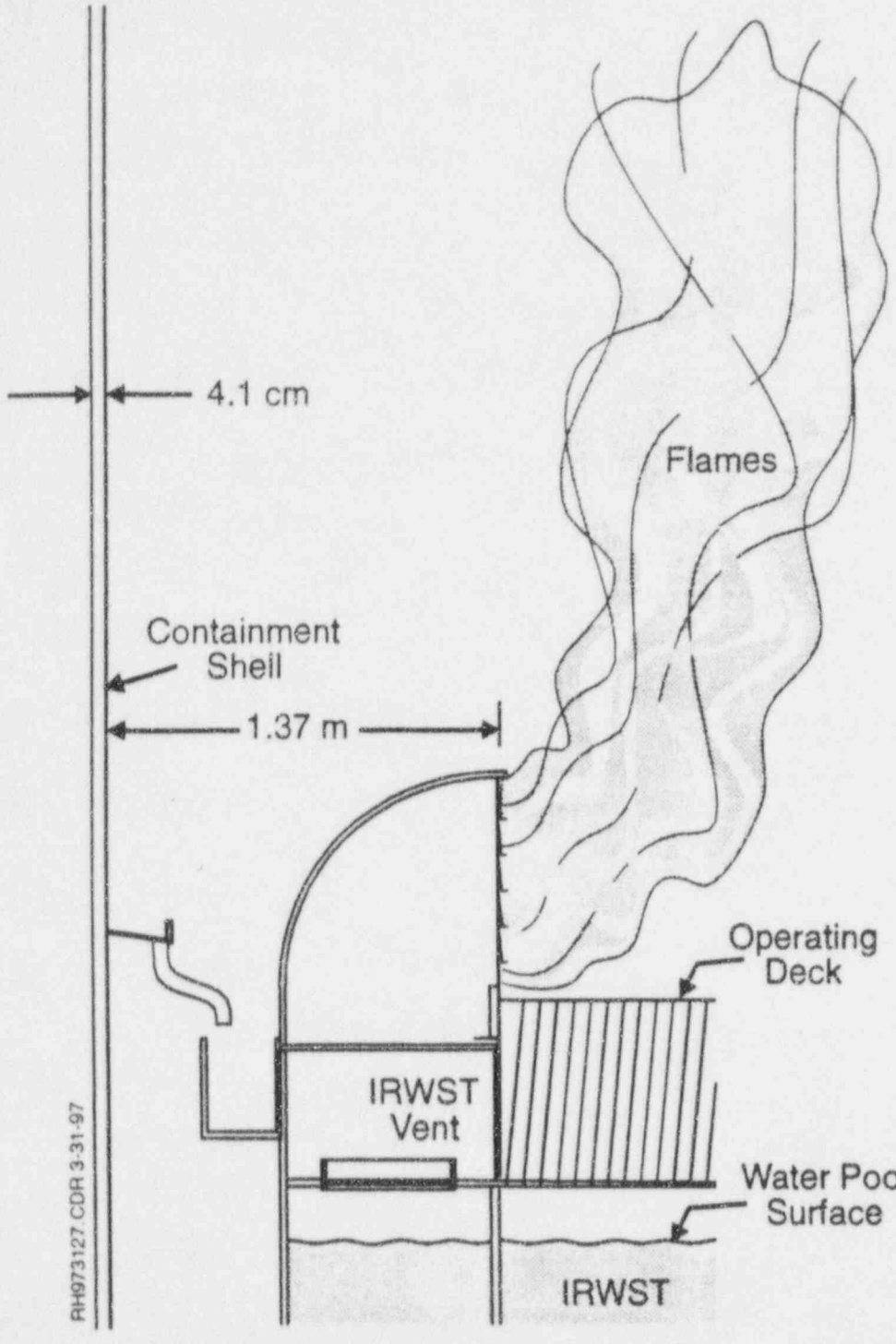


Figure 11 Localized heating of containment shell by standing diffusion flames on IRWST vents.

- Quantify the radiative heat transfer from the diffusion flame to the containment wall.
- Quantify the number of vents participating to define the azimuthal extent of the localized heating.

The diffusion flame temperature is assessed from fire plume data. Measurements of centerline values of mean excess temperature $\Delta T_o$ in fire plumes irrespective of the fuel type and size have been found to obey the following relation (Heskestad, 1988)

$$\Delta T_o = 910 \left( \frac{T_\infty}{g\, C_p^2\, \rho_\infty^2} \right)^{1/3} \xi^{-\frac{5}{3}} \qquad (6\text{-}1)$$

with

$$\xi = \frac{z - z_o}{\left( \frac{Q_c}{1000} \right)^{0.4}} \qquad (6\text{-}2)$$

where

$\Delta T_o$ is a centerline mean temperature (K) minus $T_\infty$,

$T_\infty$ is an ambient temperature (K) (in this case the containment gas temperature),

$\rho_\infty$ is the containment gas density ($kg/m^3$),

$Q_c$ is a convective heat rate [w] (assume 80% of the total reaction heat rate Q),

$z$ is elevation [m],

$z_o$ is virtual origin of the flame that can be calculated from

$$z_o = 1.02D + 0.83 \left( \frac{Q}{1000} \right)^{2/5} \qquad (6\text{-}3)$$

The plot of Eq. (6-1) is a straight line with a slope of -5/3 as shown in Figure 12. The plateau on the left side of the plot occurs when $\xi < 0.1$ which indicates that the temperature does not change significantly in that region.

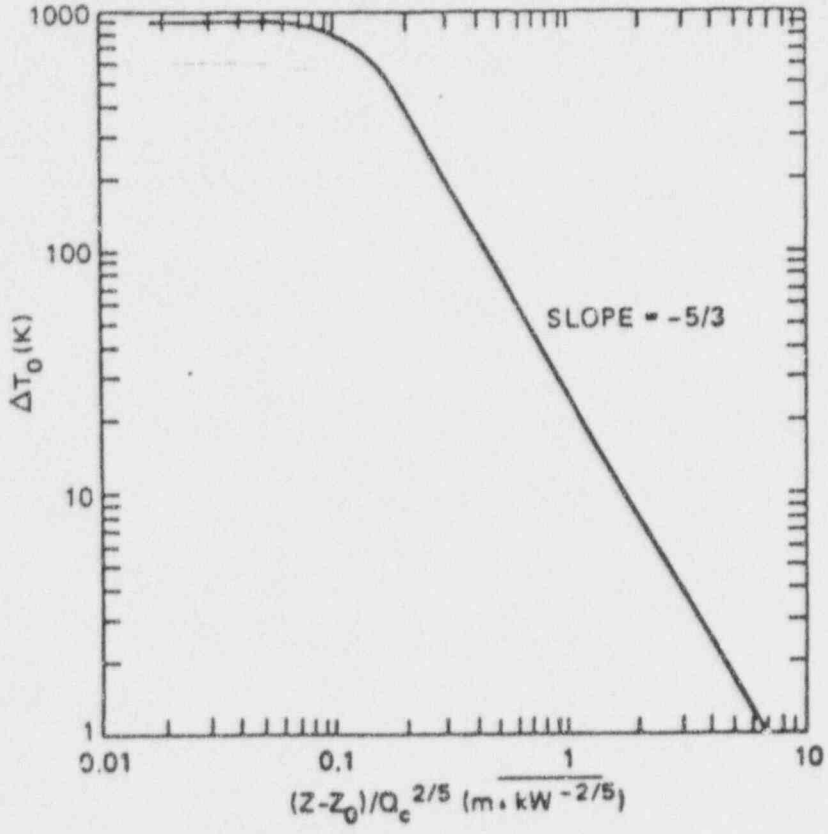


Figure 12 Correlation of centerline mean excess temperature in fire plumes as a function of elevation.

Substituting Eq. (6-3) for $z_o$ in Eq. (6-2) yields

$$\xi = \frac{1}{Q_c^{0.4}} \left[ z - 1.02D - 0.83 \left( \frac{Q}{1000} \right)^{2/5} \right] \qquad (6\text{-}4)$$

For an AP600 value of Q = 0.55 x $10^6$ W, and a flame height in the range of 1 - 2.6 m, the corresponding value of $\xi$ is from 0.05 to 0.1. Therefore, from Figure 12, the centerline mean excess temperature of the AP600 diffusion flames is about 900 K (1620°F) for the height range being considered. It is conservative to assume that the diffusion flames are uniformly at a temperature of 900 K (1620°F) above the containment temperature for heat transfer analysis in the following section.

A transient heat transfer model was developed based on the above steps and used to calculate the energy exchange between the diffusion flame, containment wall, PCCS baffle, and surrounding concrete structure (see Appendix B for details). Energy was transferred to the containment wall by radiation and convection due to the diffusion flame and its thermal plume. Radiation between the heated portion of the containment wall, baffle plate and surrounding concrete structure were quantified. Additionally, convective cooling due to air flow through the PCCS flow passages was calculated for the outer surface of the containment shell, both sides of the baffle, and the inner surface of the surrounding concrete structure. The basic assumptions that were made to construct this energy balance are:

a. A series of time intervals were used to represent the transient flame height. A constant flame height was used for each interval. The thermal conditions reached at the end of each interval were used as the initial conditions for the next time interval.

b. A uniform flame temperature is applied for the entire calculated flame height. Experimental results demonstrate that the flame temperature actually starts to decay for heights above the continuous flame. The flame height correlations are for the flame tips which exceed the height of the continuous flame.

c. No credit for water films is included on the inner or outer surface of the containment wall. This precludes the concern about the degree of wetting on the outer surface by the passive spray included in the PCCS. The likelihood of a water film on the inner surface due to steam condensation on the containment shell is high. Detailed transient calculations should include vaporization of the water film when assessing the containment's temperature response.

d. Only one-dimensional conduction in the containment wall is modeled. Multi-dimensional conduction and the flow of energy to regions of the containment shell that are not significantly heated by the local diffusion flame have not been explicitly quantified.

Two flame height profiles are assessed for the IRWST exits. The first addresses flames near the containment shell standing at the IRWST vents and the other profile shows flames produced by diffusion flames standing at the overflow openings (see Figure 10). The azimuthal extent of the multiple diffusion flames standing on the IRWST exits is significantly larger than that for the localized heating due to standing diffusion flames on the overflow openings.

The results for this assessment indicate that a global flow pattern is established in the upper containment region, down into the IRWST node without the spargers, into the IRWST gas space region with the spargers and back through vents in that region into the upper compartment. Burns are predicted to occur in the IRWST until the oxygen concentration is reduced such that combustion can not be supported within the IRWST gas space. This reduced oxygen condition occurs despite the global flow through the IRWST gas space and its limited ability to resupply oxygen through the vents on the PRHR side of the IRWST. The diffusion flame temperature was found to be 1350°K (1970°F). The hot spot temperatures for the containment shell local to the standing diffusion flames at the IRWST vents are summarized in Table 3. The results are shown to be dependent on the calculated peak flame height that has been associated with each of the intervals listed in the table. Hydrogen burns (standing diffusion flame) occurred over a total interval of approximately 5000 sec during which time the containment pressure was approximately 1.5 bar (22 psi) (absolute). A higher containment pressure of 2.2 bar (32 psi) (absolute) was calculated during a global deflagration in the upper containment prior to this diffusion flame interval and its concomitant localized containment wall temperature. However, no local wall heating (hot spot) existed during the global burn.

As mentioned above, the thermal response of the containment wall for the CMT floor elevation was assessed for a standing diffusion flame at either valve vault room exit. Essentially the same approach as outlined above for the IRWST exits was employed for diffusion flames on the CMT floor. However, the boundary condition of the containment wall's outer surface is different at this lower containment elevation. The PCS annulus does not extend down to this elevation. The different geometry was included in the heat transfer model. Again, a transient calculation was performed. The diffusion flame height and duration for a DVI line break was quantified and used to assess the thermal response of the containment wall and its penetrations at this plant elevation. The view factor for the radiation heat flux for the part of the containment wall closest to a diffusion flame on the CMT floor is smaller than that for the wall adjacent to the IRWST

Table 3 Calculated Hot Spot Containment Shell Temperature
Above Operating Desk Local to IRWST Vents

| Interval Duration (sec) | Flame Height (m/ft) | Average [1][2] Hot Spot Temperature (K/R) |
|---|---|---|
| 200 | 1.5/4.9 | 412/742 |
| 400 | 1.7/5.6 | 503/905 |
| 900 | 1.6/5.2 | 639/1150 |
| 500 | 1.5/4.9 | 741/1330 |
| 400 | 1.7/5.6 | 785/1410 |
| 200 | 1.1/3.6 | 803/1450 |
| 200 | 2.3/7.5 | 817/1470 |
| 300 | 1.5/4.9 | 834/1500 |
| 400 | 1.2/3.9 | 837/1510 |
| 900 | 1.1/3.6 | 835/1510 |
| 400 | 3.3/10.8 | 872/1570 |
| 100 | 1.6/5.2 | 902/1620 |
| 100 | 1.0/3.3 | 899/1620 |
| 200 | 1.6/5.2 | 898/1620 |
| 200 | 0.8/2.6 | 891/1600 |
| 2200 | 0.4/3.0 | 816/1470 |
| 400 | 1.0/3.3 | 798/1440 |

(1) Time averaged temperature for each interval.
(2) The average hot spot temperature for flames standing at the overflow vents are lower due to the geometric effects of the further displacement between those flames and the containment wall and the orientation of those flames (see Figure 10).

vents. The smaller view factors are due to the different geometric arrangement on the CMTfloor and the larger displacements between either diffusion flame location and the different containment boundary components. The peak calculated containment shell temperature for the CMT elevation is 417°K (291°F) (see Table 4). This result is bounded by the IRWST vent diffusion flame result (see Table 3).

### 6.2 Containment Wall Structural Response

Membrane tension at temperature will be the controlling loading condition of interest for considering the impact of a localized hot spot in the containment wall due to standing diffusion flames. A simple hoop stress expression (Pr/t) is a sufficient means of estimating the wall's response for the membrane tension.

In practice some strain could readily be tolerated without failure of the containment wall. The possibility of creep of the containment wall due to an extended exposure to high temperature and wall stress was reviewed. The general approach used in MAAP4 based on the Larson-Miller formulation was reviewed and felt to be reasonable for application to the containment wall. If a wall temperature of 930°K (1210°F) is assumed for an AP600 containment loading of 1.5 bar (22 psi absolute) and, using a Larson-Miller parameter of thirty-four, the time required to induce creep failure is approximately 2 hours. The Larson-Miller parameter (LMP) of thirty-four applies for low carbon steel. Other carbon steels are known to have larger LMPs such as thirty-six to thirty-seven at similar stress levels. A LMP value of thirty-seven would imply a creep failure time of approximately 130 hours. Thus, some margin appears to exist in the 2 hr estimate that assumes low carbon steel. The anticipated duration of a hydrogen diffusion flame at the IRWST vents producing such a 930°K (1210°F) containment shell hot spot temperature is less than 0.3 hours. Thus, when the estimated high local containment wall temperature is applied for its calculated interval shell failure would not be expected by the creep mechanism. The calculated thermal response of the containment shell adjacent to the outboard IRWST vents near the ADS spargers could produce this limiting condition. The calculated thermal response of the containment shell due to standing diffusion flames at the IRWST overflow openings is much lower (600°K) (620°F) and the time required to induce creep failure is very long, i.e., practically infinite since the material's strength is essentially not diminished at that temperature.

Table 4 Peak Containment Shell and Penetrations Temperatures on CMT Floor

A. Standing Diffusion Flame at North Valve Vault Room Exit[1]

| Duration (sec) | Flame Height (m/ft)[2] | Hot Spot Temperature (K/F)[3] Containment Shell | Electrical[4] Penetration |
|---|---|---|---|
| 300 | 6.5/21.3 | 396/253 | 423/301 |
| 300 | 4.8/15.7 | 401/262 | 446/343 |
| 300 | 4.4/14.4 | 404/267 | 457/363 |
| 550 | 0 | 403/265 | 439/330 |
| 450 | 6.2/20.3 | 412/282 | 468/382 |
| 450 | 4.2/13.8 | 417/291 | 474/393 |

B. Standing Diffusion Flame at South Valve Vault Room Exit

| Duration (sec) | Flame Height (m/ft)[2] | Hot Spot Temperature (K/F)[3] Containment Shell | Personnel Hatch | Equipment Hatch |
|---|---|---|---|---|
| 300 | 5.9/19.4 | 396/253 | 395/251 | 407/273 |
| 300 | 4.2/13.8 | 401/262 | 397/255 | 418/292 |
| 300 | 2.8/9.2 | 403/265 | 398/256 | 424/303 |
| 550 | 0 | 401/262 | 395/251 | 420/296 |
| 450 | 5.3/17.4 | 409/276 | 401/262 | 440/332 |
| 450 | 2.9/9.5 | 412/282 | 402/264 | 448/346 |

[1]Exit covered with plate so partial opening of 3 x 3 ft at southwest corner.
[2]Flame temperature taken as 1385°K (2030°F) for all thermal assessments.
[3]Peak temperature at the end of each of the six sequential intervals.
[4]Temperature of air trapped within penetration enclosure.

Predicated on this consideration of the controlling structural loading mechanisms and the thermal loading produced by a standing diffusion flame, the definition for the heat affected zone of the containment wall due to hydrogen flames standing on the IRWST vent exit is as follows:

1. The extent of the high temperature region for the containment wall local to the IRWST vents (see Region Ⓐ of Figure 13 and Figure 14) can be approximated by a zone 2.6 m (8.5 ft) high with a 60° arc of the containment wall circumference. The extent of the high temperature region for the containment wall local to the overflow openings can be approximated by a zone 7.8 m (25.6 ft) high with a 3° arc of the containment wall circumference (see Region Ⓑ of Figure 13).

2. The temperature of the affected zone should be viewed as uniform in the azimuthal direction over the entire 60° (Region Ⓐ) and 3° (Region Ⓑ) arcs.

3. The vertical temperature distribution for each affected zone varies linearly by approximately 90°K (160°F). However, a first approximation can conservatively apply the hot spot temperature for the entire heat affected zone.

The calculated thermal response of the containment shell for CMT floor elevation (107′ 2″) is lower (412°K/282°F) than either result for the IRWST diffusion flames. Thus, the time required to induce creep failure of the containment shell at this plant elevation by diffusion flame heating is also very much longer than the loading condition interval. The bounding containment shell loading condition due to a local hot spot is produced by a standing diffusion flame at the IRWST vents.

### 6.3 Equipment and Personnel Hatches Thermal Responses

The heating of the equipment and personnel hatches by a standing diffusion flame at the south valve vault room was quantified. A simple model of each hatch was constructed to perform a transient lumped heat balance for each hatch and the air enclosed within them (see Appendix B for details). Heat loss to the auxiliary building was not modeled. The peak temperature calculated for the equipment hatch was 448°K (346°F) and for the personnel hatch was 402°K (264°F).

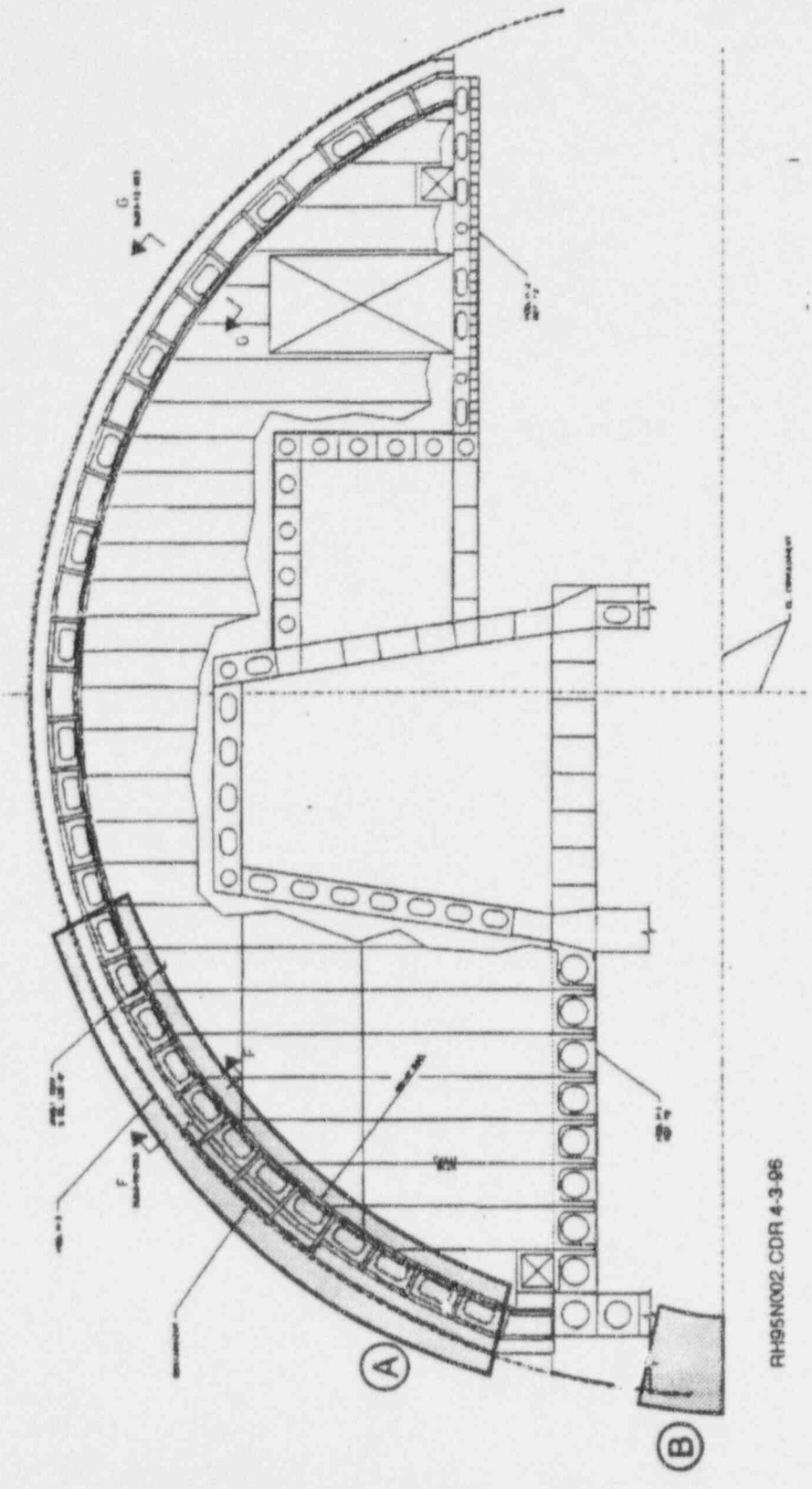


Figure 13 Azimuthal Extent of High Temperature Zone of Containment Wall ( Ⓐ opposite IRWST vents and Ⓑ opposite overflow opening).

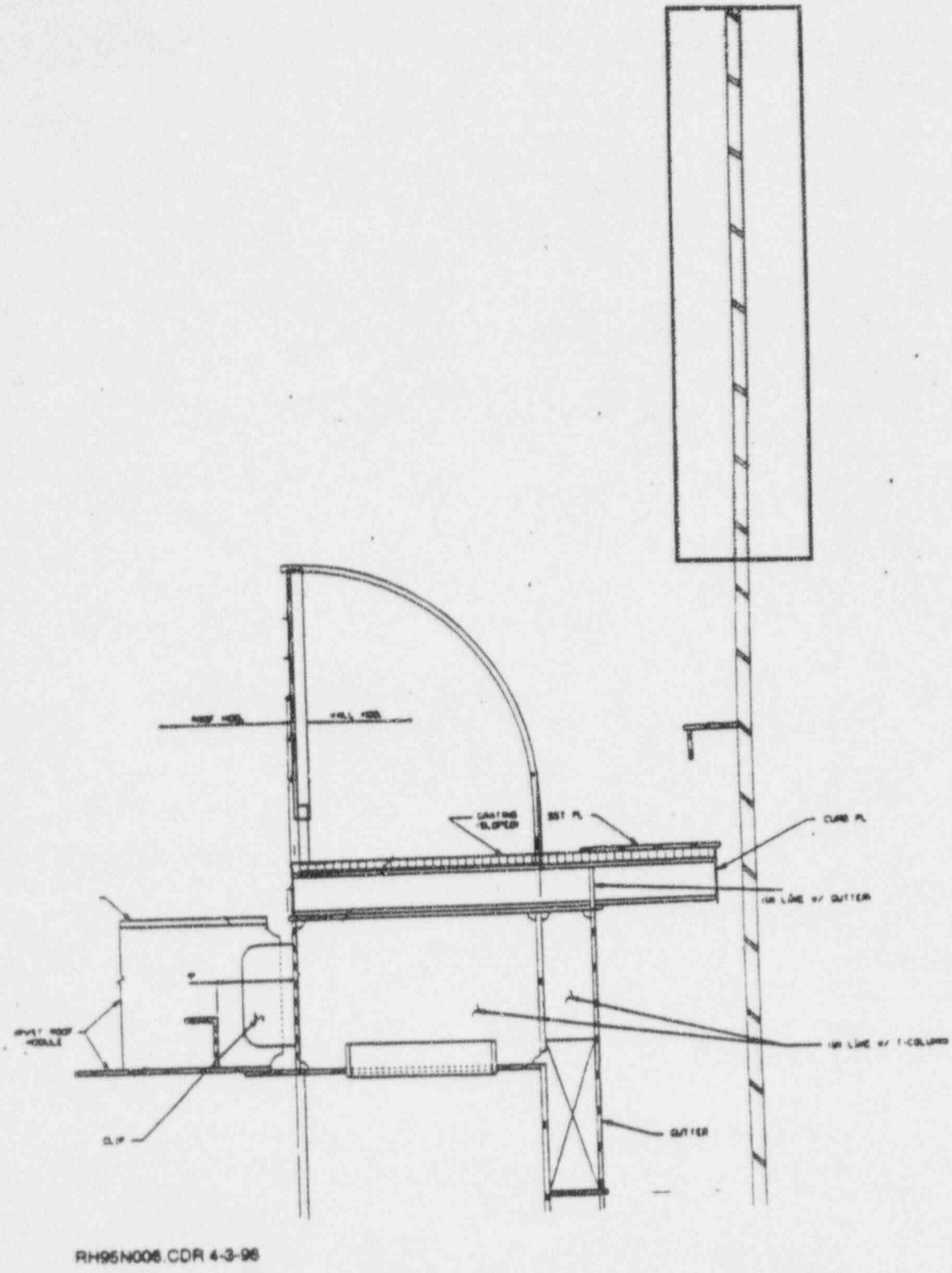


Figure 14 Vertical Extent of High Temperature Zone of Containment Wall.

## 6.4 Electrical Penetration Thermal Response

The heating of the electrical penetration closest to the north valve vault room was quantified. This single calculation was selected to represent the bounding effect of a standing diffusion flame on all the electrical penetrations. This provides significant margin in the calculated peak temperature for those electrical penetrations that are further from the valve vault room exit. A simple model was used to perform a transient lumped heat balance for a penetration enclosure and the air enclosed within it (see Appendix B for details). The thermal response of the electrical penetration internals and sealing material was not assessed. The back wall of the penetration enclosure was assumed to be at the local containment wall hot spot temperature. No heat loss to the auxiliary building was modeled. The peak temperature calculated for the air in the penetration enclosure was 474°K (393°F).

# 7.0 SUMMARY

The issue of potential standing diffusion flames at the IRWST exits producing locally high temperatures on the containment boundary were identified for evaluation. An evaluation of the potential impact on the containment boundary integrity during severe accidents was conducted. A three stage ADS sequence was defined to evaluate the impact of the IRWST vent configuration including the flappers on standing diffusion flames. The three stage ADS scenario was taken as a loss of feedwater transient with system failures leading to a severe accident with large hydrogen release rates and inventories. This sequence only involved the first three stages of the ADS system and assumed the complete failure of the fourth stage ADS. These stages all discharge through spargers submerged in the IRWST water pool. It is important to note that the failure frequency of the 4th stage ADS is very low ($10^{-8}$ per year). Under most circumstances the 4th stage ADS will be actuated. When the 4th stage ADS is actuated, most hydrogen would bypass the IRWST and be directly released to the containment. The level of hydrogen buildup in the IRWST would be much lower and unlikely to support any standing flames.

The assessment of this three stage ADS indicated that there is a potential for producing standing diffusion flames. The height and temperature of the standing diffusion flames were used to perform a thermal assessment of the local containment shell. The degree of containment shell heating was quantified and based on the coincident wall stresses due to containment pressurization for the transient interval of localized shell heating; it was estimated that the containment shell would survive. A material creep assessment based on the Larson-Miller parameter for containment steel was used to make this determination for these severe accident conditions. Thus, based on mechanistic rather than probabilistic arguments the bounding three

stage ADS assessment concluded that the containment shell would survive the effect of localized heating due to a standing diffusion flame at the IRWST exits.

Subsequently, an expanded set of accident sequences have been used to further evaluate the potential for diffusion flames locally heating the containment boundary. The expanded set of sequences include all four stages of the ADS valves and the operation of the IRWST drain line. The fourth stage ADS flow path does not pass through the IRWST, but discharges from the primary system (hot leg) directly to the steam generator compartments which directly communicate with the upper containment region. For sequences with the fourth stage effective, unlike the base case with only the first three stages of ADS considered, standing diffusion flames at the IRWST vent exits are not produced. The rate of hydrogen inflow to the IRWST through the spargers is reduced due to the availability of the fourth stage ADS valves or large LOCAs in the RCS piping and their direct path from the primary system to the steam generator compartments. This flow path has less flow restrictions and, therefore, the majority of the flow from the primary system is to the steam generator compartment. The reduction of the hydrogen inflow to the IRWST is sufficient to prevent the formation of standing diffusion flames at its exit for this family of severe accident sequences.

The expanded set of sequences included LOCAs produced by a break in the direct vessel injection (DVI) lines. A DVI line is located in each of the valve vault rooms which are dead-end compartments with a single flow path in their ceilings. This flow path connects the vault rooms to the CMT floor which is at elevation 107′ - 2″. The potential for forming standing diffusion flames at each of the valve vault room exits following a DVI line break initiated LOCA has also been assessed. This assessment also studied the impact of the initiation of the IRWST drain line operation during DVI line break initiated LOCAs. It was found for those sequences that do not flood the DVI line break elevation with IRWST water that no standing diffusion flame is produced at the valve vault room exit. This is due to the highly steam inerted and low hydrogen concentration mixture produced in the valve vault room gas space for these types of sequences. For those DVI line break sequences which flood the break elevation prior to the release of steam and hydrogen from the primary system, the steam is stripped from the escaping gases and a high hydrogen, non-inerted concentration is produced in the valve vault room gas space. The water level in the valve vault room may even be high enough to flood the igniter located in that compartment. However, the oxygen supply available to the valve vault room gas space is insufficient to support continual burning of the hydrogen released into that room even if the igniter is operable. Thus, the availability of the igniter is not a critical consideration for sequences which have high water levels in the affected valve vault room. The inability to inert the gas space in the valve vault room or to burn the hydrogen as it is released can produce high hydrogen concentrations which can exit the vault room and produce a standing diffusion flame

at its exit. Thus, the potential for a standing diffusion flame at each valve vault room exit must be assessed for the CMT floor. However, only one valve vault room exit at any given time would experience a diffusion flame since DVI line breaks are addressed one at a time.

The sensitive components on the CMT floor which maintain the containment integrity include the containment shell, equipment hatch, personnel hatch and electrical penetrations. Thermal assessments for standing diffusion flames have been performed individually for each of the valve vault rooms. These two valve vault rooms have been designated north and south to facilitate their reference. A review of the 107′ - 2″ floor plan view allows the determination that a standing diffusion flame at the exit to the north valve vault room would have a direct line of sight of both the containment shell and several electrical penetration assemblies but not the containment hatches. The thermal assessment of the containment shell and electrical penetrations takes into account the distances between the standing diffusion flame at the north valve vault room exit and these two components. The results show that the containment wall localized heating is significantly less than the three stage ADS assessment described above. Furthermore, the electrical penetrations will be heated to temperatures that do not exceed the equipment survivability temperature [477°K (400°F)] during the interval that a standing diffusion flame could be produced. The peak calculated transient temperature of the gas within the electrical penetration assembly is estimated to be approximately 474°K (393°F).

A standing diffusion flame at the south valve vault room exit would have the potential of heating the containment shell, the equipment hatch and the personnel hatch. The displacement between that diffusion flame and the containment shell is even larger than the displacement between the diffusion flame at the north valve room exit and the containment shell. Thus, lower temperatures for the containment shell on the CMT floor elevation would be produced for the flame at the south valve vault room than for the diffusion flame on the north valve vault room. Likewise, an assessment of the thermal response of both the equipment and personnel hatches shows that their peak temperatures during the interval with the standing diffusion flame are lower than the 477°K (400°F) temperature used in the containment failure assessment incorporated in the PRA (AP600, 1996). Thus, a standing diffusion flame at the exits to the valve vault rooms do not produce containment shell or hatch temperatures which exceed those employed in the PRA containment failure assessment. Since the limiting temperature of 477°K (400°F) used in the AP600 PRA evaluation is not exceeded by the localized diffusion flame heating, it is concluded that the PRA evaluations are bounding.

## 8.0 REFERENCES

AP600, 1996, Chapter 42, Conditional Containment Failure Probability Distribution, AP600 Probabilistic Risk Assessment.

Heskestad, G., 1988, "Fire Plume," The SFPE Handbook of Fire Protection Engineering, Chapter 6, pp. 1-107 to 1-115.

Steward, F. R., 1970, Combustion Science and Technology, 2, 203.

Tamanini, F., et al., 1988, "Hydrogen Combustion Experience in 1/4 Scale Model of a Mark III Nuclear Reactor Containment (Volumes 1 and 2) Prepublication Copy," EPRI Project PRY101-01.

# APPENDIX A

## Plots of Hydrogen Generation, Containment Gas Composition, IRWST and Valve Vault Rooms Junction Flow Rates, Containment Pressure and Containment Temperatures for Three Stage ADS and DVI Break in South Valve Vault Room

Notes: 1. The plots for the IRWST are for a two node model and are representative of the values for the three node model used in the transient results presented in the main body of the report.

2. The plots for a DVI Break in North Valve Vault Room are essentially the same as those for the South Valve Vault included in this appendix.

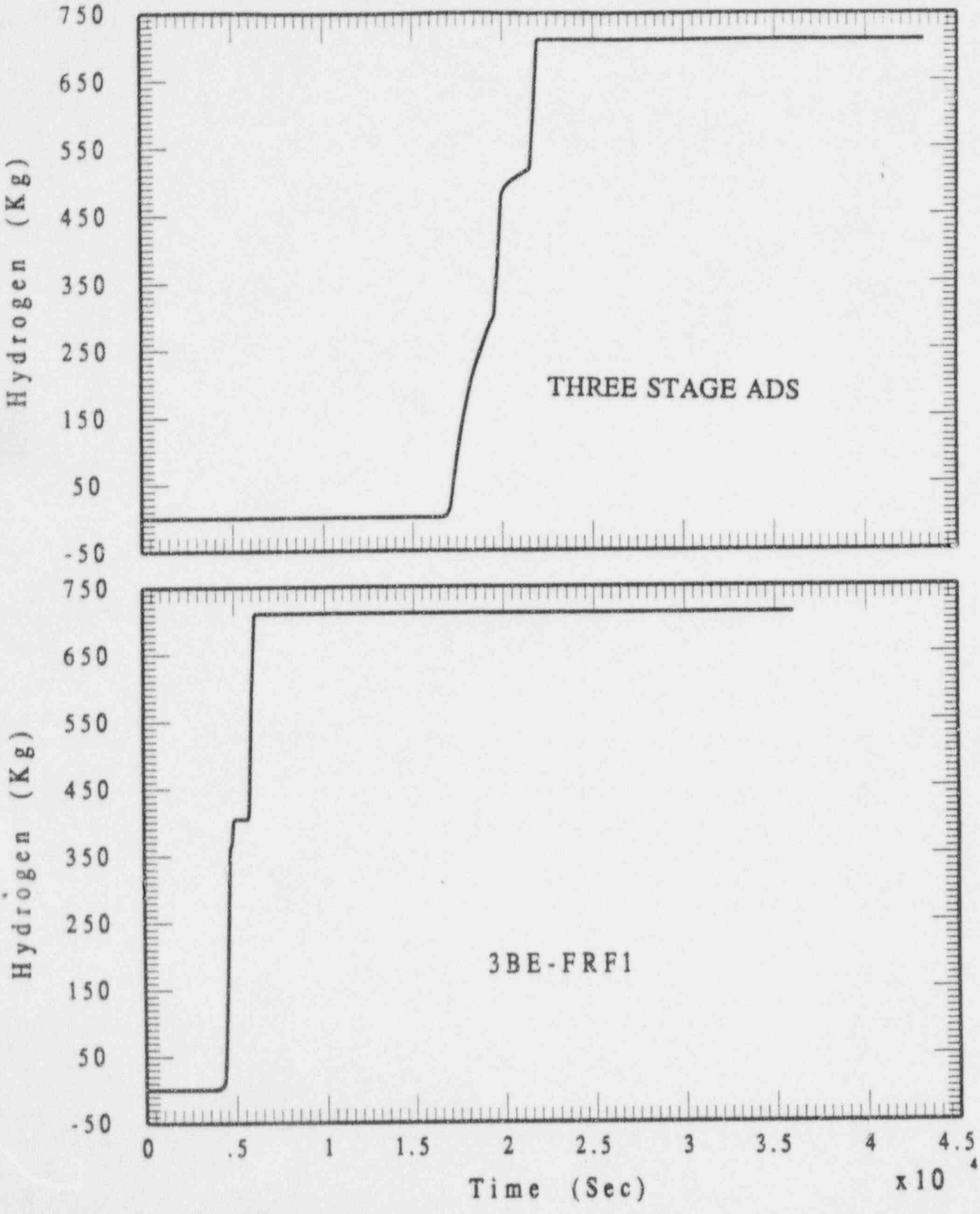


Figure A-1. Integrated In-Core Hydrogen Generation History

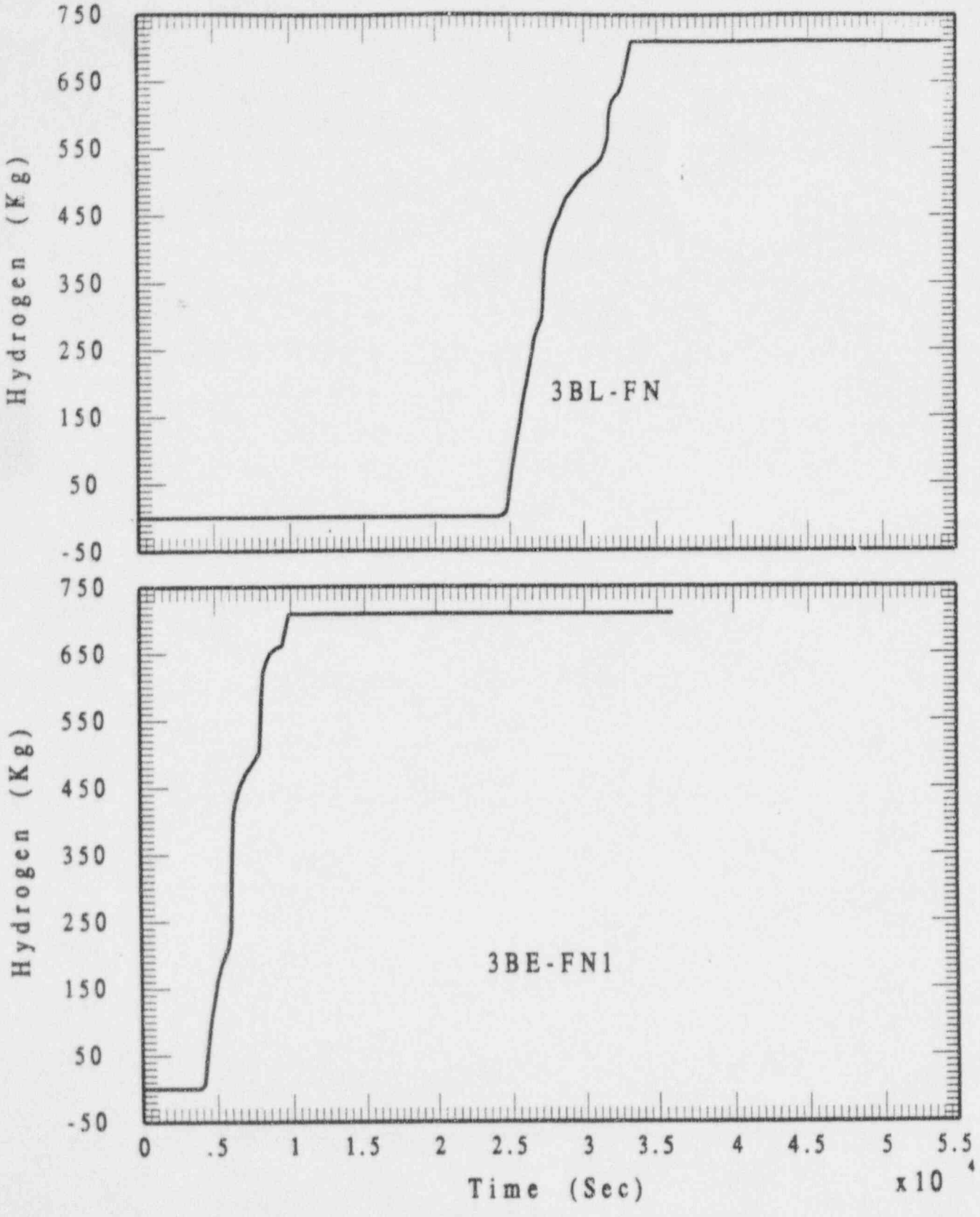


Figure A-2. Integrated In-Core Hydrogen Generation History

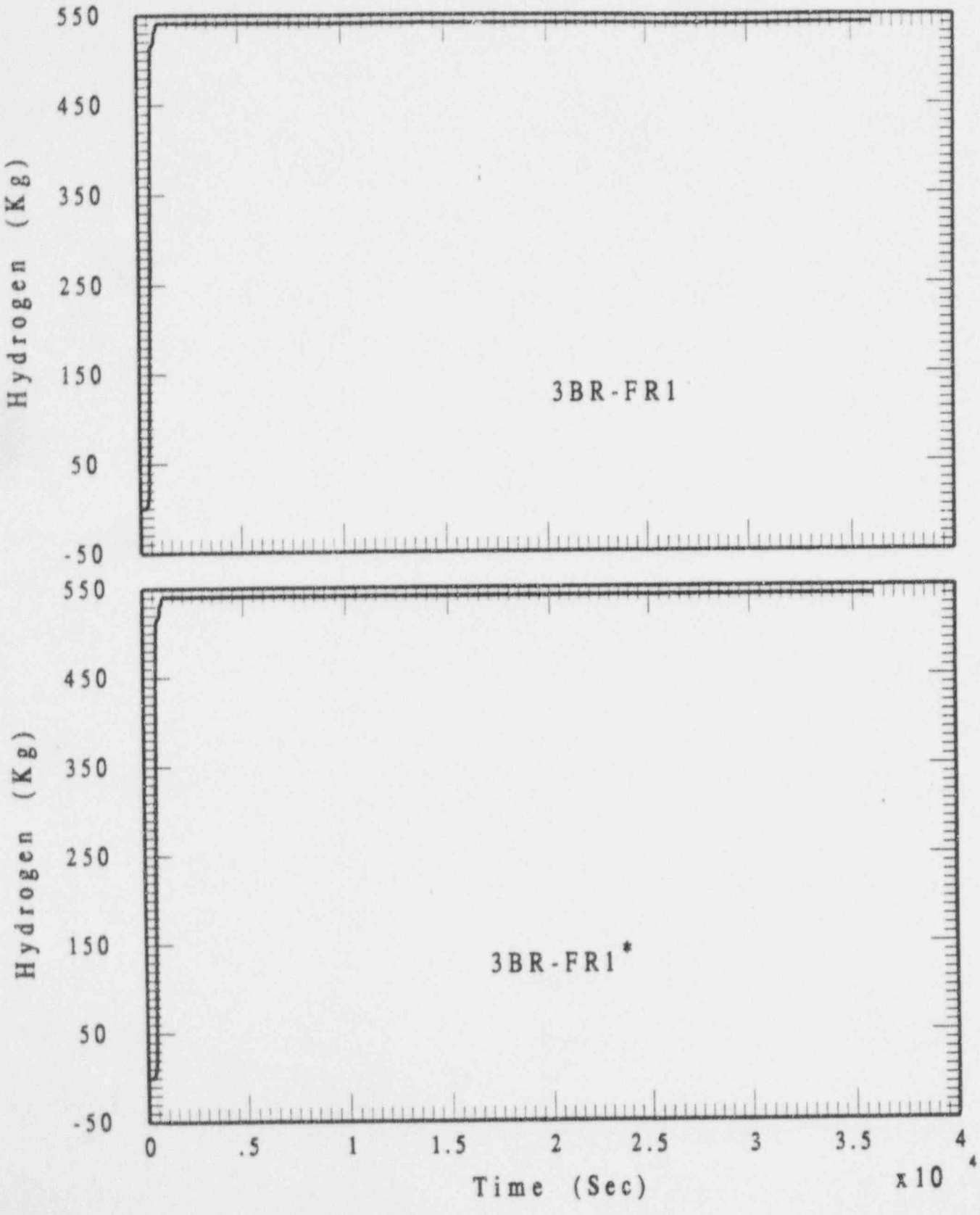


Figure A-3. Integrated In-Core Hydrogen Generation History

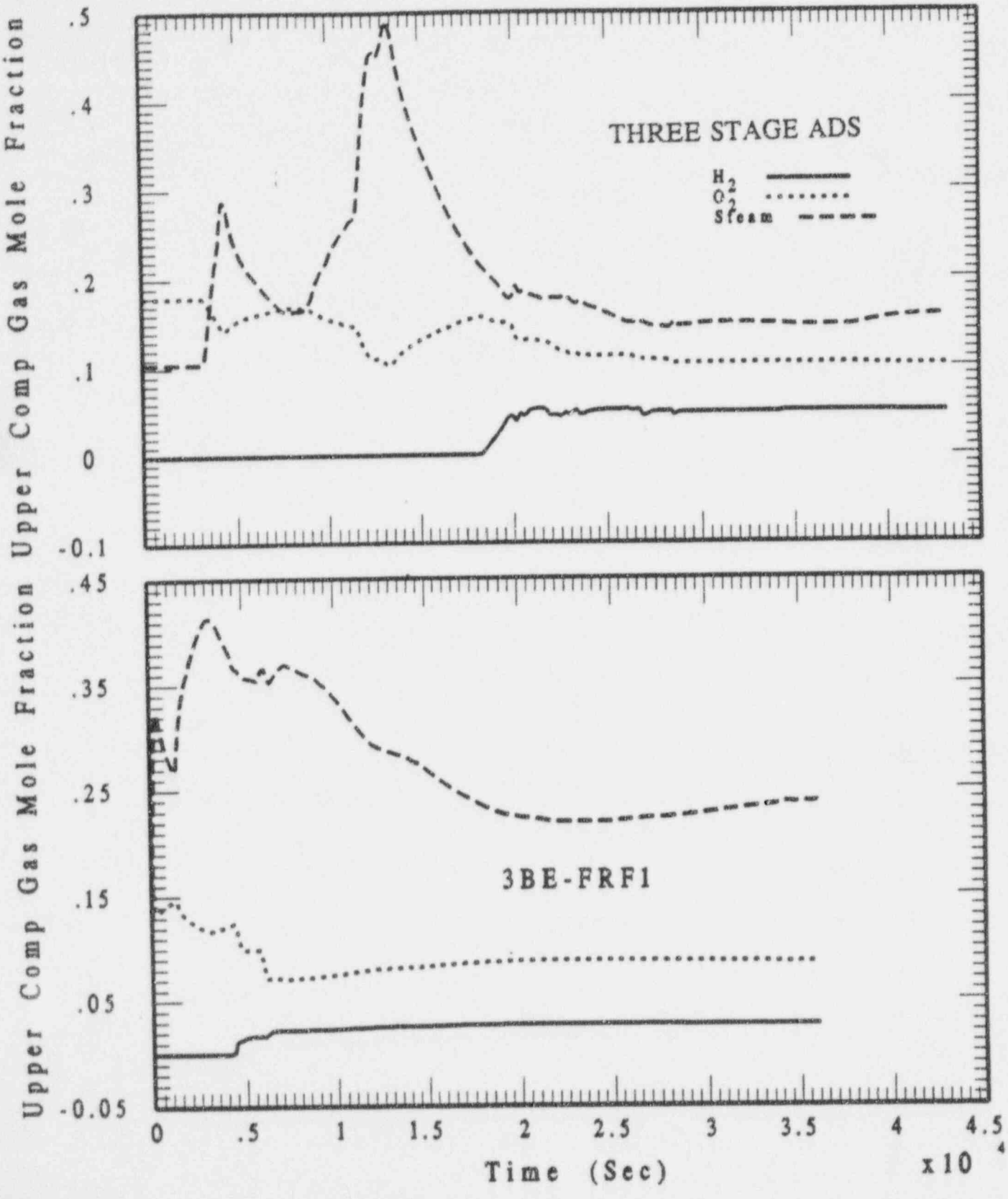


Figure A-4. Upper Compartment Gas Composition

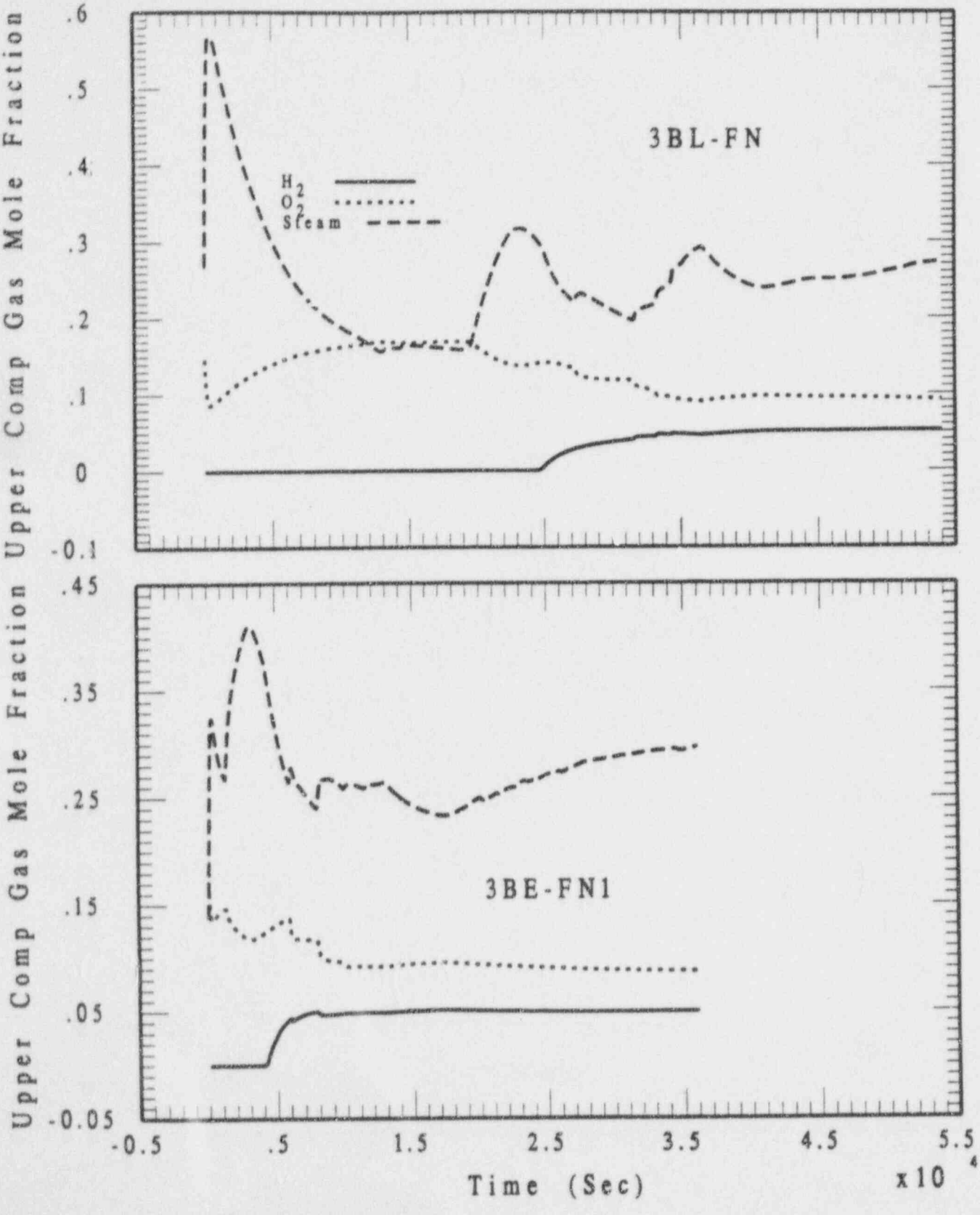


Figure A-5. Upper Compartment Gas Composition

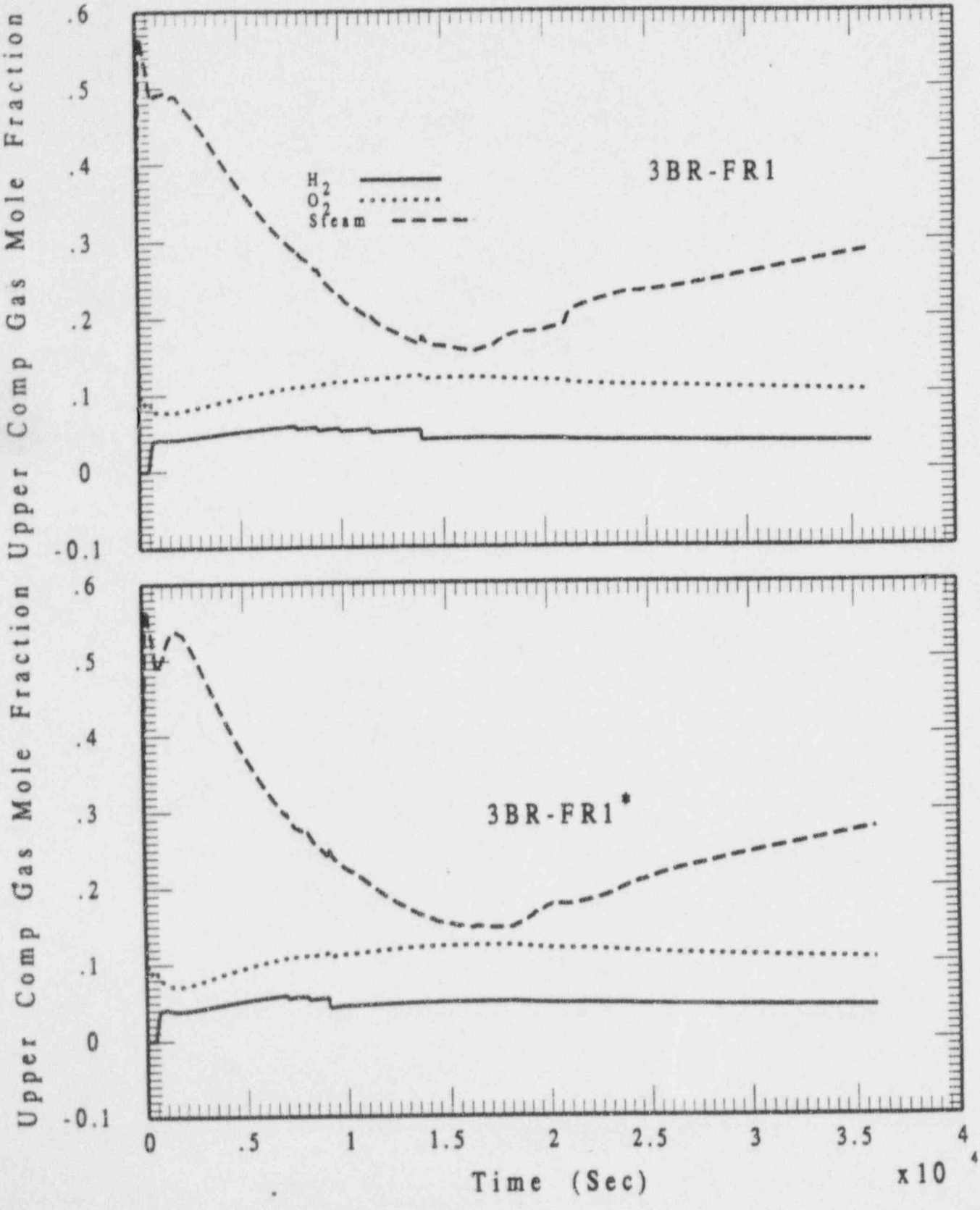


Figure A-6. Upper Comp Gas Composition

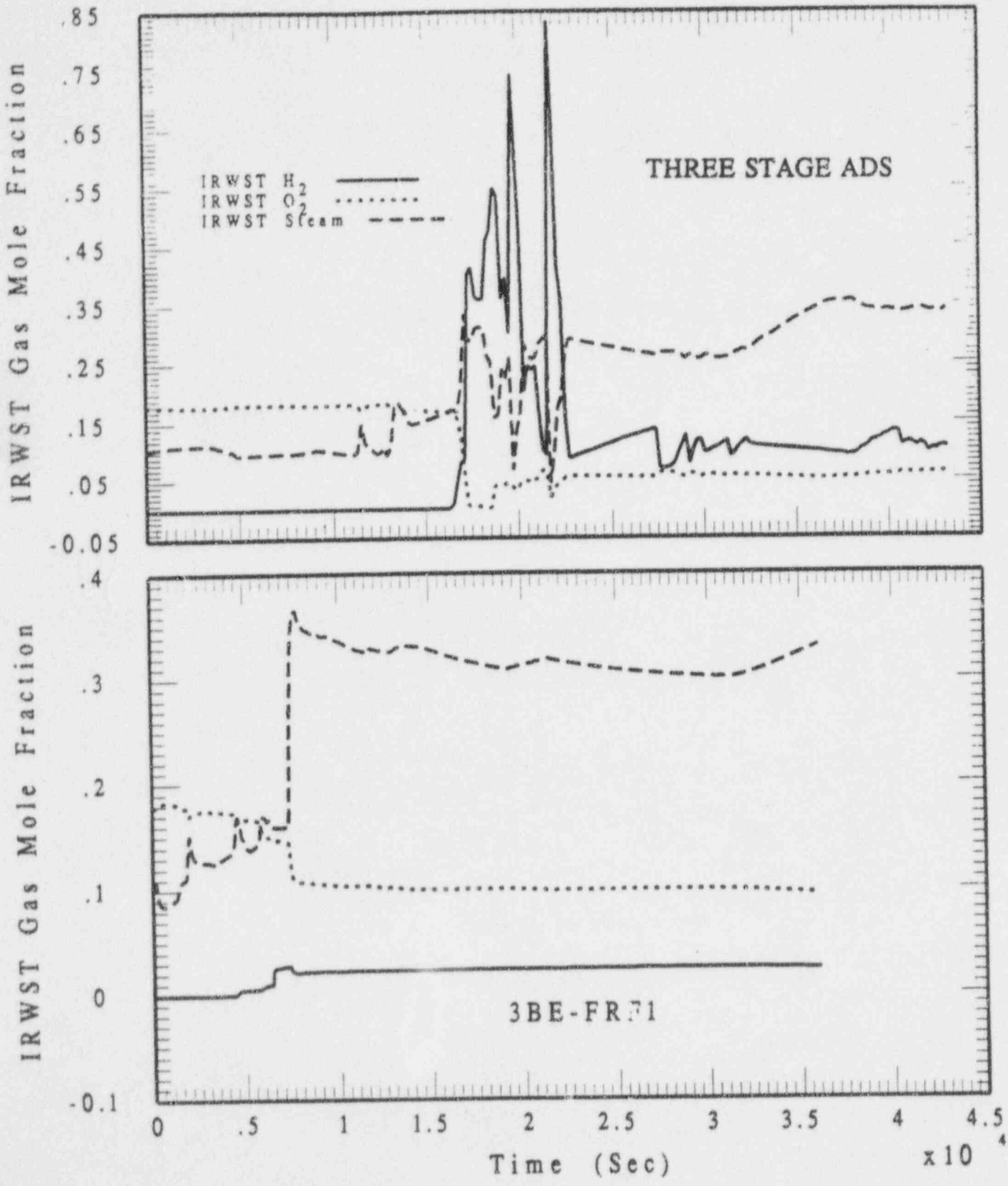


Figure A-7. IRWST Gas Composition

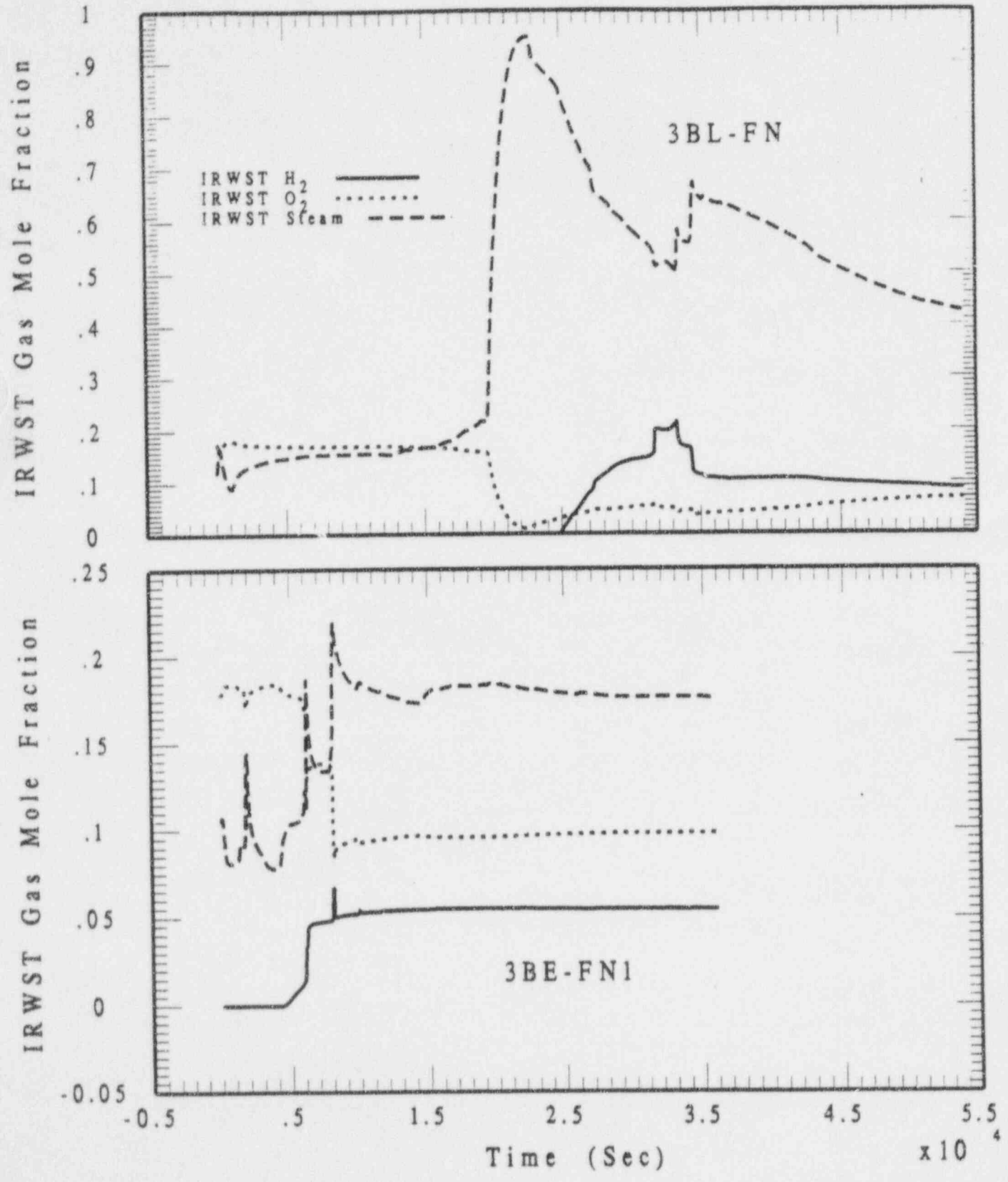


Figure A-8. IRWST Gas Composition

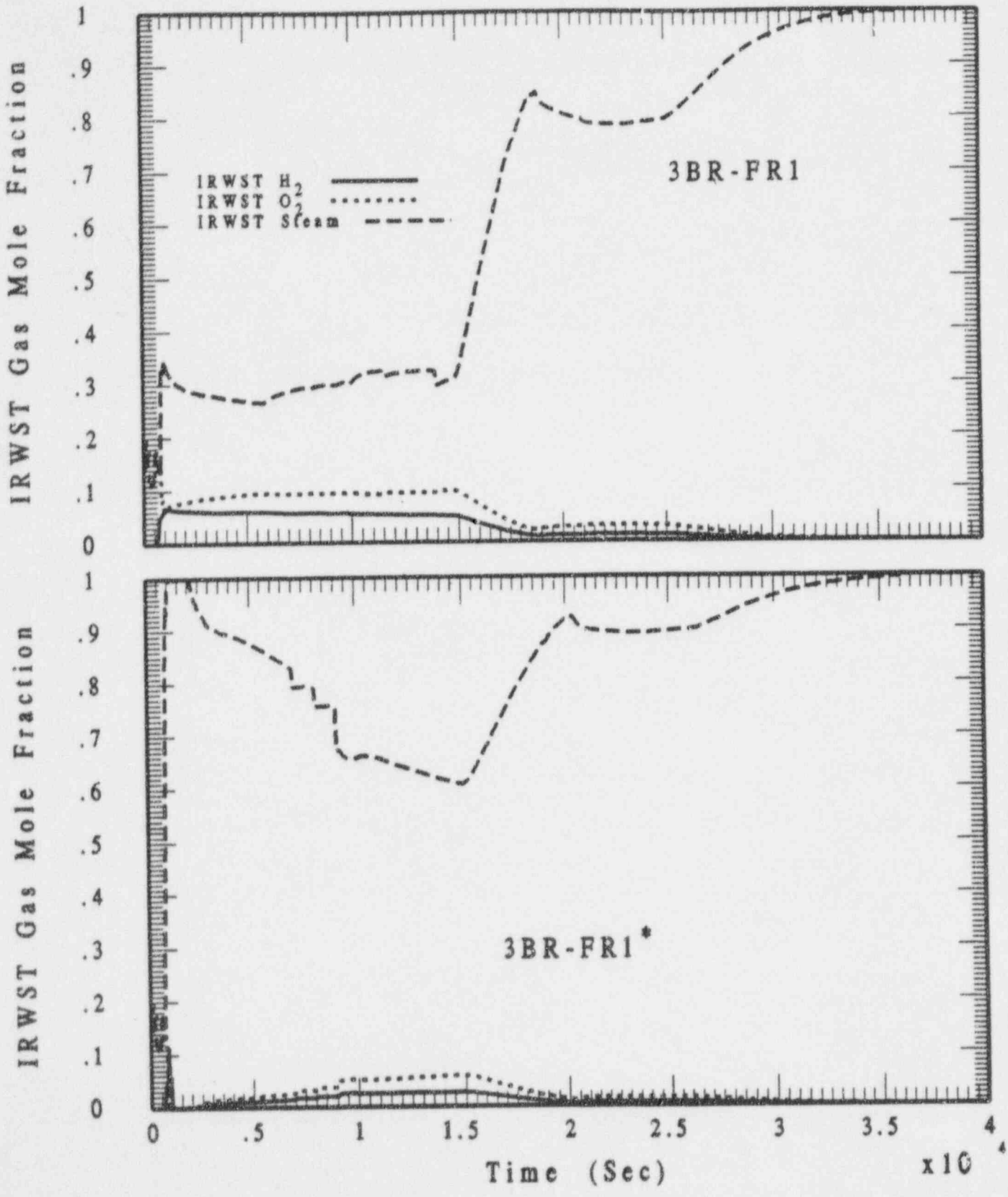


Figure A-9. IRWST Gas Composition

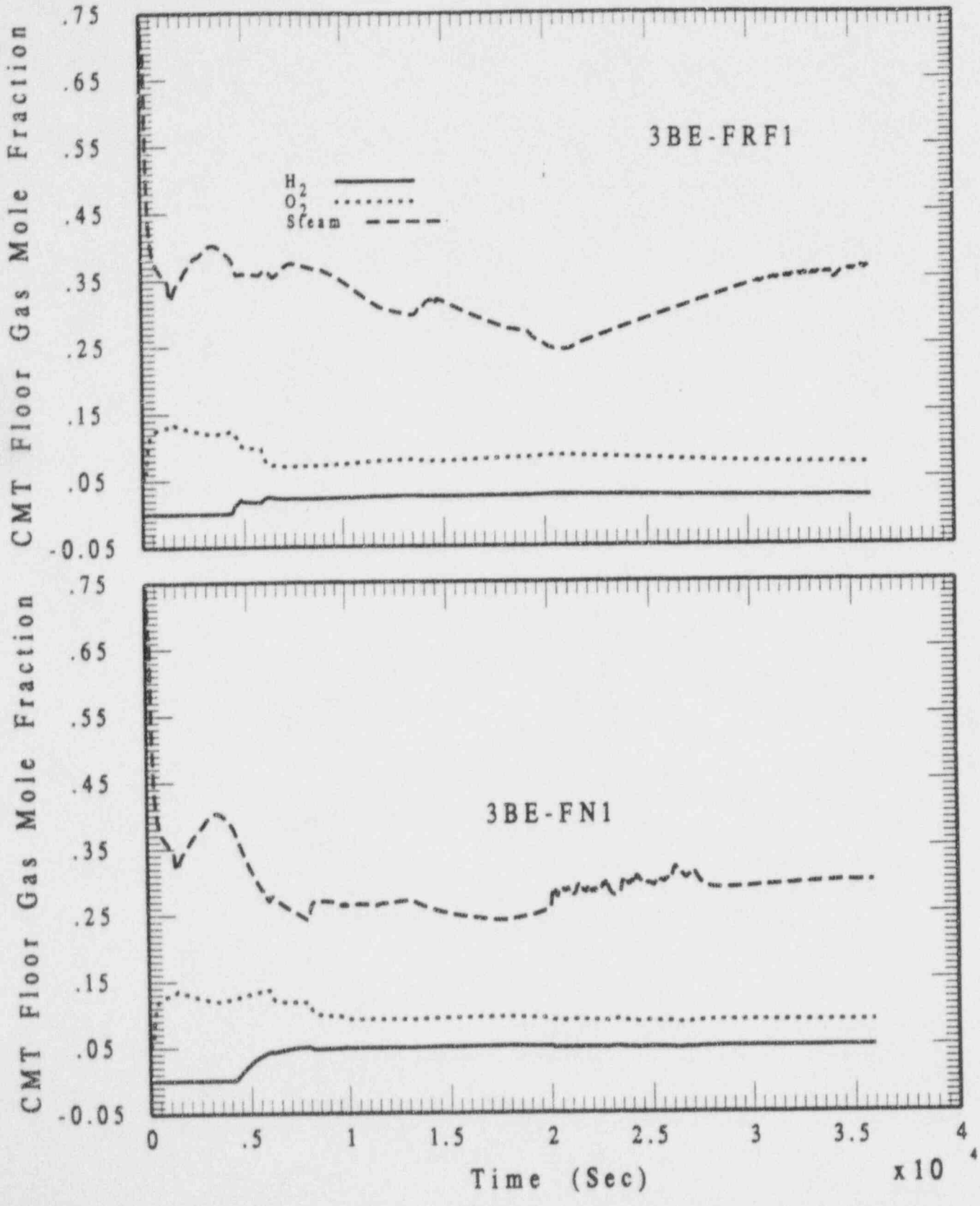


Figure A-10. CMT Floor Gas Composition

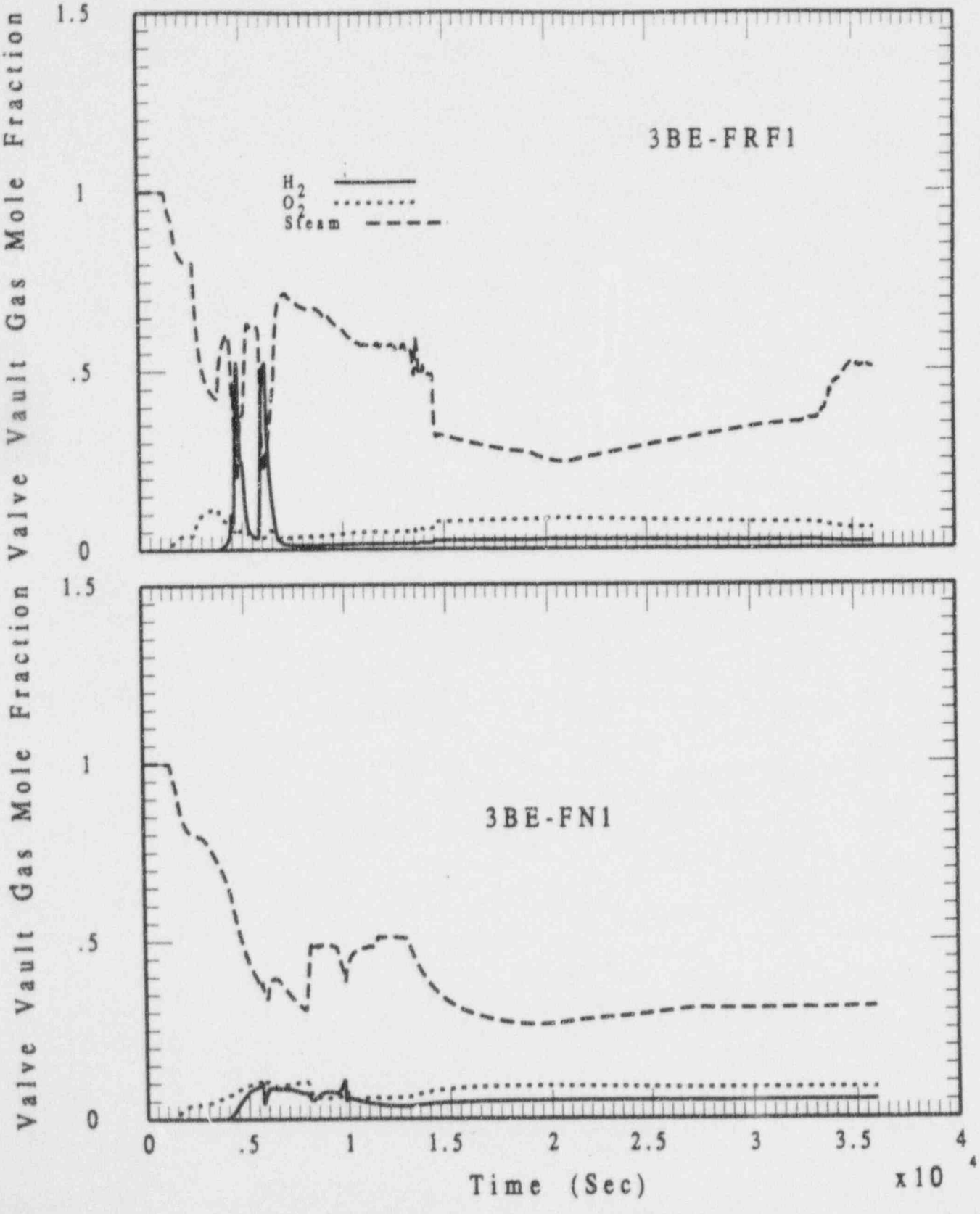


Figure A-11. Valve Vault Gas Composition

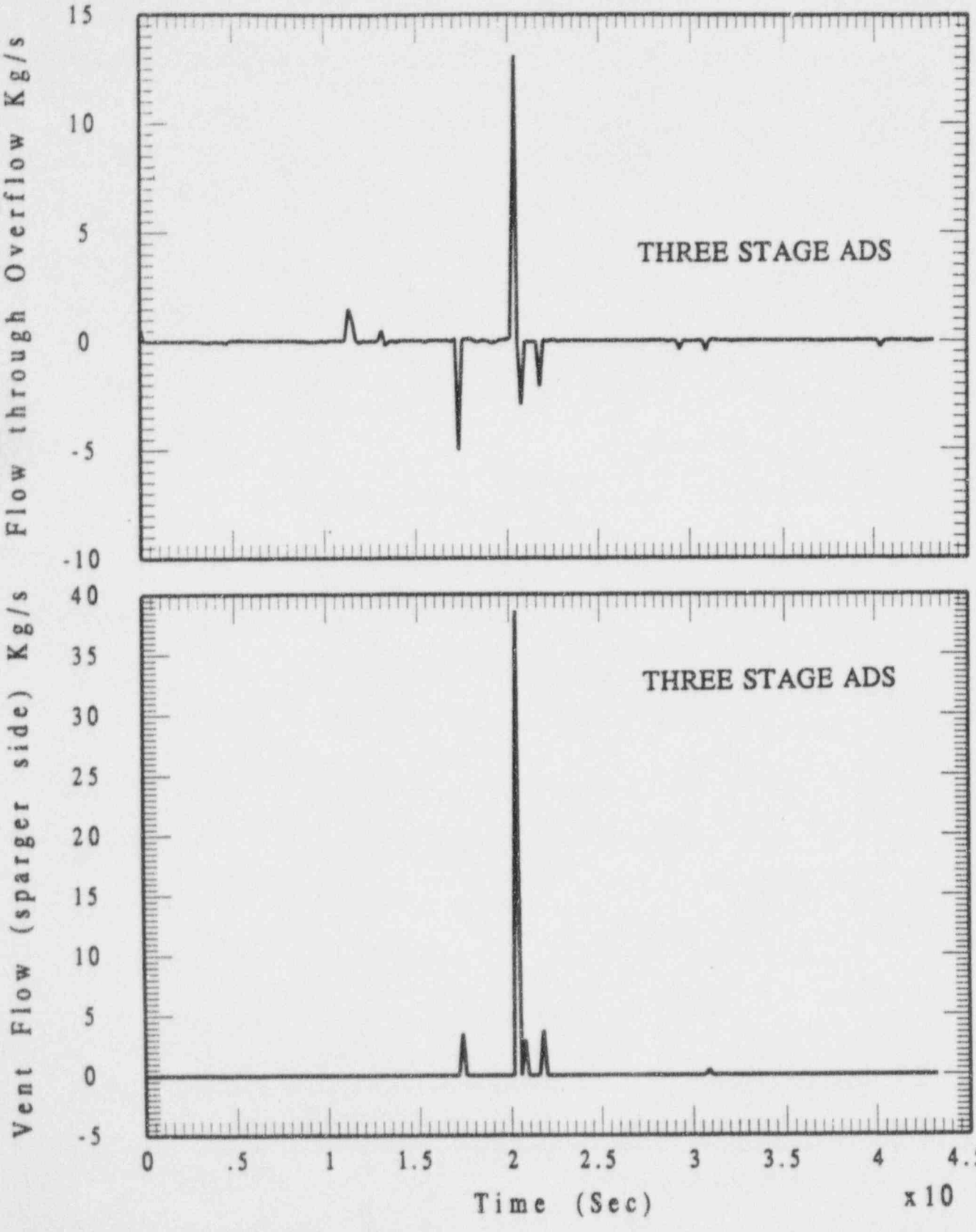


Figure A-12. IRWST Gas Exchange Flow Rates

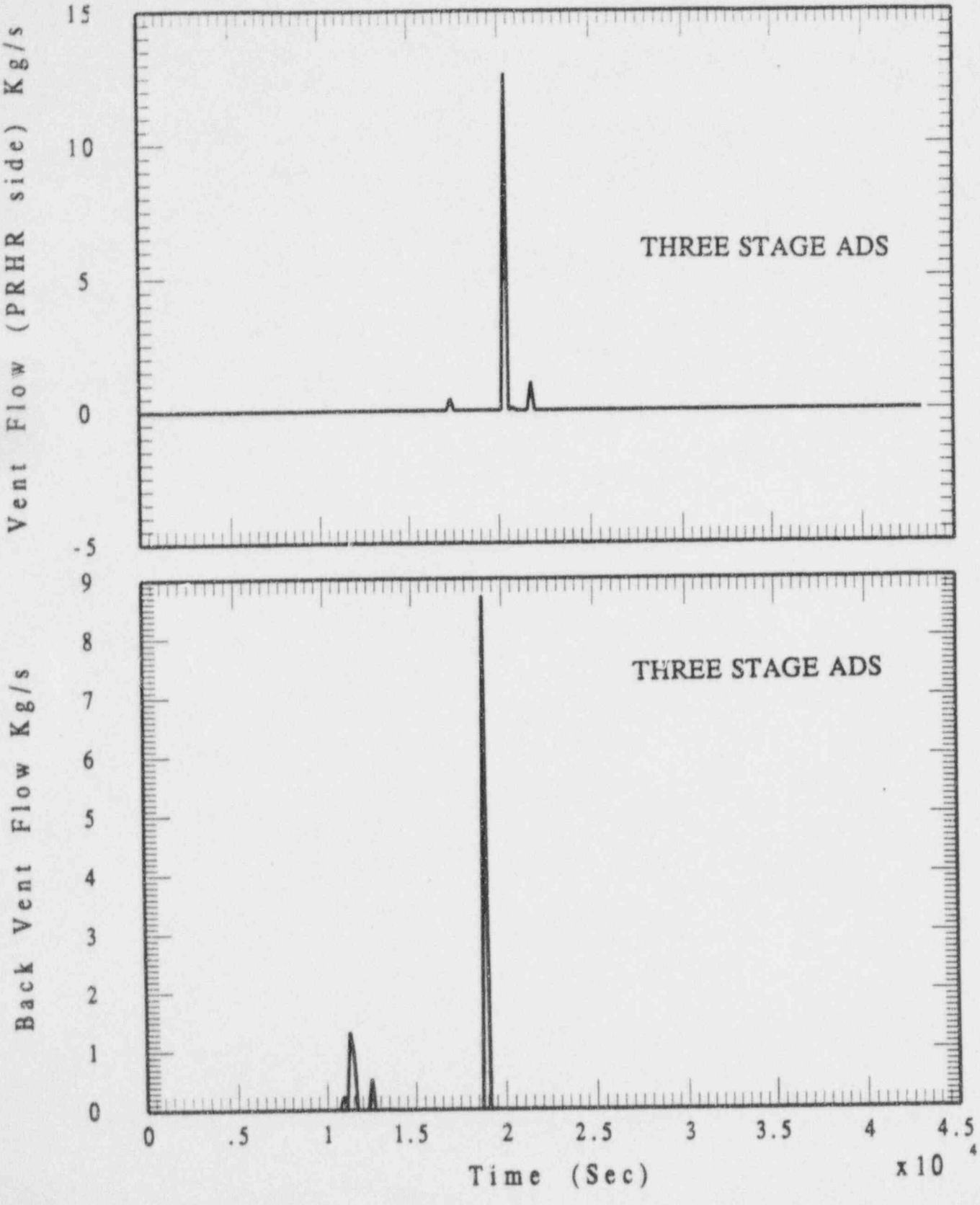


Figure A-13. IRWST Gas Exchange Flow Rates

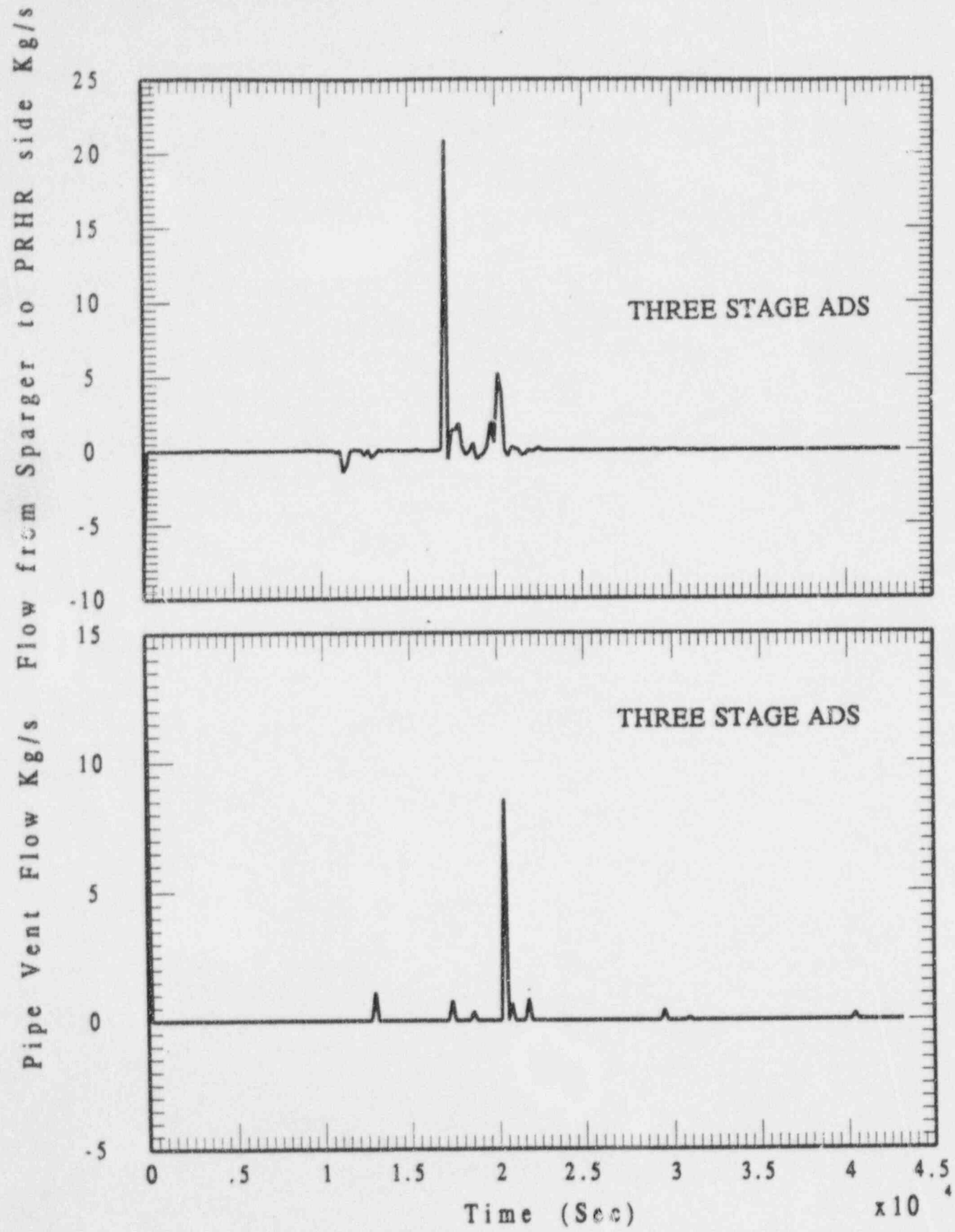


Figure A-14. IRWST Gas Exchange Flow Rates

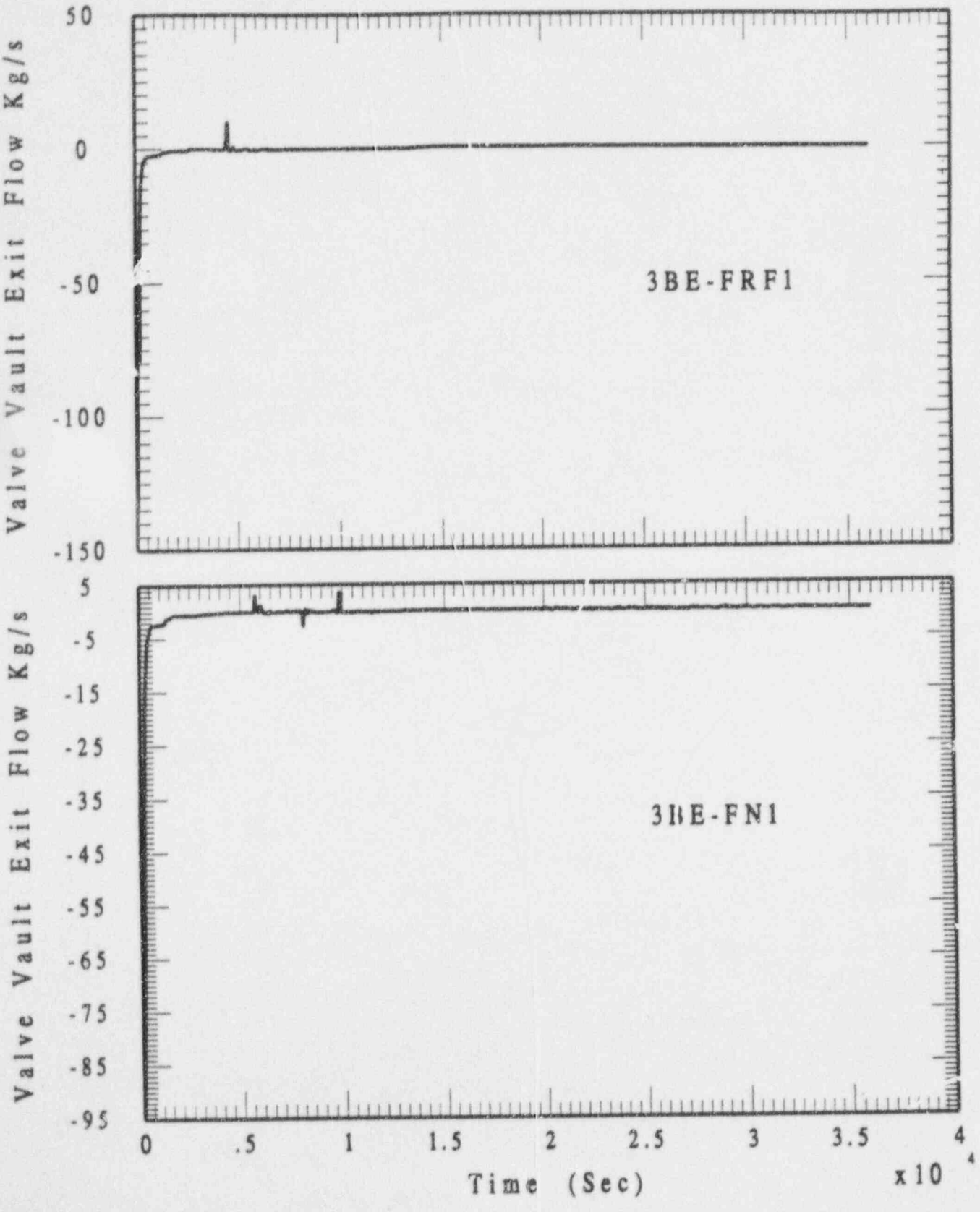


Figure A-15. Valve Vault Exit Flow Rates

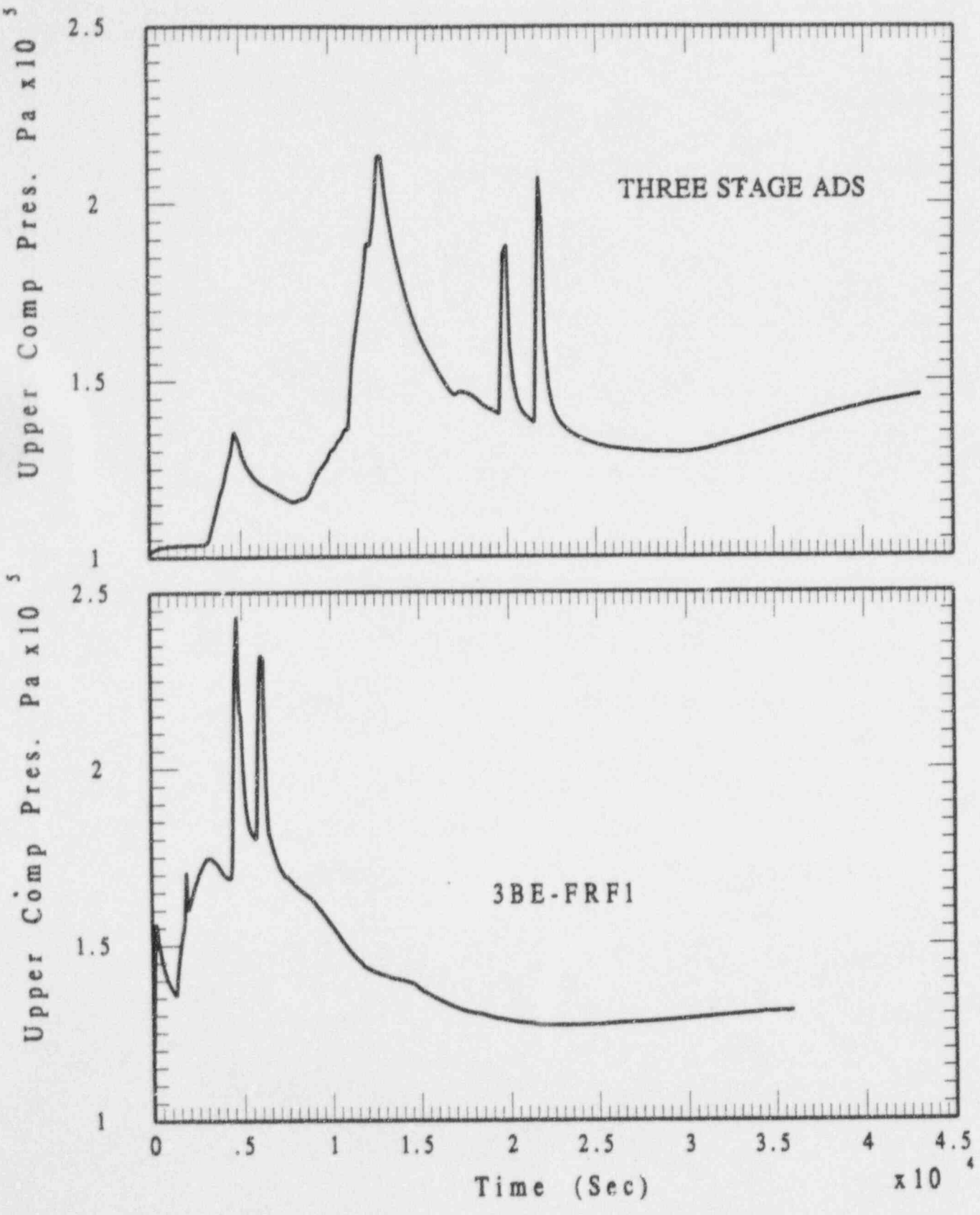


Figure A-16. Upper Compartment Pressure

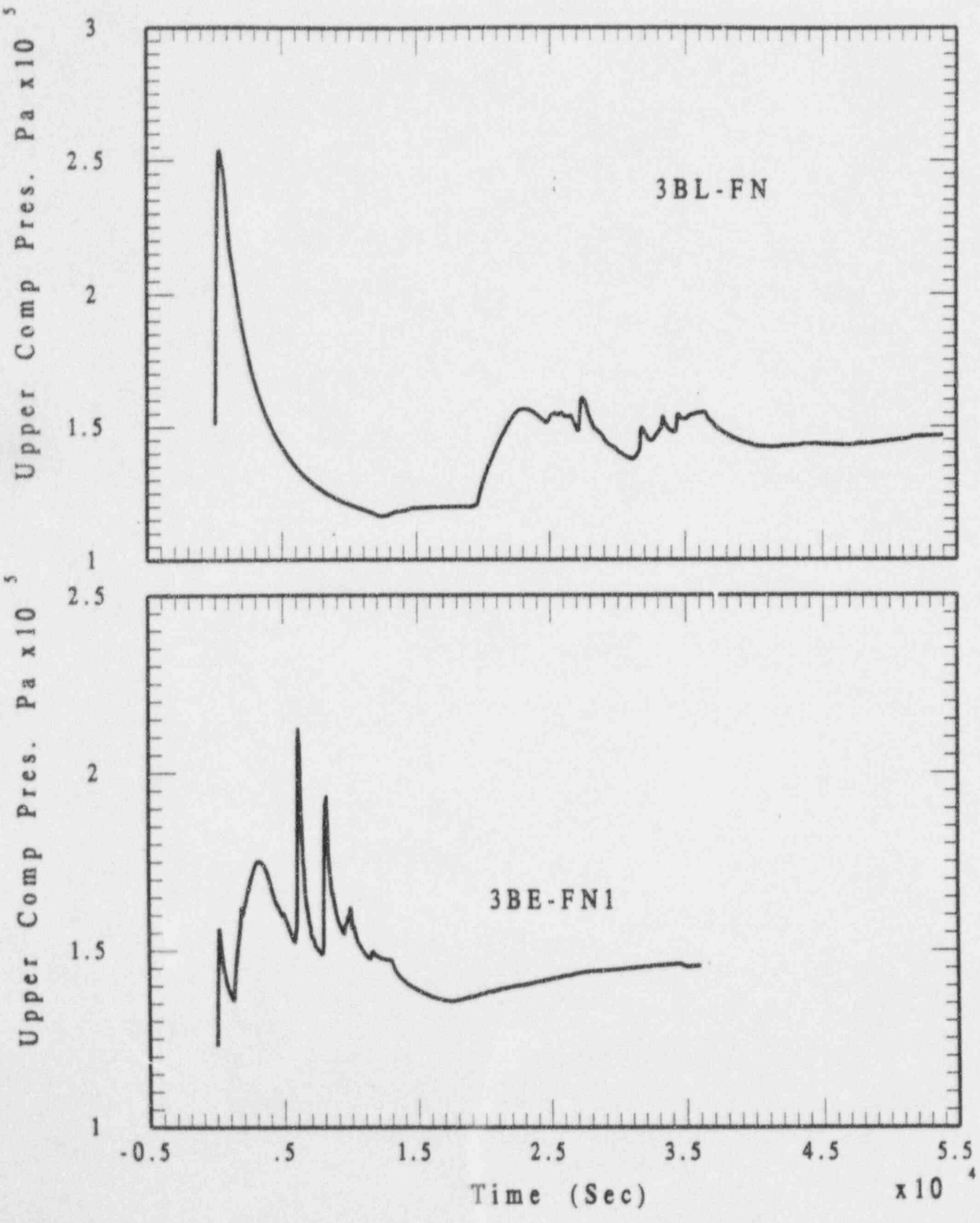


Figure A-17. Upper Compartment Pressure

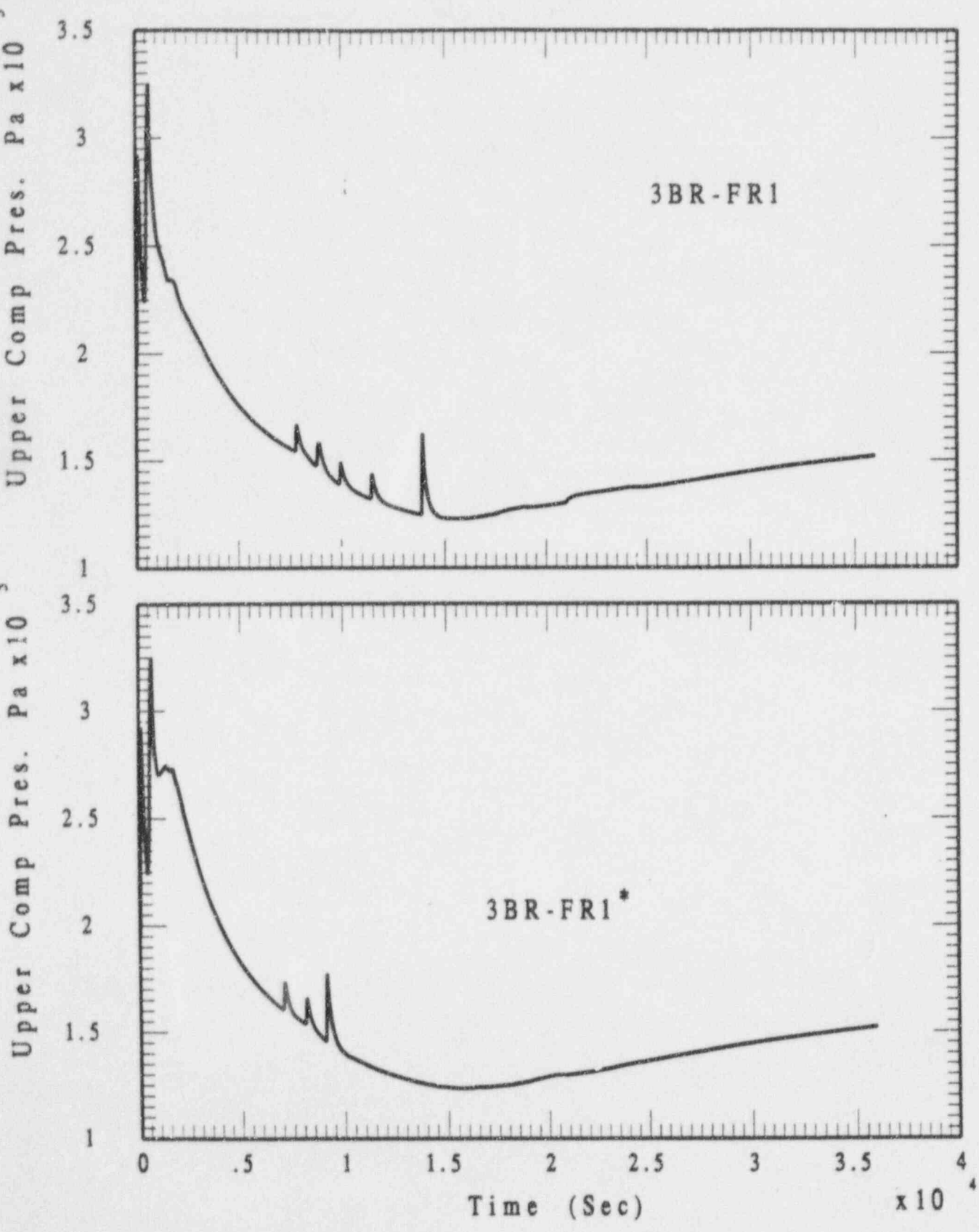


Figure A-18. Upper Compartment Pressure

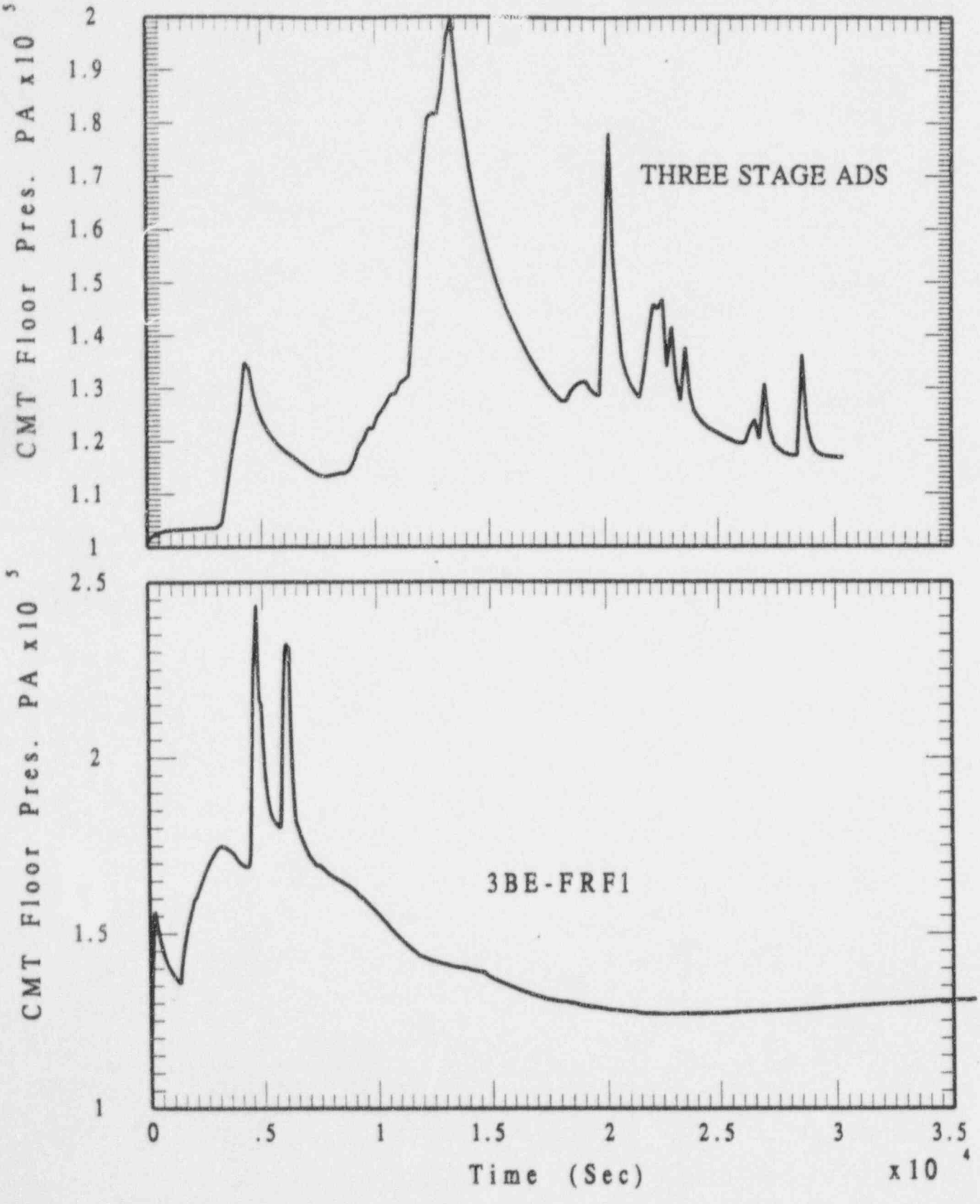


Figure A-19. CMT Floor Pressure

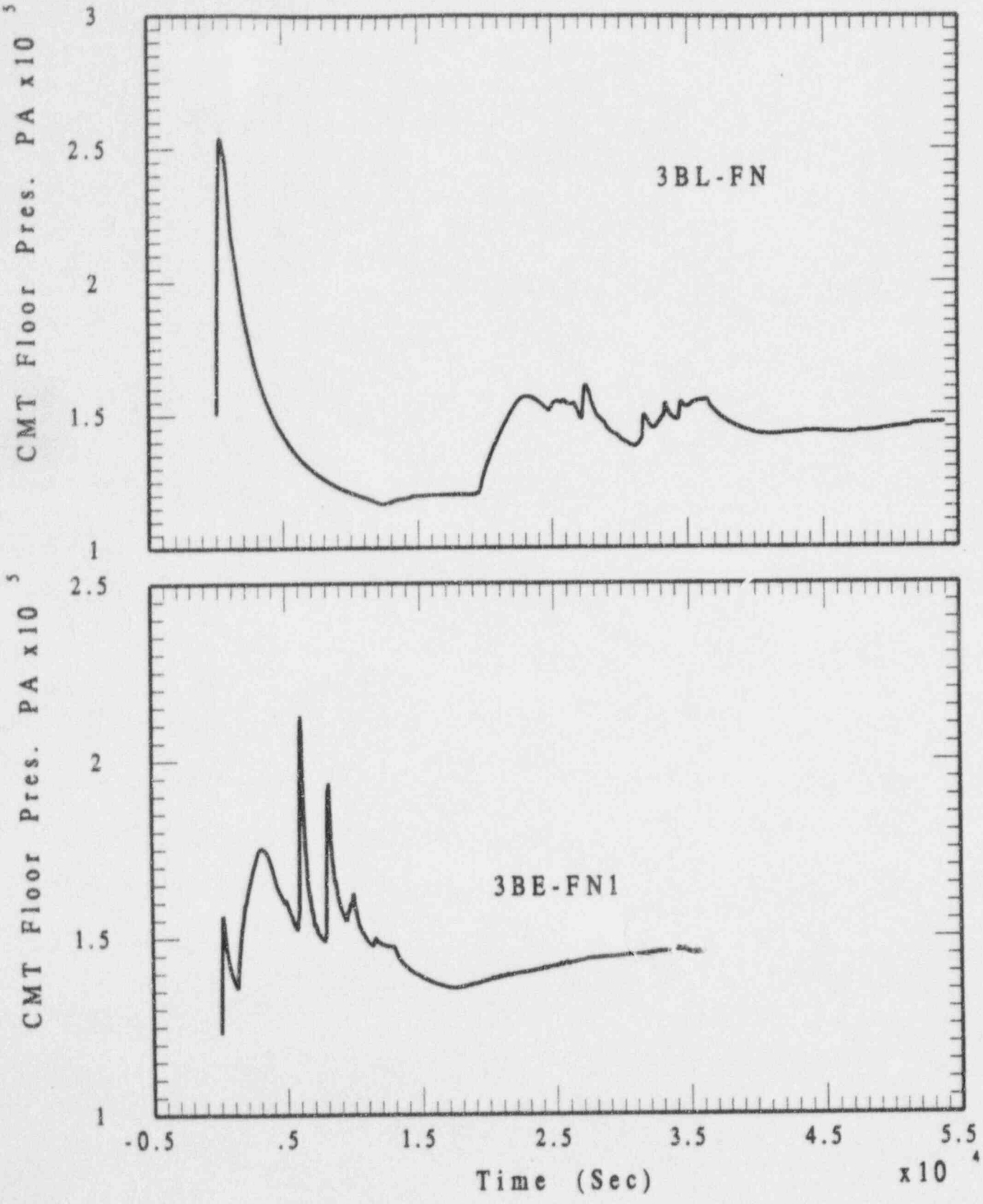


Figure A-20. CMT Floor Pressure

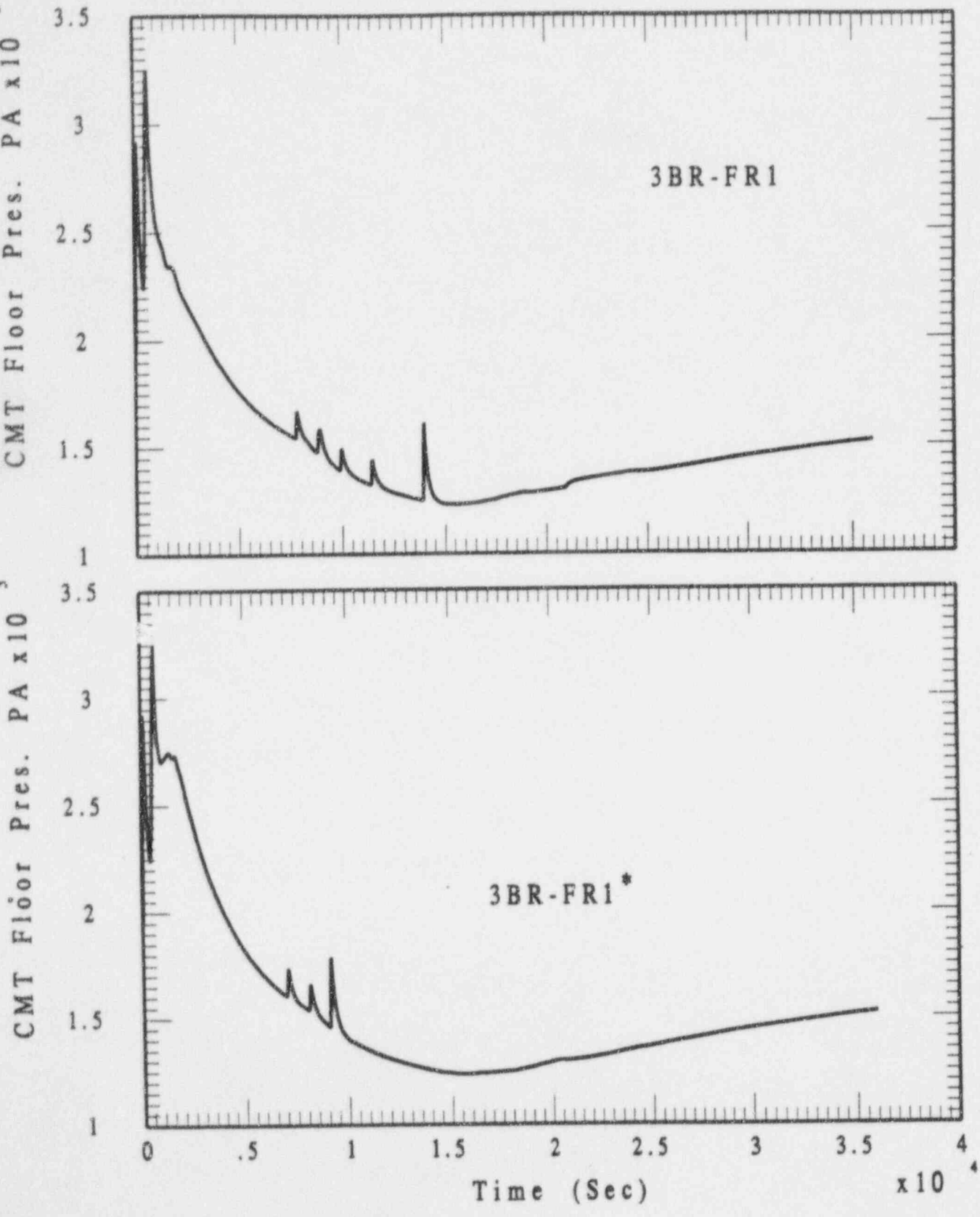


Figure A-21. CMT Floor Pressure

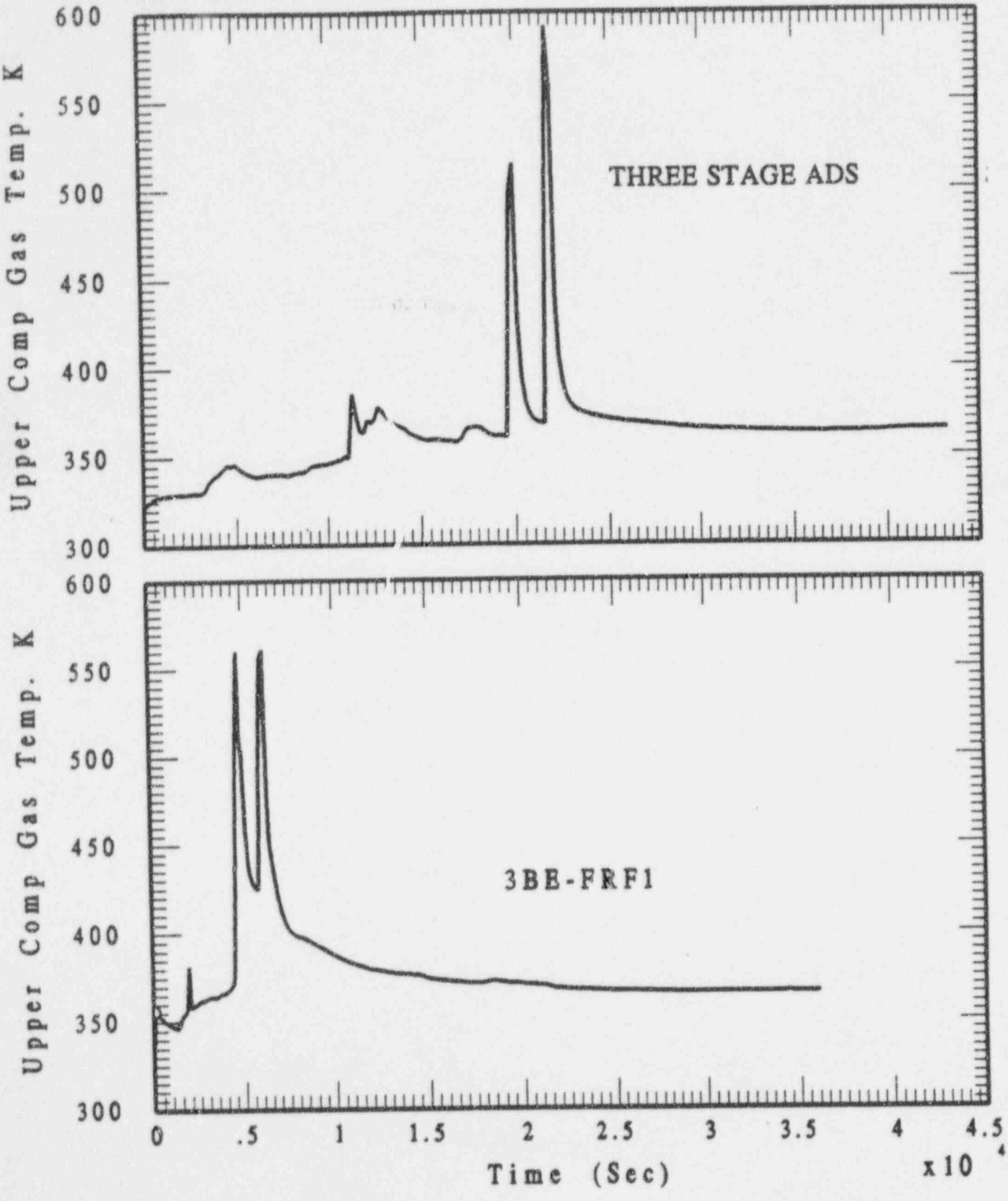


Figure A-22. Upper Comp Gas Temperature

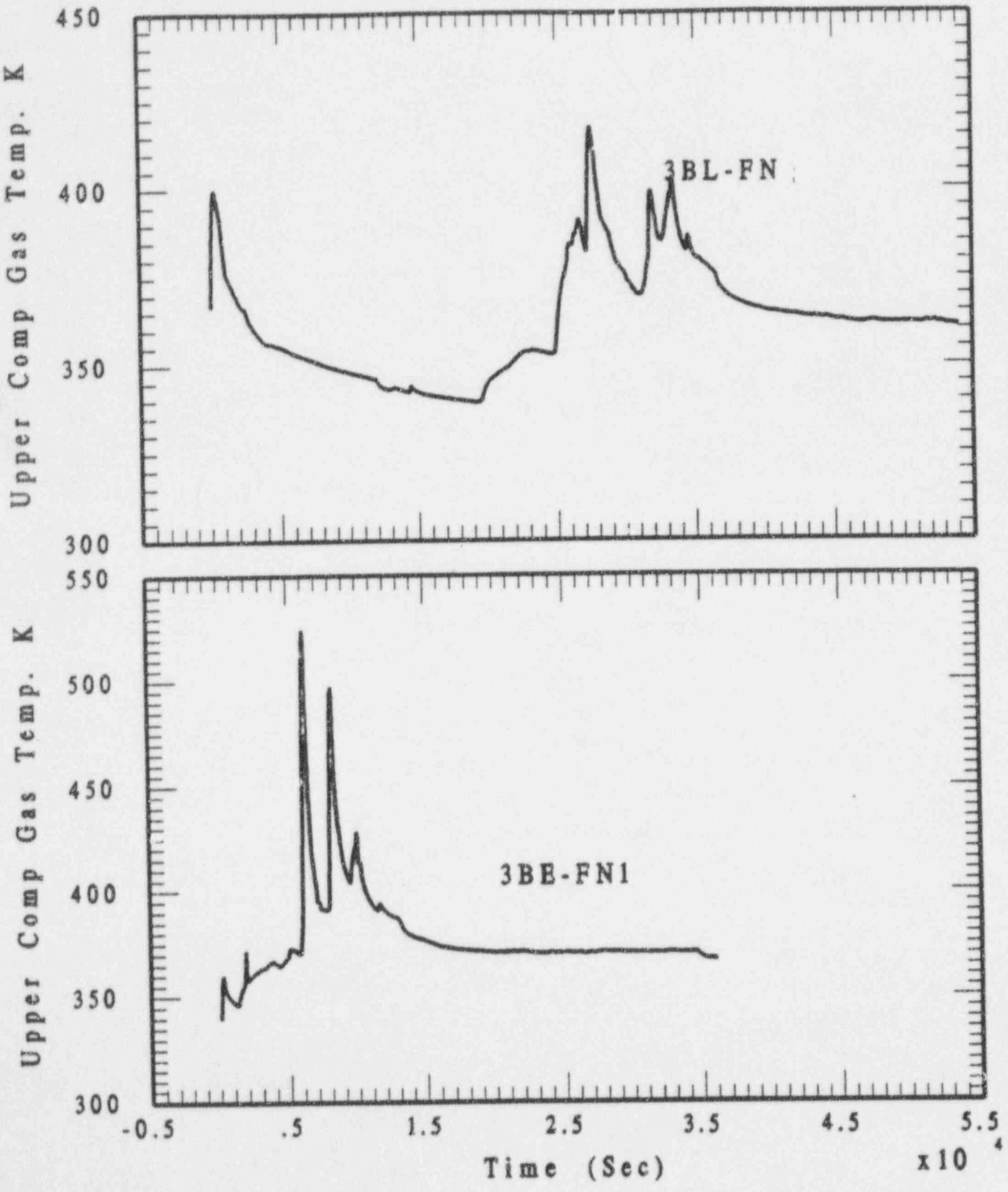


Figure A-23. Upper Comp Gas Temperature

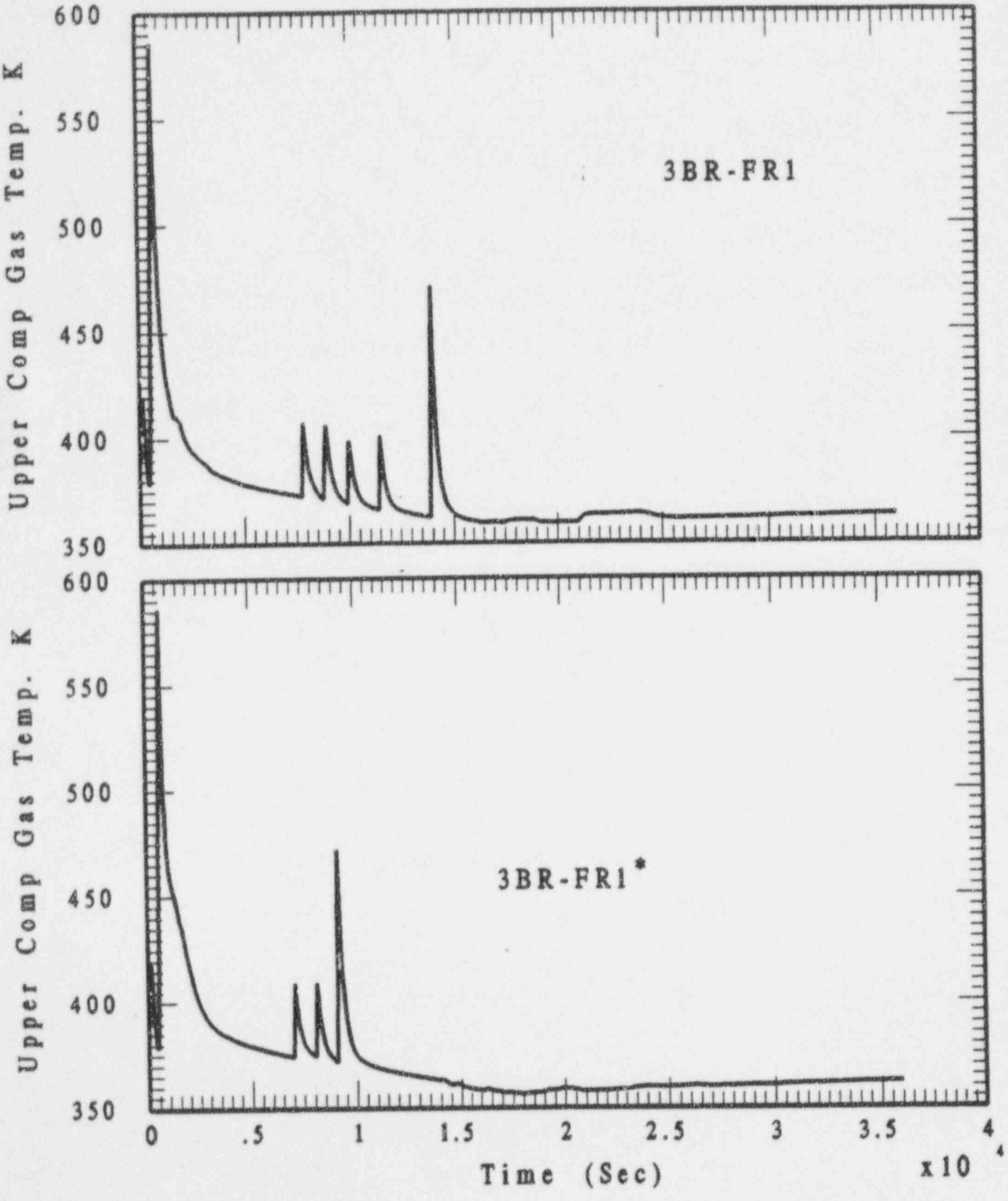


Figure A-24. Upper Comp Gas Temperature

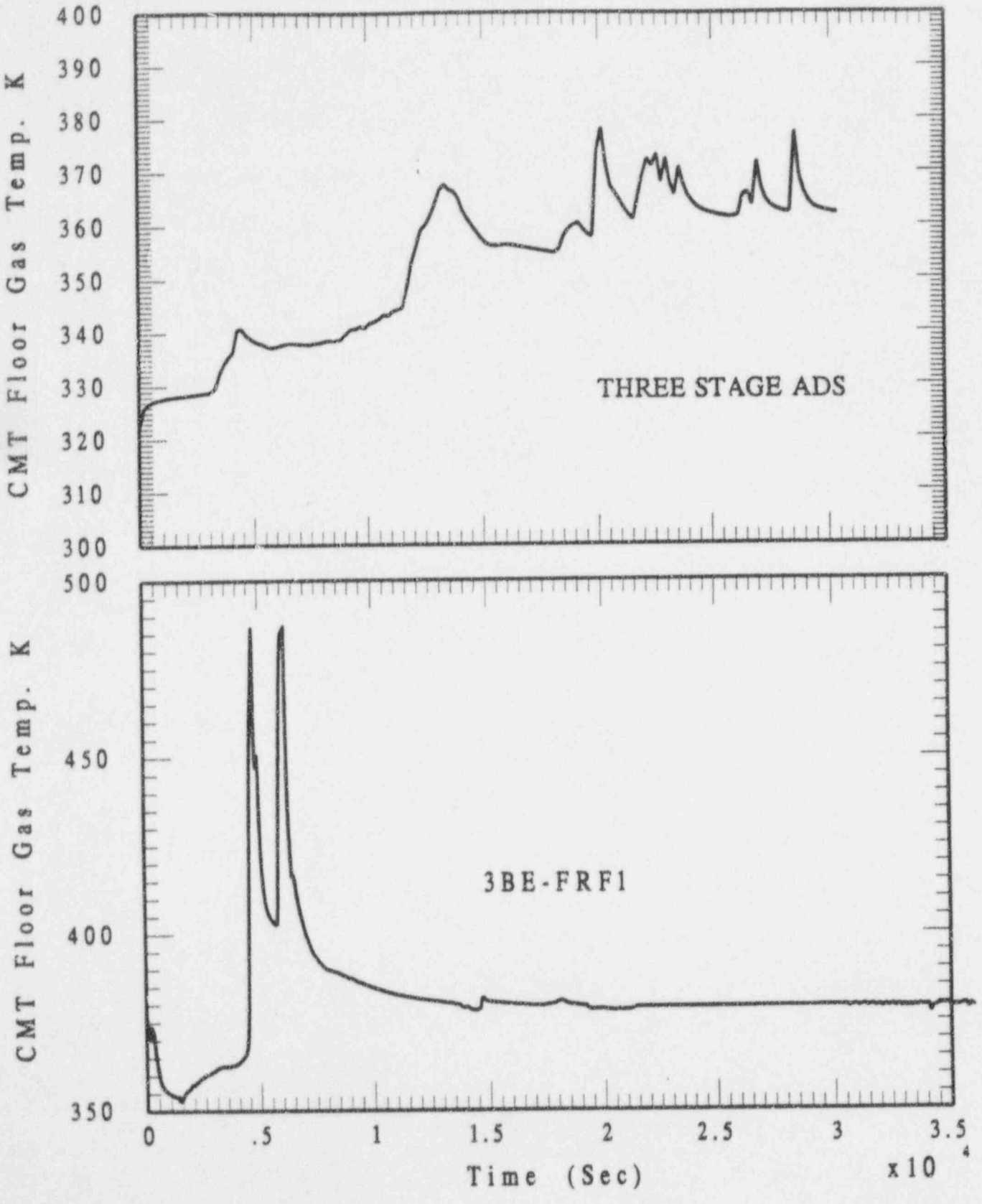


Figure A-25. CMT Floor Gas Temperature

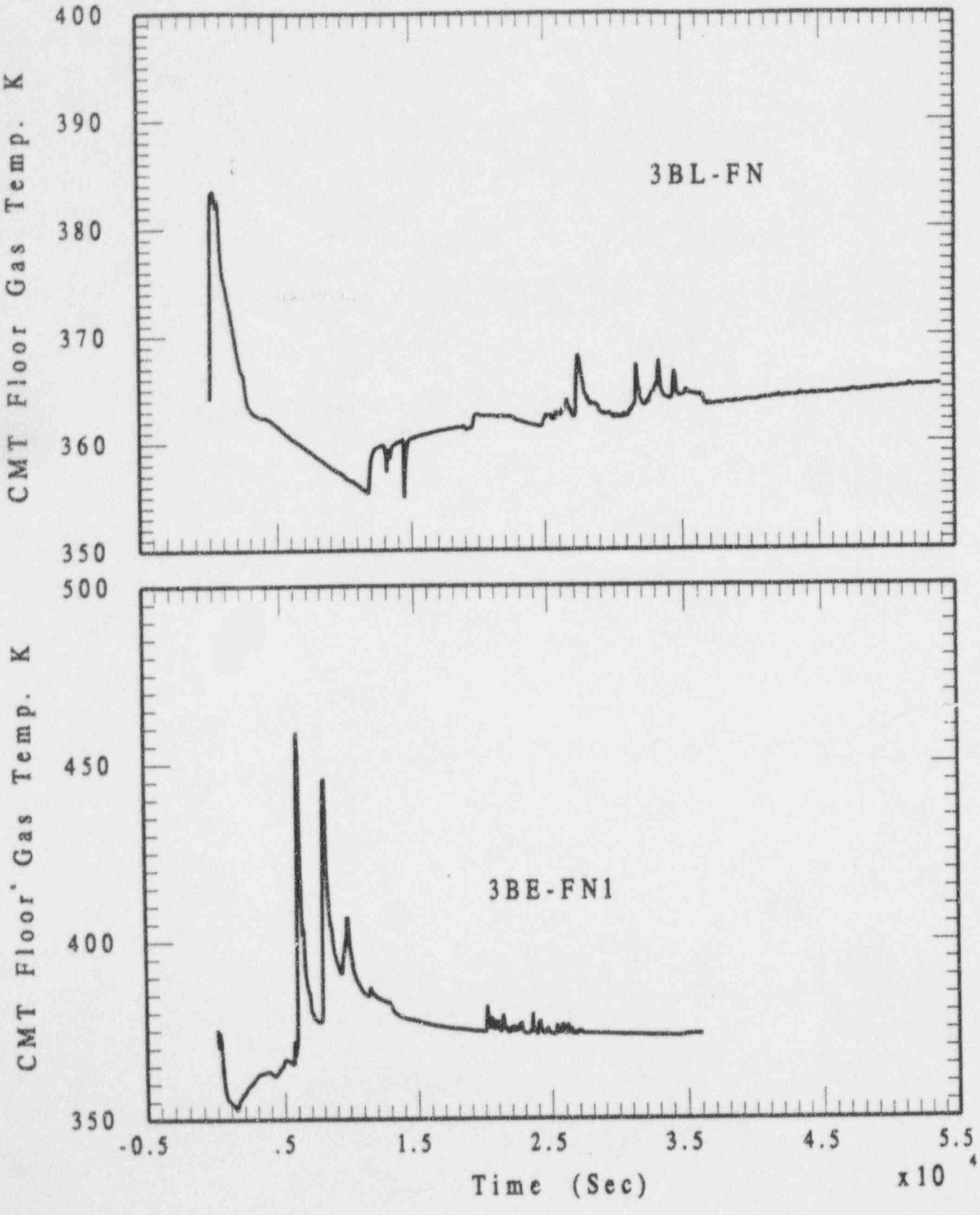


Figure A-26. CMT Floor Gas Temperature

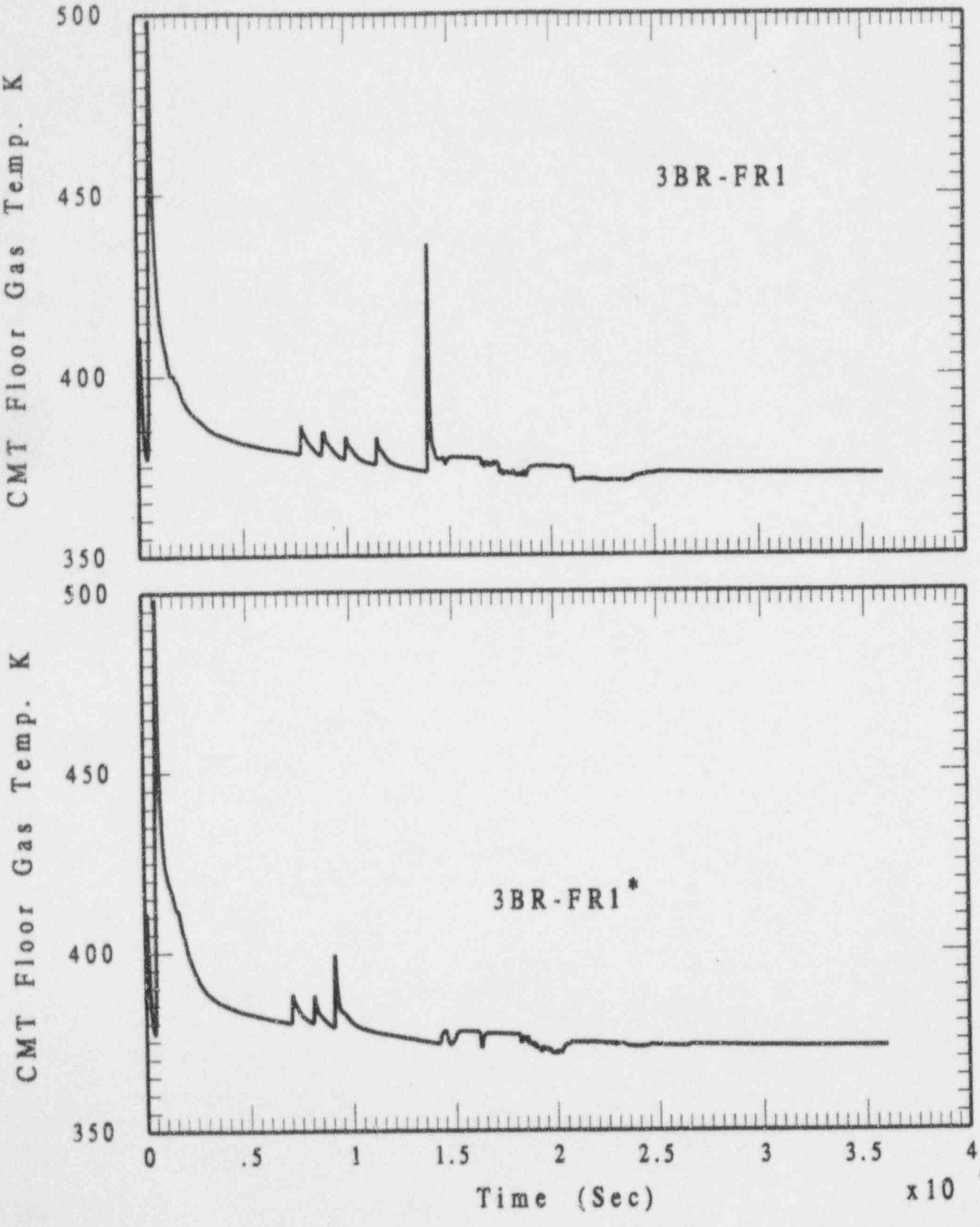


Figure A-27. CMT Floor Gas Temperature

# APPENDIX B

## Heat Transfer Models for Equipment and Personnel Hatches, Electrical Penetrations and Containment Shell

## B.1 Equipment and Personnel Hatches

The model to evaluate radiative heating onto the equipment and personnel hatches due to standing diffusion flames at the south opening in the CMT room is depicted in Figure B-1. The hatch wall, which is also part of the containment boundary, receives radiation heat fluxes from flames on one side and loses heat by radiation and natural convection on the other side. The hatch wall is assumed to be a flat 4 cm (1.6 in) thick circular disk subject to the same level of radiation fluxes to the hot spot. Hence, the calculated hatch wall temperature will be the hot-spot temperature. Air, trapped within the hatch enclosure bounded by the hatch wall and the door in the auxiliary building, would be heated by the hatch wall. This air loses heat to the colder structures including the door on the auxiliary building side and approximately the portion of the enclosure wall lying beyond the containment shell line. This portion of the enclosure is not directly subject to any heating processes inside the containment. The length of this portion is indicated by W in Figure B-1. This portion and the door on the auxiliary building side is assumed to be 4 cm (1.6 in) thick steel. These combined masses constitute relatively large heat sinks such that heat losses from them can be neglected in these transient calculations.

The model described above can be written into three ordinary differential equations governing the behavior of the hatch wall temperature ($T_s$), the enclosure air temperature ($T_a$), and the temperature of the lumped heat sinks ($T_c$) as follows

$$d\,\rho_s c_s \frac{dT_s}{dt} = q_r''(T_f,T_s,F) - h_n(T_s,T_a)\,(T_s - T_a) - \frac{\sigma\left(T_s^4 - T_c^4\right)}{\left(\frac{1}{\varepsilon_s} - 1\right)\frac{1}{1+\frac{4W}{H}} + \frac{1}{\varepsilon_s}} \qquad \text{(B-1)}$$

$$L\,\rho_a c_a \frac{dT_a}{dt} = h_n(T_s,T_a)\,(T_s - T_a) - h_n(T_a,T_c)\,(T_a - T_c)\left(1 + \frac{4W}{H}\right) \qquad \text{(B-2)}$$

$$\Delta X\,\rho_s c_s \frac{dT_c}{dt} = \frac{\sigma\left(T_s^4 - T_c^4\right)}{\frac{1}{\varepsilon_s} - 1 + \frac{1}{\varepsilon_s}\left(1 + \frac{4W}{H}\right)} + h_n(T_a,T_c)\,(T_a - T_c) \qquad \text{(B-3)}$$

The same initial conditions as specified for the containment shell assessment ($T_s$ = 390 K (242°F); $T_a$ = 360 K (188°F); $T_c$ = 330 K (134°F) are also applied here. These equations can be applied to both the equipment hatch and the personnel hatch. The only differences are geometric parameters d, L, H, ΔX, and W. Values for these parameters for each hatch are shown in Figure B-1.

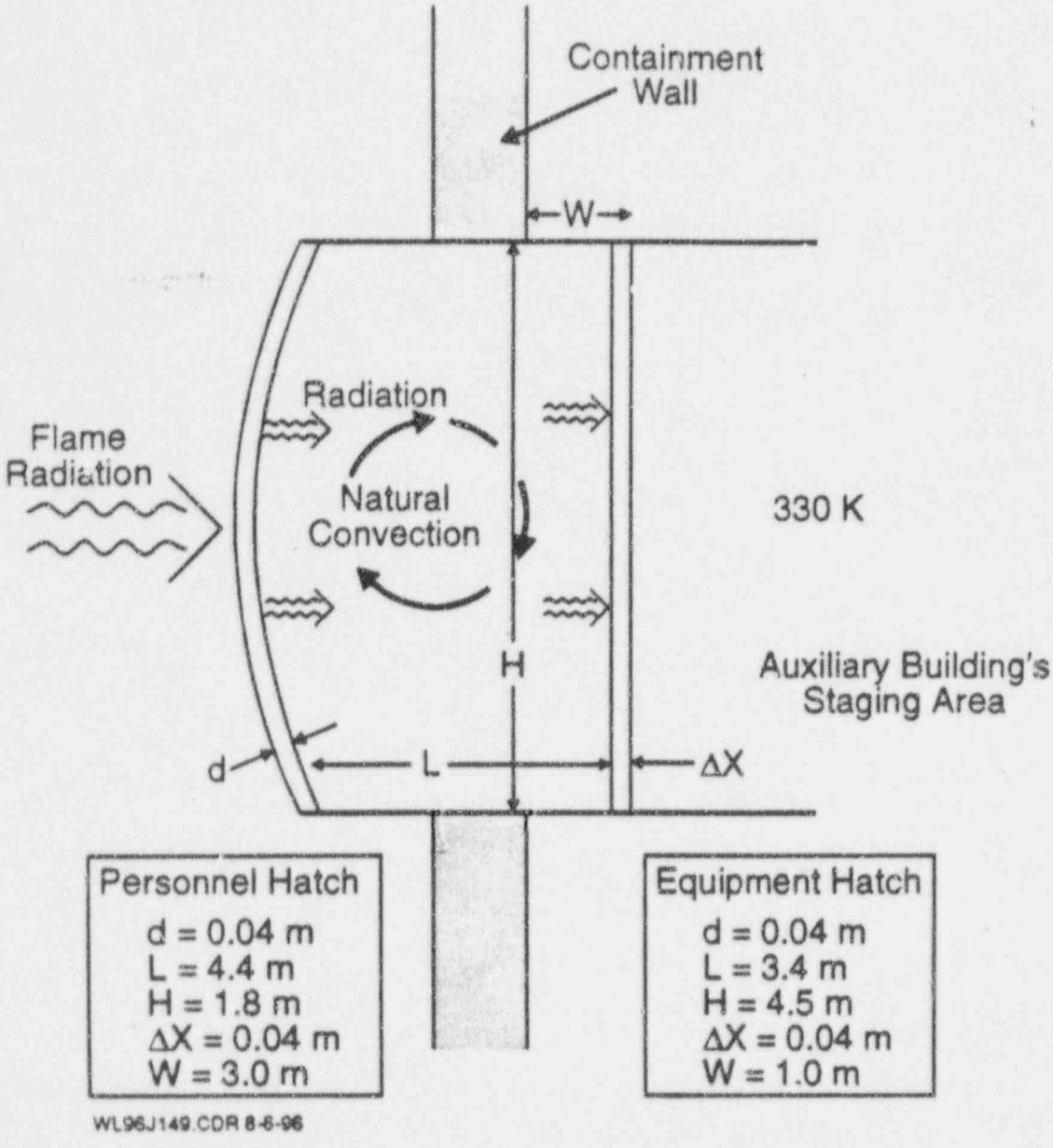


Figure B-1 Model for equipment and personnel hatches.

## B.2 Electrical Penetration Boxes

The model to evaluate radiative heating onto the electrical penetration boxes due to standing flames at the north opening in the CMT room is depicted in Figure B-2. The whole box is inside the containment with the back end connected to the containment shell. The front wall of the box is assumed a 6 mm (0.25 in) thick circular plate made of steel. The front wall receives radiation heat fluxes from the flames on one side and loses heat to air inside the box by natural convection and to other parts of the box by radiation. The penetration box is relatively small compared to the flame height, its elevation is also fixed. This elevation does not necessarily correspond to one half flame height which is the height where hot spot occurs. However, we will assume that the box's front wall always receives heat fluxes at the same level as at the hot spot regardless of the change in flame height. Therefore, very conservative radiation heat fluxes are used here. Radiation heat loss from the front wall is assumed to be limited to only the back end of the box with the same area.

Air inside the box may also be heated by horizontal side walls of the box which are inside the containment. The back end of the box may also be heated by conduction from the adjacent containment shell that is heated by the same flames. Since we already calculate the containment shell temperature separately, we can assume that the back end of the box is at the same temperature as the containment shell hot spot. This is another conservative assumption. In order to calculate heating of air by the side walls, we assume that the side wall temperature is approximated by an average of the front wall temperature and the containment shell hot-spot temperature.

The model described above can be written into two ordinary differential equations governing the behavior of the front wall temperature ($T_s$) and the temperature of air in the box ($T_a$) as follows:

$$d\,\rho_s c_s \frac{dT_s}{dt} = q_r''(T_f,T_s,F) - h_n(T_s,T_a)\,(T_s - T_a) - \frac{\sigma\left(T_s^4 - T_c^4\right)}{\left(\frac{1}{\varepsilon_s} - 1\right) + \frac{1}{\varepsilon_s}} + q_g'' \tag{B-4}$$

$$L\,\rho_a c_a \frac{dT_a}{dt} = h_n(T_s,T_a)\,(T_s - T_a) - h_n(T_a,T_c)\,(T_a - T_c)\,\frac{A_2}{A_1} + h_n\left(\frac{T_s + T_c}{2}, T_a\right)\left(\frac{T_s + T_c}{2} - T_a\right)\frac{A_3}{A_1} \tag{B-5}$$

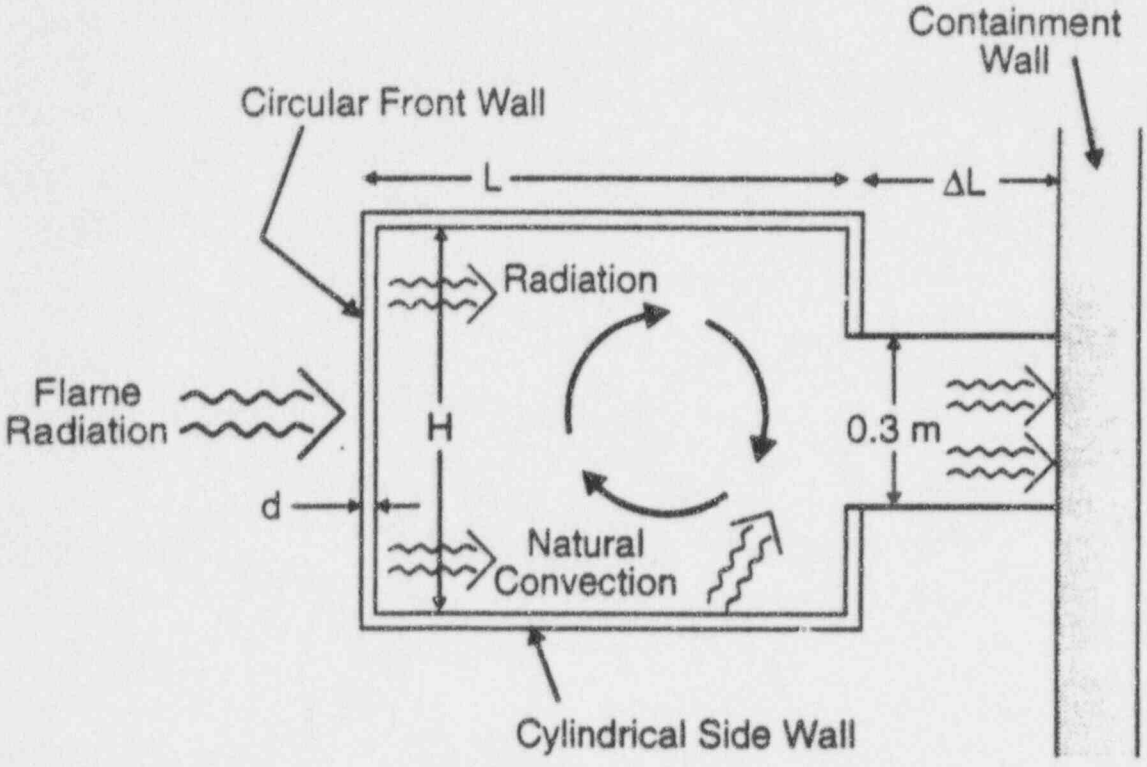


d = 6 mm
L = 0.6m
H = 0.9 m
ΔL = 0.3 m

WL96J151.CDR 7-29-96

Figure B-2 Schematic of heat transfer model for electrical penetration box.

where

$$q_g'' = \begin{cases} h(T_g - T_s) & \text{if } T_g > T_s \text{ for convective heating from containment gas} \\ h_n(T_g, T_s)(T_g - T_s) & \text{if } T_g < T_s \text{ for convective cooldown when there is no flame} \end{cases}$$

$T_g$ = CMT room gas temperature (500 K for heating and 420 K for zero-flame cooldown are conservatively assumed)

$h$ = heat transfer coefficient (assumed value of 3.1 $W/m^2 \bullet K$)

$T_c$ = calculated containment shell hot-spot temperature

$$A_1 = \frac{\pi H^2}{4}$$

$$A_2 = \frac{\pi}{4}(0.5H)^2$$

$$A_3 = \pi HL$$

The initial conditions consistent with the values in the neighborhood of 390 K as used for containment shell and hatches are assumed:

$$\text{at} \quad t = 0 \;,\; T_s = 390 \text{ K} \quad T_a = 389 \text{ K} \quad T_c = 388 \text{ K} \tag{B-6}$$

In practice, it is much more convenient to use the containment shell hot-spot temperatures averaged over each flame height duration. This strategy is adopted here. The necessary geometric parameters (d, H, L) for the calculation are shown in Figure B-2.

## B.3 Containment Shell

The heat transfer model used to perform the containment shell heatup calculations consists of four transient heat balance equations for (1) the containment shell, (2) the PCS baffle, (3) the containment building concrete wall, and (4) the PCS cooling air. The solutions to this set of equations yield the temperature of each object as a function of time.

The containment shell receives radiation and convective heat fluxes from the flames and plumes on the inner side, and on the outer side loses heat to the PCS air by convection and to the baffle by radiation (see Figure B-3).

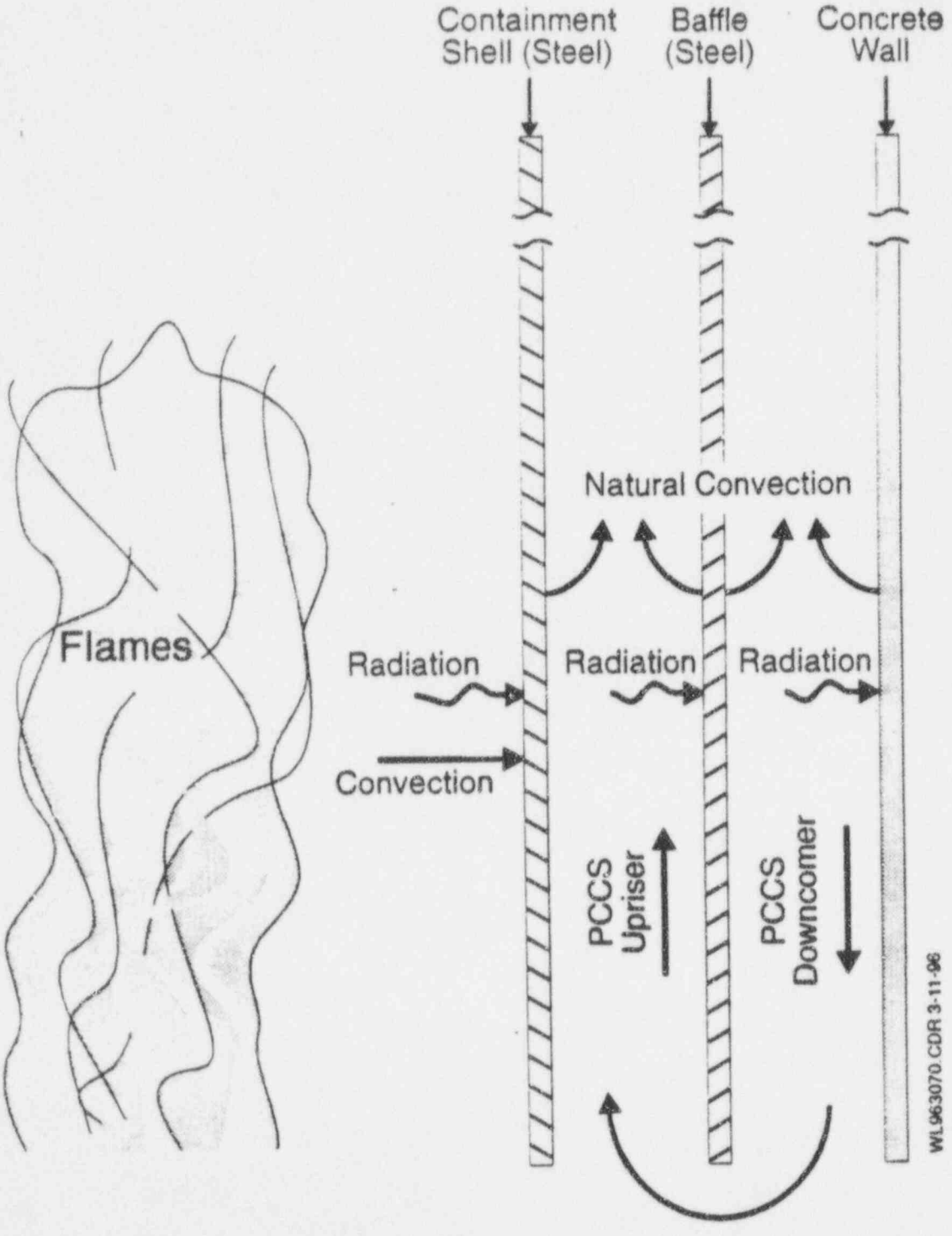


Figure B-3 Containment Shell Heat Balance for Standing Diffusion Flames.

Different portions of the containment shell receive different levels of heat fluxes imposed by the flames. It is conservatively assumed that the temperature of the entire affected portion of the containment shell is represented by a single value representative of the hot spot temperature.

The hot spot on the affected containment shell is located at an elevation corresponding to half flame height where the radiation view factor is maximized for a given flame. The heat balance for the containment shell can be written as

$$d_s \rho_s c_s \frac{d T_w}{dt} = \dot{q_r} + \dot{q_c} + \dot{q_n} (T_w, T_a) - \dot{q_{rb}} (T_w, T_b) \quad \text{(B-7)}$$

where

$T_w$ is containment shell hot spot temperature
$d_s$ is containment shell thickness
$\rho_s$ is containment shell (steel) density
$c_s$ is containment shell (steel) specific heat

The heat flux terms on the RHS of Eq. (B-7) are

(1) radiation heat flux from flame incident on containment shell

$$\dot{q_r} = \sigma \left( F \varepsilon_f \varepsilon_w T_f^4 - \alpha_g T_w^4 \right) \quad \text{(B-8)}$$

where

F = maximum view factor of a hot spot
$\varepsilon_f$ = flame emissivity (0.36)
$\varepsilon_w$ = containment shell emissivity (0.9)
$T_f$ = flame temperature (1350 K)
$\sigma$ = Stephen-Boltzman constant
$\alpha_g$ = gas absorptivity (assumed same as $\varepsilon_f$)

(2) convective heat flux from plume to containment shell

$$\dot{q_c} = h (T_g - T_w) \quad \text{(B-9)}$$

where

$T_g$ = temperature of hot gas induced by flame
h = convective heat transfer coefficient

(3) convective heat flux from containment shell to PCS air

$$q_n^{\cdot}(T_w, T_a) = h_f (T_w - T_a) \tag{B-10}$$

where

$T_a$ = PCS air temperature
$h_f$ = heat transfer coefficient associated with PCS air cooling

(4) radiation heat flux from containment shell to baffle

$$q_{rb}^{\cdot}(T_w, T_b) = \sigma \cdot \frac{T_w^4 - T_b^4}{\frac{1}{\varepsilon_w} + \frac{1}{\varepsilon_b} - 1} \tag{B-11}$$

where

$T_b$ = baffle temperature
$\varepsilon_b$ = emissivity of baffle

The baffle is made of steel with small thickness. The temperature difference across the baffle is negligible. The temperature of the affected baffle can be approximated by a single temperature ($T_b$). The balance between heat inputs and heat outputs for the baffle leads to the following equation.

$$d_b \rho_s c_s \frac{d T_b}{dt} = q_{rb}^{\cdot}(T_w, T_b) - 2q_n^{\cdot}(T_b, T_a) - q_{rb}^{\cdot}(T_b, T_c) \tag{B-12}$$

where

$d_b$ is thickness of the baffle

$q_{rb}^{\cdot}(T_w, T_b)$ is given by Eq. (B-11)

$q_n^{\cdot}(T_b, T_a) = h_f (T_b - T_a)$ is the convective heat flux from baffle to PCS air (B-13)

$q_{rb}^{\cdot}(T_b, T_c) = \sigma \cdot \frac{T_b^4 - T_c^4}{\frac{1}{\varepsilon_c} + \frac{1}{\varepsilon_b} + 1}$ is the radiative heat flux from the baffle to the concrete wall (B-14)

To model heat transfer to the thick concrete wall, a thin (5 mm) layer on the concrete wall surface is assumed to receive heat from the baffle and transfer heat to the bulk of concrete by conduction as well as to the PCS air. The equation can be written as

$$\rho_c \, c_c \, d_c \, \frac{d\,T_c}{dt} = \dot{q}_{rb}\,(T_b, T_c) - \dot{q}_n\,(T_c, T_a) - \dot{q}_{cd} \qquad \text{(B-15)}$$

where

$d_c$ = thickness of the concrete surface layer
$\rho_c$ = concrete density
$c_c$ = concrete specific heat capacity

$$\dot{q}_{cd} = \frac{k_c\,(T_c - T_\infty)}{\sqrt{\pi \alpha_c\,(t + \delta)}} \quad \text{is the conduction heat flux into the concrete wall} \qquad \text{(B-16)}$$

$T_c$ = temperature of the concrete surface layer
$T_\infty$ = ambient air temperature
$k_c$ = concrete thermal conductivity
$\alpha_c$ = concrete thermal diffusivity
$t$ = time
$\delta$ = accident time when diffusion flames are initiated

The use of time, $\delta$, is included to approximate the thermal boundary layer in the concrete wall when the diffusion flames begin to avoid excessive credit for that heat sink.

The last equation is the energy balance for the PCS air in the affected region. The height of the affected region is about the flame height and is relatively small compared to the total height of the containment shell. The width of the affected region is also small compared with the circumference of the containment. Hence, extra PCS air could be drawn from adjacent regions to the affected region when the containment shell heats up. The heatup of PCS air in the affected region can be represented by the following equation

$$\frac{d\,T_a}{dt} = \frac{h_f\,(T_w, T_a)}{2\,\rho_a\,c_p}\left(\frac{1}{2\,D_x}\right)(T_w + 2\,T_b + T_c - 4\,T_a) - \frac{U}{2\,H_f}\,(T_a - T_\infty) \qquad \text{(B-16)}$$

where

$T_a$ is the PCS air temperature for the affected region
$H_f$ is the flame height

$D_x$ is the spacing between the containment shell and the baffle.

The induced air velocity (U) can be derived from the balance between the buoyancy force and the frictional head loss. Assuming the frictional loss associated with PCS downcomer and upriser, to follow a fraction factor of flow in a pipe ($f = 0.316\ Re^{-1/4}$), we have

$$U = \left( \frac{g\ \beta\ (T_w - T_a)\ D_x^{3/4}\ \nu^{1/4}}{0.316} \right)^{4/9} \tag{B-18}$$

where

$g$ = gravitational acceleration
$\beta$ = volumetric expansion coefficient of air
$\upsilon$ = kinematic viscosity of air

With air velocity from Eq. (B-18), the heat transfer coefficient for convective heat removal by PCS air is assumed to follow the Dittus-Boelter correlation, which is

$$h_f = \frac{k_a}{D_x} Nu_f \tag{B-19}$$

where

$$Nu_f = 0.023\ Re_f^{4/5}\ Pr^{0.4} \tag{B-20}$$

$$Re_f = \frac{D_x U}{\nu} \tag{B-21}$$

The heat transfer coefficient (h) in Eq. (B-9) for flame-induced convective heating can be approximated by the flat plate correlation.

$$Nu = 0.664\ Re^{0.5}\ Pr^{1/3} \tag{B-23}$$

The velocity and the temperature of the fire plume decreases with increasing elevation as well as increasing distance from the plume center line. The containment shell is initially about 1.4 m away from the edge of the flame. The induced hot gas velocity and temperature at the containment shell would be mild resulting in low Reynolds number and small convective heat fluxes. Nevertheless, the calculation conservatively assumes a constant value of $T_g$ = 1000 K in Eq. (B-9).

For the purpose of determining a radiative view factor, a series of isolated flames on the IRWST vents are conservatively viewed as a single long continuous flame as if the flames form a wall of a large vertical cylinder whose radius is the distance from the center of the containment to the IRWST vent hood. The height of the cylinder is as tall as the flame height. The maximum view factors from the cylindrical flame to hot spot on the containment shell at flame's mid-height elevation were used in the calculation. Furthermore, it is also conservatively assumed that the flame temperature for the full height is uniformly 900 K above the containment gas temperature. The flame temperature is 1350 K for a containment gas temperature of 450 K.

### B.4 Solution Technique

The transient heat-up calculations were performed for a series of consecutive intervals used to characterize the standing diffusion flame at each valve vault exit or IRWST vent. The flame height is held constant for each interval. Each interval has a different flame height. The first interval uses the initial conditions described above. The second interval uses the end values of the first interval as initial conditions. Similarly, each subsequent interval use the end values of the immediately preceding interval as its initial conditions.